7-18-2014

Probabilistic Seismic Loss Analysis for Design of Steel Structures - Optimizing for Multiple-Objective Functions

Sanaz Saadat

PROBABILISTIC SEISMIC LOSS ANALYSIS FOR DESIGN OF STEEL STRUCTURES - OPTIMIZING FOR MULTIPLE-OBJECTIVE FUNCTIONS

by

Sanaz Saadat

A Dissertation

Submitted in Partial Fulfillment of the

Requirements for the Degree of

Doctor of Philosophy

Major: Engineering

The University of Memphis

August 2014

ABSTRACT

Saadat, Sanaz. Ph.D. The University of Memphis. August 2014. Probabilistic Seismic Loss Analysis for Design of Steel Structures - Optimizing for Multiple-Objective Functions. Major Professor: Charles Camp, Ph.D.

An optimized seismic performance-based design methodology considering structural and non-structural system performance and seismic losses is considered to design steel structures. Multi-objective optimization methodology is implemented considering various sets of optimization objectives which would take into account minimization of the initial construction cost, associated with the weight of the structural system, and the expected annual loss considering direct economic losses, and a social loss parameter defined as expected annual social loss. A non-dominated sorting genetic algorithm method is implemented for the multi-objective optimization. Achieving the desired confidence levels in meeting performance objectives of interest are set as constraints of the optimization problem. Inelastic time history analysis is used to evaluate structural response under different levels of earthquake hazard to obtain engineering demand parameters. Hazus fragility functions are employed for obtaining the damage probabilities for the structural system and non-structural components. The optimized designs and losses are compared for example steel structures, located in two geographic locations: Central United States and Western United States.

ACKNOWLEDGEMENTS

I sincerely appreciate all the supports that I have received during the completion of this dissertation at the Civil Engineering Department, Herff College of Engineering, the University of Memphis. I especially would like to thank my main advisor Dr. Charles Camp who has supported and encouraged me along the way. I am so grateful to him for his guidance, patience and kindness. I am also so thankful to Dr. Shahram Pezeshk who has been a great support for me during these years. I would like to express my sincere appreciation to Dr. Christopher Foley for his helpful suggestions and comments to improve this research. I would like to thank Dr. William Segui, Dr. Roger Meier, and Dr. Adel Abdelnaby for their help and advice. I would like to sincerely thank my family, especially my dear parents and husband, and my friends for their constant encouragements and supports.

TABLE OF CONTENTS

APENDICES

LIST OF TABLES

LIST OF FIGURES

CHAPTER 1

INTRODUCTION

Civil structures are typically designed, based on their location and type, to withstand different types of hazards such as earthquakes, wind, etc. Performance-based design (PBD) is an alternative to traditional design procedures, which are generally force-based design methods (Bazeos 2009) and provide only qualitative expressions for the level of protection for life safety or earthquake-induced damages (Hamburger et al. 2004). PBD in its current form originated in the 1990s and is based on a Federal Emergency Management Agency (FEMA) report (FEMA 1997a) that addressed seismic strengthening of existing buildings and initial concepts of performance levels defined in terms of damageability and varying levels of seismic hazard (FEMA 2012). The current forms of PBD pursue meeting the performance objectives, which are defined as statement of the acceptable risk of meeting specified performance levels specified as expressions of acceptable damage for certain hazard levels. PBD can provide more understanding on the performance of a structure to probable hazards. In addition, it facilitates meaningful discussions between stakeholders and design professionals on the development and selection of design options (FEMA 2012). The performance objectives are based on the safety and economy of a structure. They can be used to provide standard performance at a reduced cost, or confirm higher performance needed for critical facilities (FEMA 2012). In seismic PBD, performance objectives should be met for earthquake ground motions related to different hazard levels. The uniqueness and advantage of the PBD is that it uses a probabilistic approach in evaluating the performance of a structure in meeting performance objectives (Augusti and Ciampoli 2008). In addition, the probable

performance of structures in future earthquakes could be expressed in quantitative statements of the risk of casualty, occupancy and economic losses (Hamburger et al. 2004).

Seismic risk assessment is an important part of real estate financial decision-making for regions at risk of damaging earthquakes (ASTM 2007). Estimating the variability of earthquake risk would be very useful for developing mitigation policies and planning funding levels in both the public and private sectors. Applying seismic design codes and using specialized construction techniques might reduce potential losses in new buildings; however, the economic evaluation of these solutions requires evidence of risk (FEMA 2008). Expected annualized loss (EAL) is a common term in earthquake loss estimation and an outcome of seismic risk assessment that measures the average yearly loss and accounts for frequency and severity of various levels of loss (Porter et al. 2004). The Pacific Earthquake Engineering Research Center (PEER) has presented a framework to break the loss evaluation process into four steps, beginning with seismic hazard characterization, simulation of structural response to evaluate engineering demand parameters, damage modeling and assessment, and decision variable evaluation (Moehle and Deierlein 2004). This method has been implemented to evaluate expected annual values for economic and social losses associated with earthquake events.

Different objectives can be used to optimize the PBD of structures. Beck et al. (2000) introduced an optimal PBD methodology by incorporating multiple preference functions and aggregating them using multiplicative trade-off strategy. Ganzerli et al. (2000) minimized the structural cost subjected to performance constraints on plastic rotations of beams and columns and behavioral constraints for reinforced concrete

frames. Liu et al. (2005) formulated the seismic performance-based design of steel moment frames as a multi-objective optimization problem considering present capital investment and future seismic risk, which is considered in terms of maximum interstory drift demands at two hazard levels. Xu et al. (2006) presented a multi-criteria optimization for seismic PBD of steel structures under equivalent static seismic loading that minimized cost and earthquake damage. Fragiadakis et al. (2006) performed a performance-based optimum design of steel structures with respect to initial and life cycle cost. Alimoradi et al. (2007) and Foley et al. (2007) used a multi-objective optimization in the performance-based design of steel structures in which their objectives were the weight of the structure and a confidence parameter calculated based on the procedure presented in FEMA (2000a). Genturk and Elnashai (2011) considered reducing the life-cycle cost of buildings by reductions in material usage and seismic damage cost to achieve the objectives of economy and sustainability. Rojas et al. (2011) developed a multi-objective optimization PBD of steel structures using the weight of the structure and the expected annual loss as the optimization objectives.

In this study, seismic loss evaluations are considered in optimizing the PBD of steel structures. Probabilistic hazard analysis is used to measure the potential losses due to earthquake and two different sites are considered: Memphis, TN located in the Central United States (CUS) and Los Angeles, CA, located in the Western United States (WUS). A multi-objective optimization method is applied to different sets of optimization problems that have considered minimizing combinations of the initial construction cost, modeled by the weight of the structural system, expected annual loss value associated with direct economic losses, and expected annual loss value associated with direct social

losses. Inelastic time history analysis is used to evaluate structural response under different levels of earthquake hazard to obtain engineering demand parameters such as inter-story drifts and peak floor accelerations. The calculated annualized loss values provide planners and engineers with a risk-based method for evaluating alternative structural designs and a quantitative parameter to compare seismic risks in different geographic locations.

CHAPTER 2

PERFORMANCE BASED DESIGN

In this chapter, after a general introduction to the concept of PBD, the implemented PBD method is explained. It includes the definition of performance objectives and the performance evaluation method implemented for design of steel moment frames.

2.1. Introduction to Performance-Based Design

Structural design aims to specify and proportion the elements of a structure to support the loads applied to it during its lifetime. The structural designer needs to make sure that the design provides enough strength to support the loads in a manner that is safe and convenient for the occupants and at the same time should consider factors that lower the costs without sacrificing the safety. Therefore, the primary objectives of the structural designer are safety and economy (McCormac 1992). The traditional design methods in building codes intend to meet the acceptance criteria for stiffness and strength to provide adequate ductility, promote dynamic response and avoid premature formation of collapse mechanisms and other instabilities (Hamburger et al. 2004). However, one shortcoming of these methods is that the level of protection and performance of the structure is only stated qualitatively. As a result, these methods for defining design objectives would not be of enough application to all stakeholders such as owners, occupants, and insurers.

The traditional measures of seismic performance have been in terms of force and deformation computed by structural analysis and interpreted by limits set forth in building codes. Unfortunately, this type of seismic analysis does not generally have a direct relationship to performance metrics that are of interest to or easily understood by

the building's stakeholders (ATC 2007). PBD in its current form originated in the 1990s and is based on the report on NEHRP guidelines for seismic rehabilitation of buildings (FEMA 1997a), which addressed seismic strengthening of existing buildings and initial concepts of performance levels defined in terms of damageability and varying levels of seismic hazard (FEMA 2012). In PBD, the traditional seismic metrics are used to define a series of standard performance levels that provide quantitative information about building performance that are more readily interpreted and thus of more value to decision makers (ATC 2007). Seismic PBD (SPBD) permits a realistic understanding of the structure's performance by providing a quantitative statement of the probable performance of the structure subjected to earthquake loads (Hamburger et al. 2004). SPBD can be applied to the design of new buildings or the retrofit of existing buildings by defining a set of performance objectives that achieve specific performance limits for defined hazard levels. Figure 1 shows a typical flowchart of the current PBD procedures that details the definition of performance objectives, development of a preliminary design, assessing the response of the structure in terms of the desired performance metrics, comparing the resulting performance with the defined performance objectives, and revising the design to meet the performance objectives, if necessary (ATC 2007).

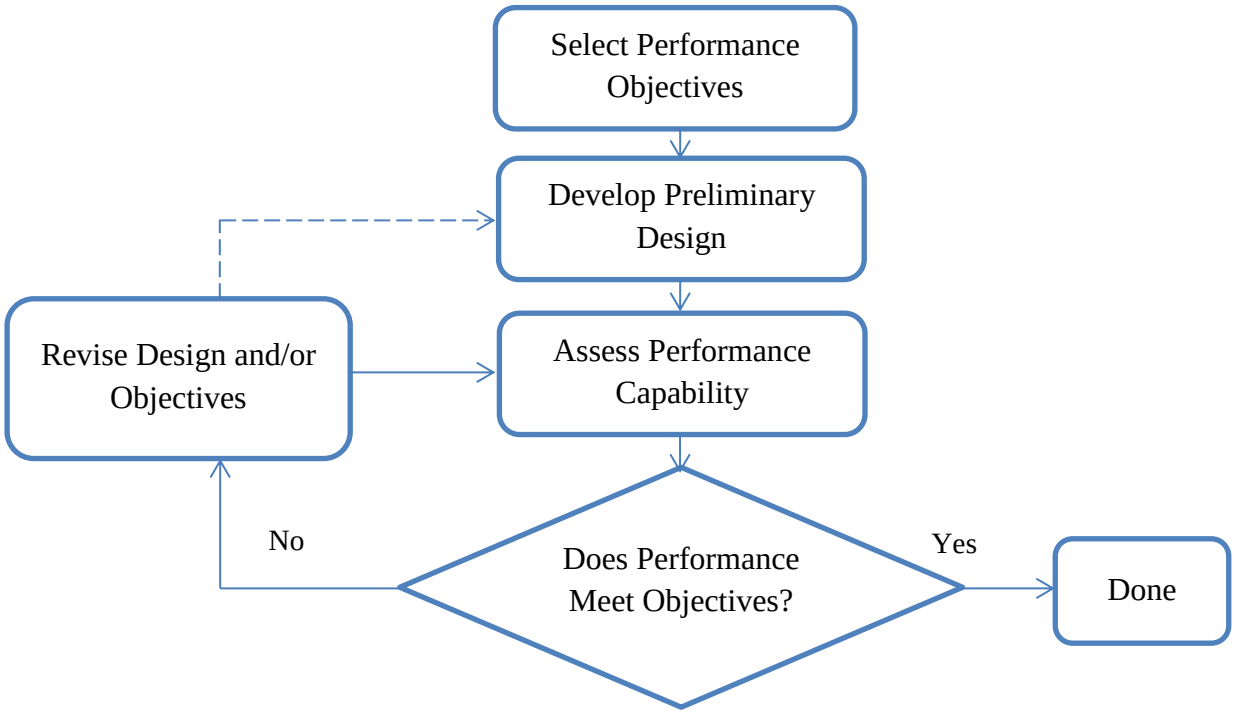

Figure 1. Performance-based design flow diagram

2.2. Performance Objectives

Performance objectives are design criteria defined in the form of probabilistic statements of the acceptable risk of incurring damage and the consequent losses. Selection of these objectives would be made considering the desires of a wider group of stakeholders who may not directly participate in the design process (ATC 2007). In order to specify the performance objectives in PBD, decision makers need to identify acceptable performance levels in the defined levels of seismic hazard. This process is explained further in the following sections.

2.2.1. Performance Level

Performance level, as described in FEMA (1997a), is defined as the intended post-earthquake condition of a building that expresses how much loss is caused by

earthquake damage. This loss can be expressed in term of casualties, or damage to property or occupational capability. Table 1 lists some performance levels as defined by FEMA (1997a).

Table 1. Definition of performance levels

Performance Level	Description
Operational Level	Very little overall damage, Backup utility services maintain functions, Structure substantially retains original strength and stiffness. No permanent drift.
Immediate Occupancy Level	Light overall damage. The building receives a "green tag" (safe to occupy) inspection rating. Repairs are minor. Structure substantially retains original strength and stiffness. No permanent drift.
Life Safety Level	Moderate overall damage. Structure remains stable and has significant reserve capacity. Some residual strength and stiffness left in all stories. Hazardous non-structural damage is controlled. Some permanent drifts.
Collapse Prevention Level	Severe overall damage. The building remains standing, but only barely, any other damage or less is acceptable. Little residual stiffness and strength, but load bearing columns and walls function. Large permanent drifts.

The discrete damage states listed in Table 1 are selected from a large spectrum of possible damage states that a structure could experience as a result of earthquake response (FEMA 2000a). Two of the most common performance levels are collapse prevention and immediate occupancy.

2.2.2. Collapse Prevention Performance Level

The collapse prevention (CP) structural performance level is defined as the damage state in which the structure is on the verge of partial or total collapse. The

structure would experience substantial degradation in the strength and stiffness of the lateral-force-resisting system along with large permanent lateral deformations. However, the gravity-load-resisting system must continue to carry gravity-load demands. Under the CP performance level the structure is not safe for re-occupancy (FEMA 2000a).

2.2.3. Immediate Occupancy Performance Level

The immediate occupancy (IO) structural performance level is defined as the damage state in which only limited structural damage has occurred that usually would not require repair. The vertical and lateral force-resisting systems retain nearly all their pre-earthquake strength and stiffness. The structure should be safe for immediate post-earthquake occupancy (FEMA 2000a).

2.2.4. Seismic Hazard

Seismic hazards imposed by earthquake events include direct ground rupture, ground shaking, land-sliding, liquefaction, and settlement. Since the most significant cause of earthquake damage to buildings is due to ground shaking, the effects of ground shaking form the basis for seismic design requirements in most design codes (FEMA 1997a). However, for the structures located where other seismic hazards could result in significant ground deformation, these hazards should also be considered in performance evaluation of the structure (FEMA 2000a).The goal of earthquake resistant design is to produce a structure that can withstand a certain level of shaking without excessive damage. Selecting the design ground motions requires considering the significant uncertainties in the size, time, and location of potential earthquakes. Seismic hazard analysis is the quantitative estimation of ground shaking hazards at a particular site (Kramer 1996).

There are two general approaches for seismic hazard analysis: deterministic seismic hazard analysis (DSHA) and probabilistic seismic hazard analysis (PSHA). DSHA involves the development of a particular seismic scenario upon which a ground motion hazard evaluation is based (Kramer 1996). Implementing a probabilistic approach to consider uncertainties associated with future earthquakes has been introduced by Cornell (1968). PSHA considers the uncertainties in earthquake size, location, and time of occurrence and integrates over all potential magnitudes and source distances to estimate the mean frequencies of earthquake ground motion occurring at the site in any given time period (Bazzurro and Cornell 1999). Hazard levels may be defined on either a probabilistic or deterministic basis. Probabilistic hazards are defined as the probability that more severe demands will be experienced (probability of exceedance) in a specific time period. Deterministic demands are defined within a level of confidence in terms of a specific earthquake scenario (a specific magnitude event on a particular fault), which would be more appropriate for buildings located in the vicinity of a major active fault (FEMA 1997a). Table 2 lists some more frequently used probabilistic hazard levels in terms of their probability of exceedance (POE) and their corresponding mean return period, which is defined as the average number of years between events of similar severity (FEMA 1997a).

Table 2. Some frequently used probabilistic levels

Earthquake Having Probability of Exceedance (POE)	Mean Return Period (years)
50% in 50 years	72
20% in 50 years	225
10% in 50 years	474
2% in 50 years	2475

Based on the recommendations of FEMA (1997b), structures could be assigned to one of three specified Seismic Use Groups (SUG): SUG-III, which includes structures that have essential facilities and are required for post-earthquake recovery and those containing substantial quantities of hazardous substances; SUG-II, in which structures have a substantial public hazard due to occupancy or use (e.g. high capacity educational structures, water treatment facilities, etc.); and SUG-I, that include structures not assigned to SUG-II or SUG-III. Figure 2 shows the recommended building performance levels for different levels of ground motion (FEMA 2000a).

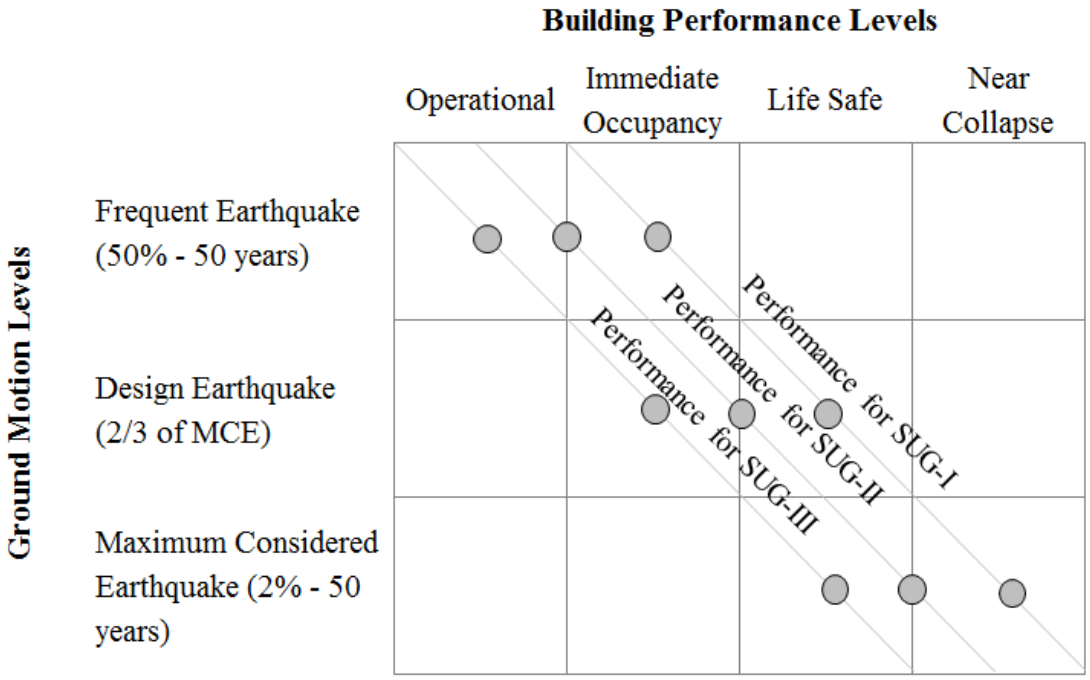

Figure 2. Recommended building performance levels for different levels of ground motion (FEMA 2000a)

In FEMA (1997a), performance objectives are presented in a deterministic manner. The definition of these performance objectives include defining the limiting damage state, termed as performance level, and correlating the performance level to the defined ground motion hazard level (FEMA 2000a).

Significant uncertainty exists in predicting the amount of damage that the building would experience for a given ground motion. This uncertainty is due to factors that affect the building behavior and response, such as stiffness of non-structural elements, quality of construction, etc.; inaccuracies associated with analysis procedures; and the uncertain character of earthquake ground motions. Therefore, it would be more appropriate to predict the performance in a probabilistic manner instead of deterministically (FEMA 2000a). To address these uncertainties, FEMA (2000a)

developed a reliability-based probabilistic approach for performance evaluation. In this method, uncertainties are expressed in terms of acceptable confidence levels and recommended methods to improve these confidence levels such as increasing the stiffness and strength of the structure and reducing uncertainties associated with performance evaluation.

2.3. Confidence Levels

As described in Section 2.2.2, in order to address the uncertainties inherent in the evaluation of structural performance in different seismic hazard levels, FEMA 350 (FEMA 2000a) has developed a reliability-based probabilistic approach for performance evaluation in which uncertainties are expressed in terms of acceptable confidence levels (CLs) in meeting the performance objectives. In this study, the FEMA (2000a) methodology for the calculation of CLs is implemented. Structural analysis is used to estimate various structural response parameters such as interstory drift and axial forces on individual columns under different loading conditions which include seismic ground motions for different hazard levels. Predicted demands, calculated from structural analysis, are later adjusted for an analytical uncertainty factor accounting for the uncertainty inherent in the analytical technique, and a demand variability factor accounting for sources of variability in structural response. These predicted demands are compared with structural capacity modified by resistance factors to account for uncertainties inherent in predicting capacity. The ratio of factored demand-to-capacity is implemented to calculate confidence level (FEMA 2000a).

Selected performance objectives are CP for hazard level of 2% POE in 50 years and IO for hazard level of 50% POE in 50 years, which are the two performance levels

considered in the FEMA (2000a) PBD recommended procedure. Structural demands for the earthquake ground motions associated with selected hazard levels are considered as the median values of maximum inter-story drift (ISD) and maximum column compressive forces of structure for suites of ground motions in each hazard level (Rojas 2008) and are determined using non-linear time-history analysis. The confidence parameter λ_{CL} is calculated as the factored demand-to-capacity ratio as

$$\lambda_{CL} = \frac{\gamma \gamma_a D}{\phi C} \tag{1}$$

where γ is the demand variability factor accounting for the variability in predicted demand related to assumptions made in structural modeling and character of ground shaking, γ_a is an analysis uncertainty factor, D is the calculated demand on a structure, obtained from the structural analysis, C is the median estimate of the capacity of the structure, and resistance factor ϕ accounts for the uncertainty in the prediction of structural capacity. FEMA (2000a) provides recommended values for γ , γ_a and C, listed in Tables A-1 to A-3 in Appendix A.

The CL is calculated as

$$\mathrm{CL} = \Phi(K_x) \tag{2}$$

where $\Phi(K_x)$ is the normal cumulative distribution function value corresponding to K_x which is a standard Gaussian variant associated with probability x of not being exceeded (FEMA 2000a) and is back-calculated from:

$$\lambda_{CL} = e^{-\beta_{UT}\left(K_X - \frac{k}{2b}\beta_{UT}\right)} \tag{3}$$

therefore,

$$K_x = \frac{k\beta_{UT}}{2} - \frac{\ln(\lambda_{CL})}{b\beta_{UT}} \tag{4}$$

where β_{UT} is an uncertainty measure equal to the vector sum of the logarithmic standard deviation of the variations in demand and capacity resulting from uncertainty, b is a coefficient relating the incremental change in demand (ISDs and column forces) to an incremental change in ground shaking intensity at each hazard level, taken as 1.0 (FEMA 2000a), and k is the slope of the hazard curve, in natural log coordinates, at the hazard level of interest. An example of calculating k (FEMA 2000a) is

$$k = \frac{\ln\left(\frac{H_{S_1(10/50)}}{H_{S_1(2/50)}}\right)}{\ln\left(\frac{S_{1(10/50)}}{S_{1(2/50)}}\right)} = \frac{1.65}{\ln\left(\frac{S_{1(10/50)}}{S_{1(2/50)}}\right)} \tag{5}$$

where $S_{1(10/50)}$ and $S_{1\,(2/50)}$ are the spectral amplitudes for hazard levels of 10% in 50 years and 2% in 50 years, respectively; $H_{S1\,(10/50)}$ is the probability of exceedance for 10% in 50 years which is calculated as 1/475=0.0021, and $H_{S1\,(2/50)}$ is the probability of exceedance for 2% in 50 years, calculated as 1/2475=0.00040.

In order to further improve the performance-based design procedure, the aim is to consider performance measures that better relate to the decision making needs of

stakeholders and create procedures for estimating probable repair cost, casualties, and time of occupancy interruption, for both new and existing buildings. The steps for this methodology include: characterization of the ground shaking hazard, analysis of the structure to determine its probable response and the intensity of shaking transmitted to non-structural components, determination of the probable damage to the structure at various levels of response, determination of the potential for casualty, capital and occupancy losses as a function of structural and non-structural damage, and computation of the expected future losses as a function of intensity, structural and nonstructural response, and damage (FEMA 2006).

2.4. Seismic Loss Evaluation

Seismic losses are metrics for decision making in seismic risk mitigation. Evaluation of loss due to building damage from an earthquake event depends on both seismic hazard and the building vulnerability (Kappos et al. 2007). The types of losses that could be considered include casualties (loss of life and serious injuries), direct economic losses (including the cost of repair and replacement of damaged systems and components), and downtime (including the time of occupancy interruption due to damage) (ATC 2007).

Expected annual loss values are calculated by aggregating the probabilistic seismic hazard analysis (PSHA), probabilistic seismic demand analysis, probabilistic capacity analysis, and probabilistic loss analysis, using the total probability theorem.

PEER center has developed a loss assessment framework (Moehle and Deierlein 2004, Ramirez et al 2012) to calculate the mean annual occurrence rate of decision variable $\lambda[DV]$ as

$$\lambda[DV] = \iiint P[DV|DM]P[DM|EDP]P[EDP|IM]\lambda[IM]\,dDM\,dEDP\,dIM \quad (6)$$

where *DV* is the decision variable, *DM* is the damage measure, *EDP* is the engineering demand parameter, and *IM* is the intensity measure. The cumulative distribution function of the random variable *X* conditioned on random variable Y is $P[X \mid Y]$. Direct economic loss is evaluated through calculating the EAL parameter. For direct social loss calculation, a parameter defined as expected annual social loss (EASL) is considered. Therefore, in loss calculations two types of *DV* (i.e. EAL and EASL) are considered. The steps of this framework are further explained in the following sections.

2.4.1. Probabilistic Seismic Hazard Analysis

PSHA quantifies and rationalizes the uncertainties regarding the location, size, and resulting shaking intensity of possible future earthquakes at a given site (Baker 2008). This method implements the characterization of the earthquake sources and their seismicity and ground motion attenuation relationships, along with considering the uncertainties associated with these characterizations, to estimate the probabilities that the ground motion parameters will be exceeded during a particular time period (Kramer 2007).

PSHA is performed for Memphis using the EZ-FRISK software package (EZ-FRISK 2013). The New Madrid seismic zone (NMSZ) and CUS gridded data are considered as seismic sources and the attenuation relationships recommended by USGS (2008) are implemented. EZ-FRISK generates the uniform hazard response spectra (UHRS) for different hazard levels. More information about the implemented software can be found in Appendix B. Figure 3 shows the obtained response spectra for hazard

levels considered for Memphis which are 2, 5, 10 and 50 percent probability of exceedance (POE) in 50 years.

Synthetic ground motions are generated using the stochastic methods implemented in SMSIM (Boore 2000). A stochastic method for synthetic ground motion generation is used to address the need for ground motion records compatible with local seismic characteristics in regions with scarce recorded data. The ground motions are modified to match the uniform hazard response spectra for four hazard levels of earthquakes with 2, 5, 10, and 50 POE in 50 years (Shahbazian and Pezeshk 2010). The SHAKE91 computer program is used to account for site effects using the Memphis site properties considering the information given by Romero and Rix (2001) for Lowlands geological conditions and damping and modulus degradation curves adopted from EPRI (1993). The SHAKE91 program (Idriss and Sun 1992), which is a modification of SHAKE (Schnabel et al. 1972), analyzes the behavior of the horizontally layered soil deposits subjected to seismic loading. A total of 40 ground motions (10 time histories for each of the four hazard levels) are considered for calculation of losses at Memphis site. Increasing the number of considered hazard levels would result in the more accurate EAL calculation which on the other hand would be equivalent to having a more computationally expensive analysis procedure.

For a site located in Los Angeles, CA, suites of ground motions are from the SAC steel research project (Somerville et al. 1997) for three different hazard levels (2, 10, and 50 percent POE in 50 years). The ground motions are scaled so that, on average, their spectral values match with the least square error fit to the USGS national hazard mapped values at 0.3, 1.0, and 2.0 seconds, and an additional predicted value at 4.0 seconds

(Somerville et al. 1997). The weights assigned to the four period points are 0.1 at the 0.3-second period point and 0.3 for the other three period points. The target spectra provided by USGS are for the S_B/S_C soil type boundaries, which have been modified to be representative for soil type S_D (FEMA 2000b). A total of 30 ground motions are considered for the site located in Los Angeles, CA.

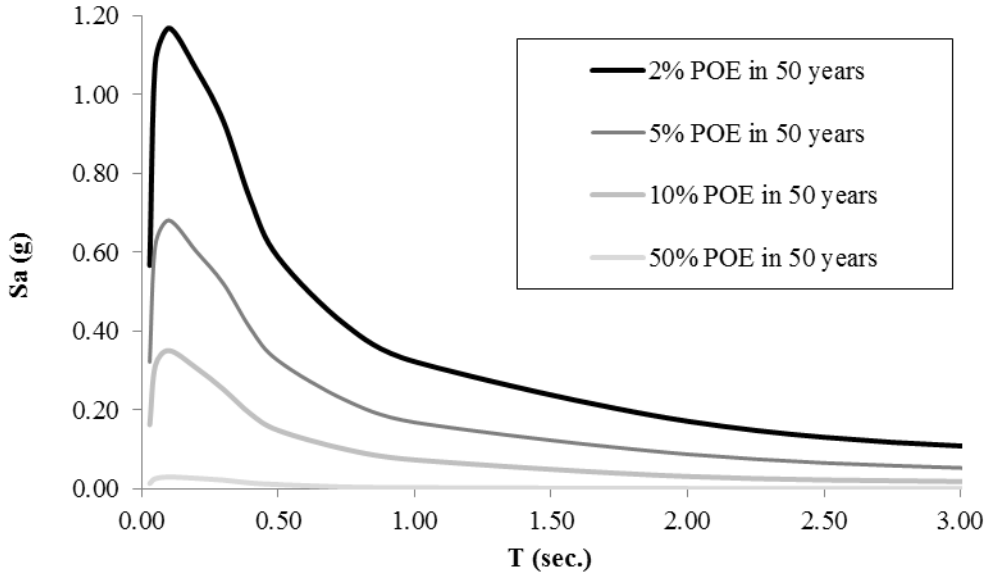

Figure 3. Spectral accelerations for different hazard levels for a site located in Memphis, TN obtained from EZ-FRISK

2.4.2. Probabilistic Seismic Demand Analysis

In the seismic demand analysis, the response of the structure subjected to the ground motions defined by the PSHA is used to calculate engineering demand parameters (EDPs). Engineering demand parameters describe structural response by simulation of the building to the input ground motions (Moehle and Deierlein 2004). Considering that ISDs and peak floor accelerations (PFAs) could be implemented to evaluate the damage

to structural and nonstructural components (HAZUS-MR 2003b), in this study, the EDPs are the ISD and PFA, calculated from a non-linear time-history analysis of the structure. The DRAIN-2DX (Dynamic Response Analysis of Inelastic 2-Dimensional Structures) computer program is used for the analysis of the structure. DRAIN-2DX is a computer program written in FORTRAN 77 and performs nonlinear static and dynamic analysis (Powell 1993 and Prakash et al. 1993). Yield surfaces for structural elements are based on the models presented in Powel (1993), Alimoradi (2004), and Rojas et al. (2011). More details are presented in Appendix C.

2.4.3. Probabilistic Damage Analysis

The EDPs for structural and nonstructural components are linked to damage measures (DMs) which describe the physical condition of these components. For the purpose of damage assessment, fragility curves for the structure of interest should be developed. Fragility functions are probability distributions to indicate the likelihood of damage to an element or system due to a given damage state as a function of a single demand parameter such as the ISD or the PFA (ATC 2007). Fragility curves are defined as lognormal distributions of the conditional probability of damage exceeding a certain *DM* given *EDP* (Hazus-MH 2003a and Rojas 2008) which can be expressed as

$$P[DM|EDP] = \Phi\left[\frac{1}{\beta_{DM}} \ln \frac{EDP}{EDP_{DM}}\right] \tag{7}$$

where EDP_{DM} is the median value of the considered *EDP* (e.g. ISD) and β_{DM} is the lognormal standard deviation of the *EDP* for the *DM* considered (such as slight, moderate, extensive, and complete)

Fragility curves are obtained using the parameters given in Hazus technical manual Hazus-MH (2003a) for structural and non-structural members for different damage states. Figures 4 through 6 show the fragility curves for a low-rise building type S1 (steel moment frames) with high-code seismic design level. Values of β_{DM} are determined from Hazus-MH (2003a). Figure 7 shows an example of damage analysis. This analysis would be performed for structural components (SS) and drift sensitive (NSD) and acceleration sensitive (NSA) non-structural components.

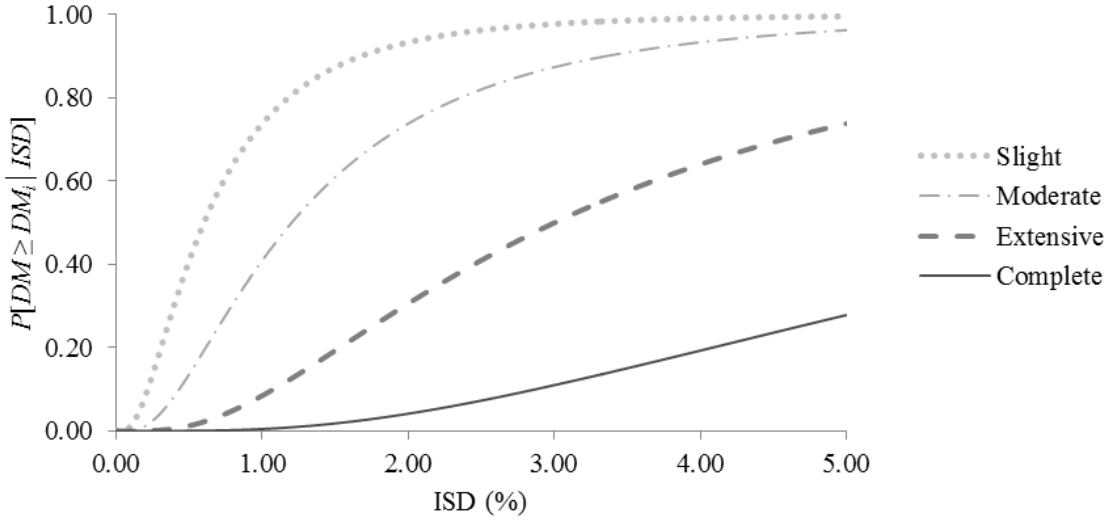

Figure 4. Fragility curves for structural (SS) elements for sample structure

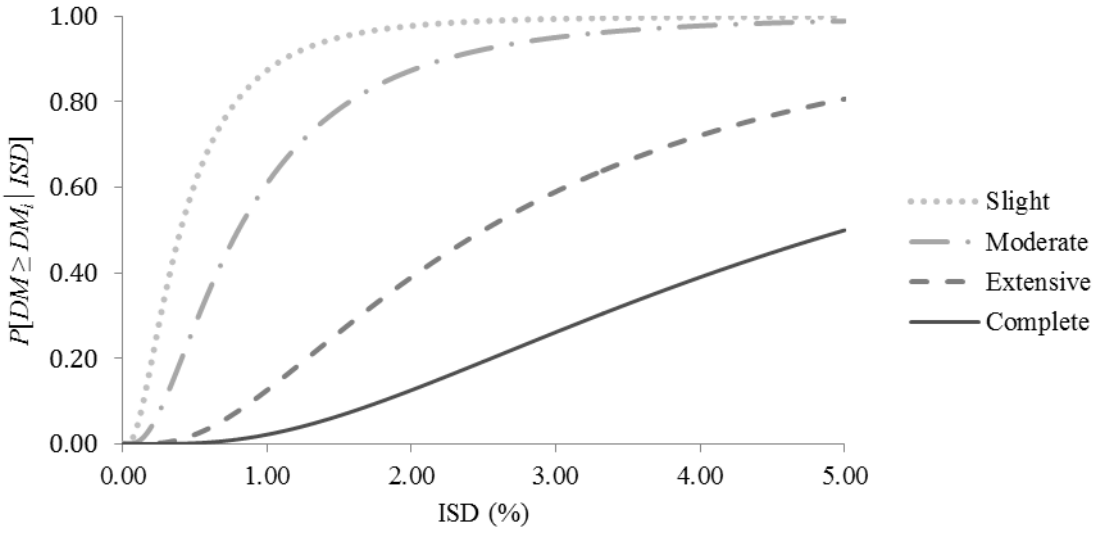

Figure 5. Fragility curves for drift-sensitive non-structural (NSD) elements for sample structure

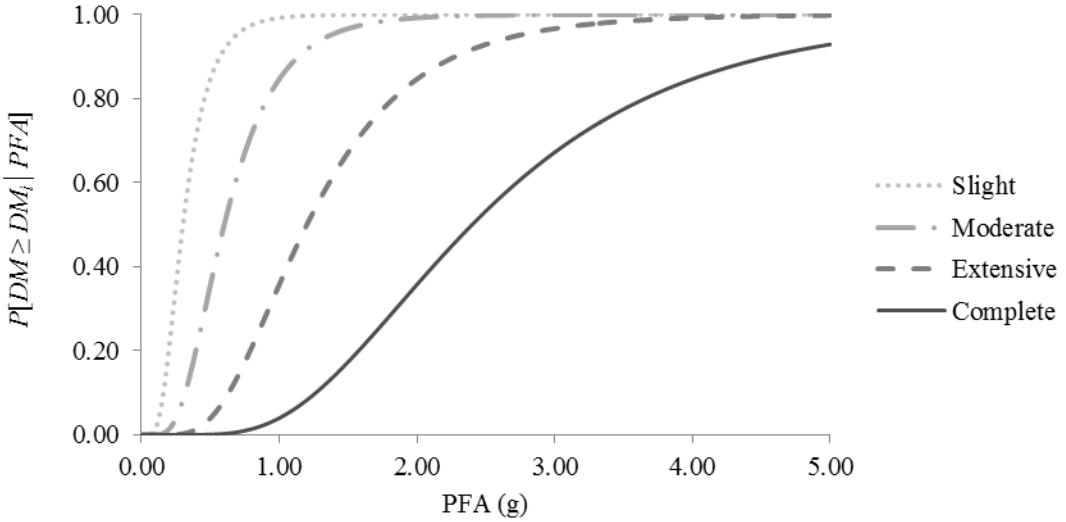

Figure 6. Fragility curves for acceleration-sensitive non-structural (NSA) elements for sample structure

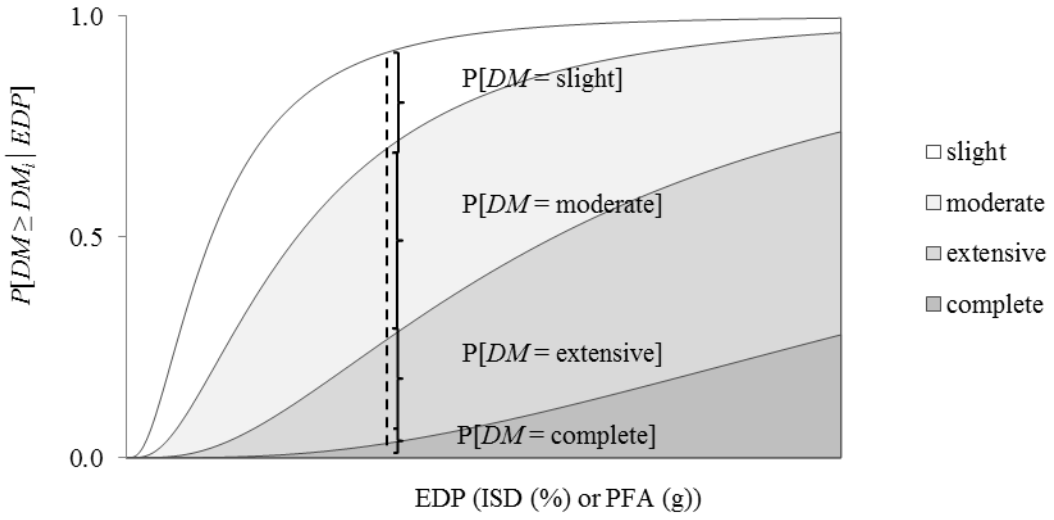

Figure 7. Damage analysis for different components

2.4.4. Probabilistic Seismic Loss Analysis

Probabilistic loss analysis estimates the consequences of structural damage from an earthquake and is used to evaluate decision variables (*DV*s). These variables are related to consequences of earthquake damage which can be expressed in terms like social losses or casualties or economic losses associated with repair cost or repair time. The DVs considered in this study are economic loss and social loss. Economic loss is expressed in terms of the percentage of the building replacement cost (%BRC).

Expected economic losses $E[L_{c,EDP}]$ (%BRC) for each component (SS, NSD, NSA), are calculated for a specific *IM* as

$$E\left[L_{c,EDP}\right] = \sum_{i=2}^{5} P\left[DM_{i,EDP}\right] \times RC_{DMi,c} \tag{8}$$

where $L_{c,EDP(IM)}$ is the loss associated with each component *c* (SS, NSD, and NSA) for the *EDP* at a specific *IM*, $P[DM_{i,EDP}]$ is calculated using fragility curves for the *EDP* at a specific

IM, and $RC_{DMi,c}$ is defined as the repair cost for each component due to DM_i which varies from slight (i=2) to complete (i=5) (Hazus-MH, 2003b). Expected loss $E[L_{EDP}]$ for a particular structure and a specific *IM* is calculated as the sum of losses for all components as

$$E\left[L_{EDP}\right] = E\left[L_{SS,EDP}\right] + E\left[L_{NSD,EDP}\right] + E\left[L_{NSA,EDP}\right] \tag{9}$$

The total loss curve is obtained from the loss curves for each hazard level and hazard curve as

$$P\left[L > l\right] = \int_{\lambda} P[L > l \left| IM \right]] d\lambda \approx \sum_{i=1}^{m} (1 - P[L < l \left| IM_i \right]]) \Delta\lambda_{IM_i} \tag{10}$$

where $P[L > l]$ is probability of loss L exceeding a specific value l, which is obtained from the loss curves for each hazard level, λ is the annual rate of exceedance for each IM_i, m is the number of hazard levels considered, and $\Delta\lambda_{IMi}$ is the change in annual rate of exceedance associated with dividing the hazard curve into m different segments, as shown in Figures 8 and 9. The hazard curve for the Memphis site is obtained using the EZ-FRISK program. For the Los Angeles site, the hazard curve is obtained from USGS (2013). For the Memphis site, since four hazard levels are considered in the analysis, the curve is divided into four segments (m=4). The segments are set to have the points associated with the four considered hazard levels (for this case, 2%, 5%, 10%, and 50% POE in 50 years) would be located at the midpoint of each segment. In the Figures 8 and 9, diamond markers show the points on the hazard curve that are associated with the hazard levels considered in the loss analysis. Same procedure is followed for the Los

Angeles hazard curve, with the difference that it is divided to three segments (m=3), since three hazard levels (2%, 10%, and 50% POE in 50 years) are considered for the Los Angeles site.

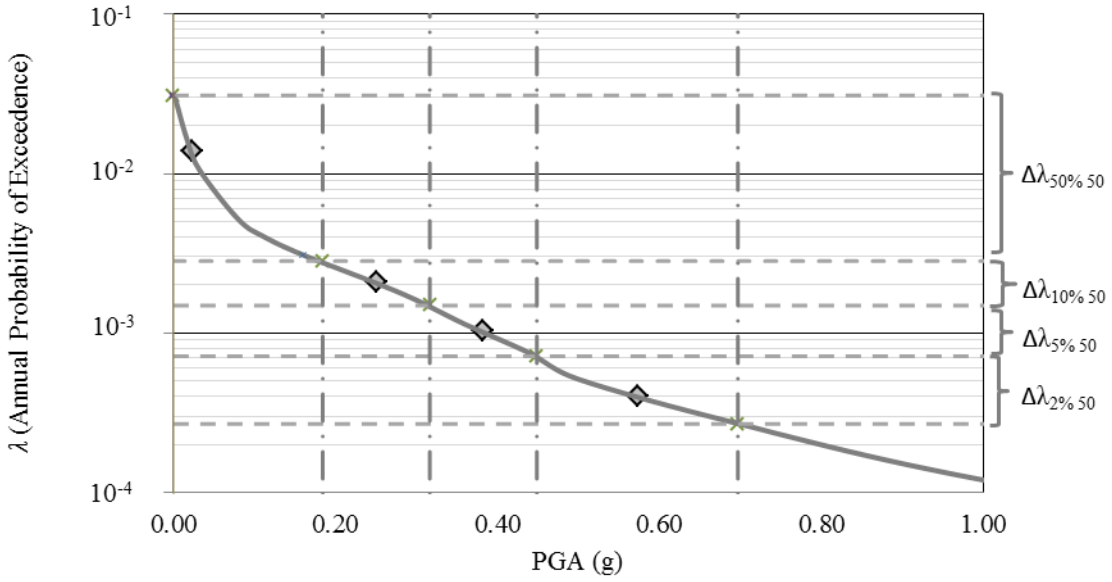

Figure 8. Memphis, TN hazard curve, amplified for soil type D

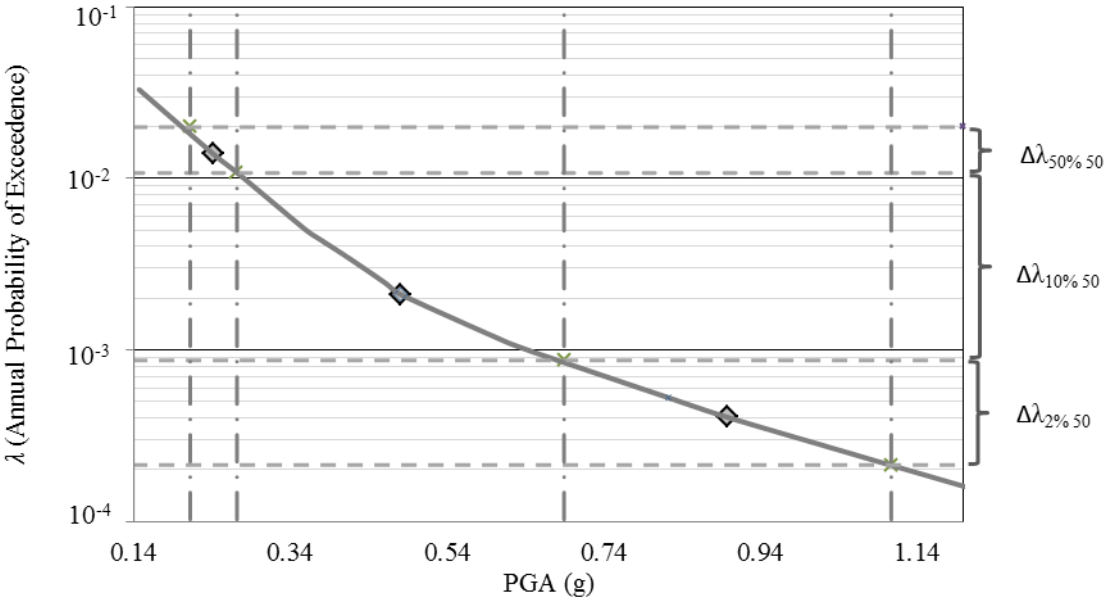

Figure 9. Los Angeles, CA hazard curve, amplified for soil type D

The EAL is the area under the total loss curve. EASL is calculated following the same procedure presented for EAL with direct social loss as the decision variable. The methodology presented in Hazus-MH (2003b) is used to perform probabilistic loss analysis with casualties as *DV*. This methodology assumes that there is a relationship between building damage and the number and severity of casualties and estimates casualties caused by both structural and nonstructural damage (Hazus-MH, 2003b).

Figure 10 shows an overview of the Hazus methodology, in which casualties caused by an earthquake are modeled by developing a tree of events leading to their occurrence (Hazus-MH 2003b). In this figure CSL_i (i= 1,4) is the casualty severity level for i equal 1 (lowest severity level associated with minor injuries) to 4 (highest severity level). More description is presented in Table A-4, Appendix A. The four damage measures are associated with slight to complete damage levels.

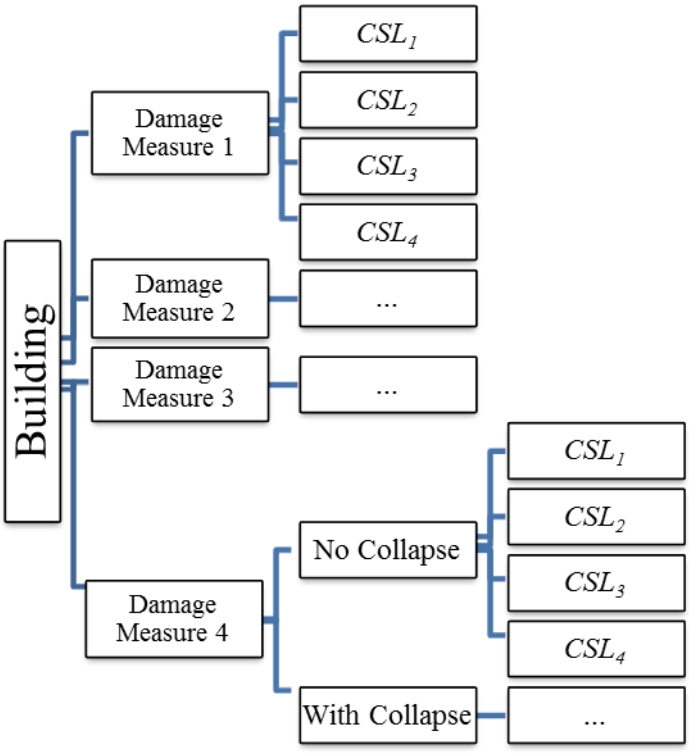

Figure 10. Injury event tree model

Equations (11) and (12) below show the aggregation of these different events to calculate the social losses. Social losses for indoors and outdoors injuries for each intensity measure *IM*, $E[SL_{indoors,EDP}]$ and $E[SL_{outdoors,EDP}]$, respectively, are calculated as

$$E[SL_{indoors,EDP}] = \sum_{i=2}^{4}\sum_{j=1}^{4} P[DM_{i,EDP}] \times P[CSL_j | DM_i] \times w_j \times \alpha + P[DM_{i,EDP}] \times \left[\sum_{j=1}^{4} (P[Collapse | DM_5] \times P[CSL_j | Collapse] + P[no-Collapse | DM_5] \times P[CSL_j | no-Collapse]) \times w_j \times \alpha \right] \quad (11)$$

$$E[SL_{outdoors,EDP}] = \sum_{i=3}^{5}\sum_{j=1}^{4} P[DM_{i,EDP}] \times P[CSL_j | DM_i] \times w_j \times \alpha \quad (12)$$

where $P[DM_{i,EDP}]$ is the probability of damage measure [slight (i=2) to complete (i=5) damage] for the *EDP* at a specific *IM*, CSL_j is the casualty severity level for j equal 1 (lowest severity level) to 4 (highest severity level), and w_j are the weights given to different *CSL*s based on financial costs. The probabilities for different *CSL*s are based on recommendations presented in Hazus-MH (2003b). The weights w_j are chosen based on the comprehensive costs for different injury levels suggested by National Safety Council (NSC) (NSC 2013) and α (in \$/person) is the comprehensive cost for CSL_i.

The expected number of occupants injured or killed, $EN_{OI,EDP}$, for a specific *IM* is calculated as

$$EN_{OI,EDP} = N_o \times \left[n_i \times E[SL_{indoor,EDP}] + n_o \times E[SL_{outdoor,EDP}] \right] \quad (13)$$

where N_o is the number of occupants in building, n_i and n_o are factors that account for the distribution of people indoors and outdoors, considering recommendations from Hazus

MH (2003b). The expected number of occupants injured or killed is calculated for all ground motions and all hazard levels. EASL is calculated using the area under the total social loss curve obtained from the aggregation of the loss curves for each hazard level and hazard curve.

Figures 11 and 12 show total loss curves for economic and social losses for Memphis, TN and Los Angeles, CA. Total economic loss curves present the annual rates of exceedance for different values of total repair cost, RC_T. Total social loss curves present the annual rates of exceedance for different values of total social cost, SC_T. The presented total loss curves in Figures 11 and 12 show that both parameters EAL and EASL, calculated as the area under the curve, are significantly larger for the site located in Los Angeles, as compared to the site located in Memphis.

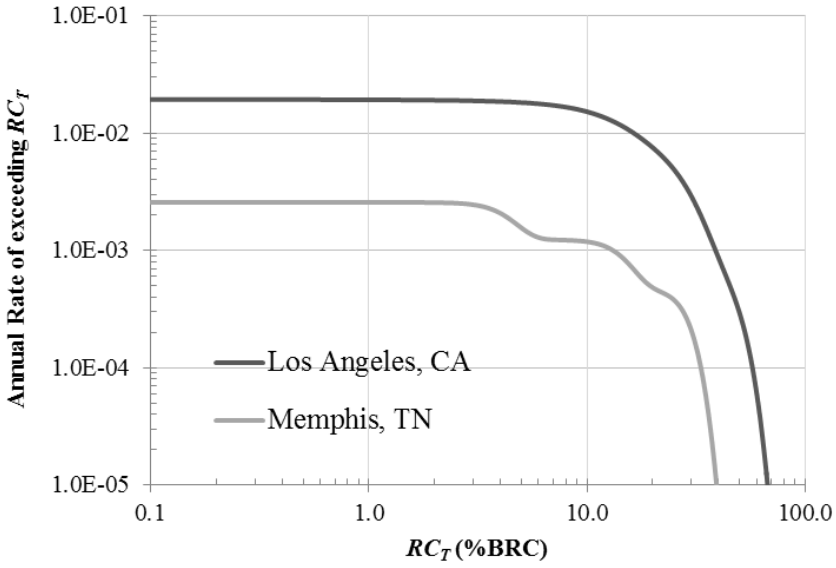

Figure 11. Total economic loss curves for Memphis, TN and Los Angeles, CA sites for an example structure

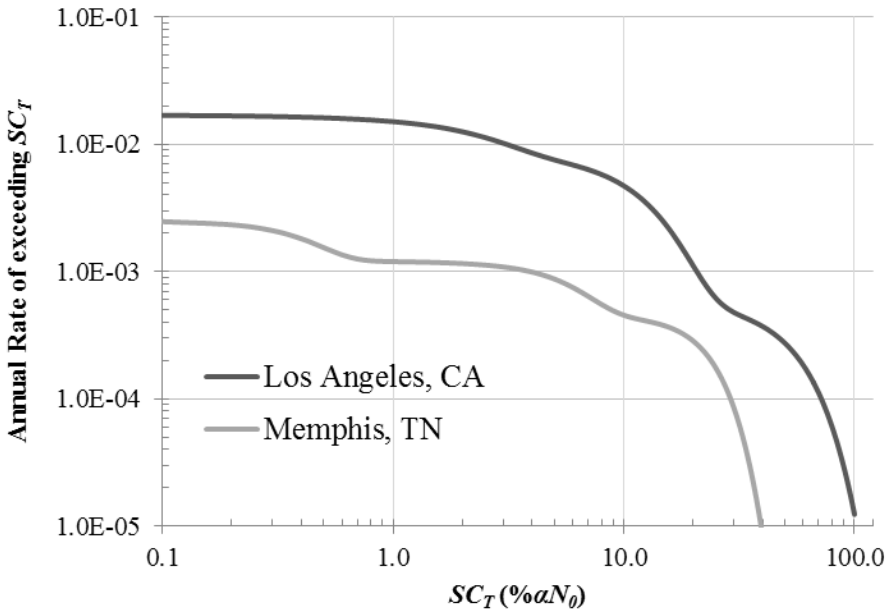

Figure 12. Total social loss curves for Memphis, TN and Los Angeles, CA sites for an example structure

CHAPTER 3

OPTIMIZATION METHOD

Optimization is the process of making a system, design, etc. as efficient as possible as measured by a set of optimization objectives. Therefore, optimization seeks to improve performance toward some optimal point or points (Goldberg 1989). Optimization in design is the determination of properties of the structure to amplify the value of a certain characteristic while the values of the rest of its characteristics are constrained to remain within prescribed limits (Vasiliev and Gurdal 1999). ASCE (1997) presented several examples of optimization methods applied to structural design problems (e.g. design of plate girders, cold-formed steel beams, composite members, reinforced and prestressed concrete beams, steel frameworks, and tall buildings).

The general form of the optimization problem can be expressed as finding a design variable vector $X_d = \{x_1, x_2, \ldots, x_n\}$ to minimize or maximize the objective function $f(X)$ as:

$$Min \text{ or } Max \quad f(X_d) \tag{14}$$

subject to

Equality Constraints $$c_i(X_d) = 0 \quad i = 1, 2, \ldots, n_E \tag{15}$$

Inequality Constraints $$c_i(X_d) \le 0 \quad i = p+1, 2, \ldots, n_I \tag{16}$$

where $c_i(X)$ are equality and inequality constraints (ASCE 1997).

Various optimization methods have been developed over the last several decades, many of which have matured to be utilized in realistic engineering systems (ASCE 1997). Some of these optimization methods are based on direct search for exact mathematical solutions, such as linear and nonlinear programming methods: sequential quadratic programming, successive linear programming, and gradient-based search methods (Soliman and Mantaway 2012). Another approach to optimization uses stochastic methods based on observations of natural phenomena. Some of the more popular techniques include genetic Algorithms (GA), simulated annealing algorithm (SAA), evolutionary algorithms (EA), artificial neural networks (ANN), ant colony optimization (ACO), and particle swarm optimization (PSO). These stochastic methods provide a means of coping with models and systems that are highly nonlinear, have high dimensionality, or are inappropriate for classical deterministic methods of optimization (Spall 2004).

Evolutionary algorithms (EA), inspired by evolutionary biology, are very flexible techniques that are capable of solving very complex optimization problems. Some examples of EAs include GAs, evolution strategies, evolutionary programming, and genetic programming (Castro 2006). These algorithms can be applied to a wide variety of subjects including the design of artificial intelligence systems, image processing, facial recognition, structural design, etc.

EAs have been applied to a variety of civil and architectural engineering problems such as structural design, structural control, damage detection, architectural design, and traffic engineering and transportation. Jenkins (1997) used a GA to optimize the geometry and design of a multi-story frame with truss-supported hangers. Camp et al.

(1998) investigated the application of a GA in two-dimensional steel structures. Matsuzaki et al. (1999) implemented a GA for solving the multi-floor facility layout problem. Li et al. (2000) used a GA for multi-level optimization of buildings with active control under wind loads. Caldas and Norford (2003) used a GA for the optimization of building envelopes and the design of HVAC systems. Park et al. (2013) applied a GA to minimize the worker vertical transportation time in high-rise building construction. The above-mentioned studies are just a few examples among so many that demonstrate the diversity of problems in civil engineering that use EAs.

3.1. Genetic Algorithm

Within the field of stochastic optimization, GAs are among the most widely used methods. Simply stated, a GA attempts to mimic the processes of natural evolution. GAs were first introduced and developed by John Holland in the 1960s (Coley 1999). Holland's goal was to implement the mathematical abstraction of the biological adaptation process into a wide range of complex systems with factors that interact in a nonlinear manner (Holland 1975). Holland's GA moves from one population of chromosomes (e.g. strings of ones and zeroes that encode and represent the values of design variables) to a new population by applying a form of natural selection using genetics-inspired operators such as crossover and mutation (Mitchell 1999). A GA combines a strategy of the survival of the fittest among the string structures with an organized and yet randomized exchange of information to form a search algorithm. GAs have proven themselves to provide robust search mechanics in complex search spaces (Goldberg 1989). During the last several decades, there has been a widespread interaction among researchers who work on various evolutionary computation methods and the term

"genetic algorithm" used by researchers is sometimes far from Holland's original conception (Mitchell 1999).

3.1.1. Selection

In a GA, chromosomes represent a population of candidate solutions within the search space of a specific optimization problem. Selection is the process of selecting individual chromosomes from the population for the purpose of reproduction. Choosing an appropriate selection method will encourage the GA to maintain the diversity within the population through exploration and at the same time moves the population towards finding the best individual (Coley 1999). Usually, selection is based on the fitness value assigned to each chromosome. There are several selection methods suggested by different researchers such as tournament selection, proportional selection methods (e.g. roulette wheel selection), truncation selection, linear ranking selection, and exponential ranking selection (Blickle and Thiele 1995). In this study, a roulette wheel selection (RWS) strategy, which is one of the commonly used selection methods in GA applications, is implemented. In this RWS method, each individual chromosome in the population is given a chance to become a parent proportional to its assigned fitness value. Therefore, individuals with a better fitness value have a higher chance of being selected. The probability of individual *i* being selected in a population of *N* individuals can be expressed as:

$$P_i = \frac{fitness(i)}{\sum_{j=1}^{N} fitness(j)} \tag{17}$$

Figure 13 shows a sample RWS, in which the largest portion of the wheel (in this example 40%) is assigned to the fittest individual based on Equation (17), leading to a higher chance of this individual being selected. To implement this method, a probability is assigned to each individual using the P_i value, and probabilities are summed cumulatively to place individuals on the considered roulette wheel. Then, a random number is generated between zero and one and based on which portion the random number has been fallen into, the associated individual would be selected. The individuals have a chance of being selected multiple times and their probability of being selected would depend on their fitness value.

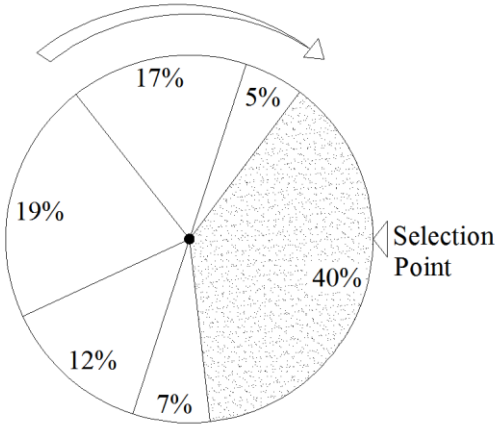

Figure 13. Roulette Wheel Selection Method

3.1.2. Crossover

Crossover is a genetic operator used in GAs to reproduce individuals from one generation for the next generation. Among the various methods proposed for crossover are: single-point crossover, multipoint crossover, and uniform crossover. Figure 14 shows some of these crossover methods that recombine pairs of individuals to generate new offspring. The difference between these methods is in the number of crossover points.

Some studies suggest that for some cases, for example for larger search spaces, uniform crossover outperforms single and double point crossover methods (Spears and De Jong 1991). In this study, uniform crossover is implemented in which, offspring is generated by swapping the bits of the chromosome string between the two parent individuals, using the crossover probability. The considered crossover probability is 0.6, which has been used in the similar optimization problems (Rojas et al 2011).

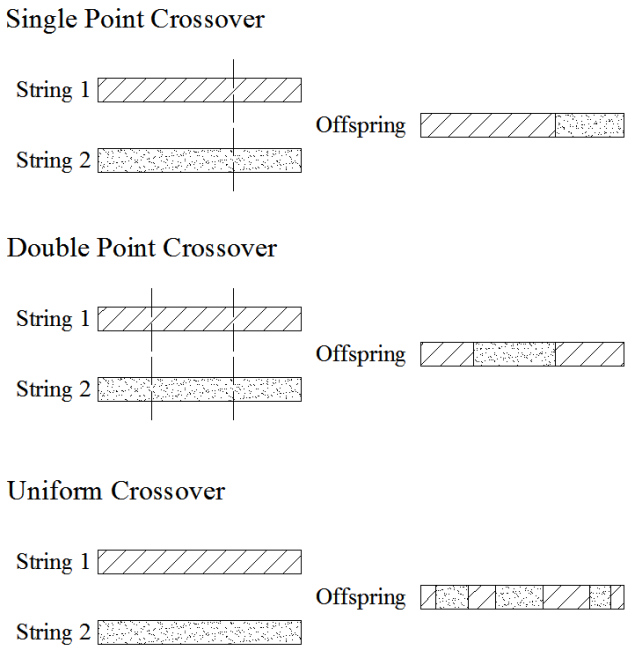

Figure 14. Different Crossover Method

3.1.3. Mutation

Mutation is a genetic operator that helps add new genetic material to chromosomes in a population to both aid in the exploration of the search space and to help the GA avoid premature convergence to a local optimum (Gen and Cheng, 2000). However, the probability of mutation is usually kept low to avoid losing the knowledge from the previous generation and turning into a random search. In this study mutation probability of 0.03 is considered. Figure 15 shows a sample mutation procedure for

binary represented individuals, in which bits on the individual are randomly switched from zero to one with the mutation probability.

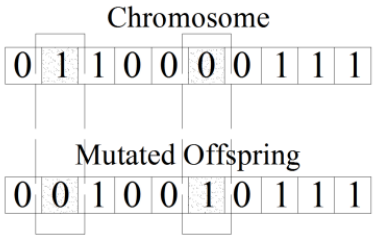

Figure 15. Sample Mutation Method

3.2. Multi-Objective Optimization

In multi-objective optimization problems, there is more than one objective function to be optimized simultaneously. In this case, due to the usual conflict among different objectives, there is not a single solution that is best with respect to all objectives. Instead, there is a set of solutions, called non-dominated solutions or Pareto optimal solutions, that cannot simply be compared with each other because no improvement is possible in one objective function without sacrificing at least one of other objective functions (Gen and Cheng 2000). Many researchers have worked on the multi-objective optimization in variety of fields, originally pioneered by Pareto (1906).

The general form of the multi-objective optimization problem can be expressed as finding a design variable vector $X_d = \{x_1, x_2, \ldots, x_n\}$ to minimize or maximize the objective functions

$$Min \text{ or } Max \ [f_1(X_d), f_2(X_d), ..., f_q(X_d)] \tag{18}$$

subject to

Equality Constraints $c_i(X_d) = 0 \quad i = 1,2,...,n_E$ (19)

Inequality Constraints $c_i(X_d) \leq 0 \quad i = p+1,2,...,n_I$ (20)

where $f_i(X_d)$ are q objective functions and $c_i(X_d)$ are equality and inequality constraints. If S is used to denote the feasible region in the decision space, the feasible region in criterion space Z can be defined as

$$Z = \left\{ z \in R^q \middle| z_1 = f_1(X_d), z_2 = f_2(X_d), ..., z_q = f_q(X_d), \ x \in S \right\} \quad (21)$$

where z $\in$ R^q is a vector of q objective function values (Gen and Cheng, 2000). For the minimization case, a solution $z^{nd} \in Z$ is considered to be non-dominated if and only if there does not exist another different solution $z \in Z$ that:

$$\begin{aligned} z_k &< z_k^{nd} \quad \text{for some } k \in \{1, 2, ..., q\} \\ z_l &\leq z_l^{nd} \quad \text{for all } l \neq k \end{aligned} \quad (22)$$

where z^{nd} is the non-dominated solution.

As mentioned, these non-dominated solutions cannot simply be compared with each other because you cannot select one solution among them which is better than the others in all objectives. Therefore, in order to select one solution from the non-dominated set of solutions, the decision maker needs to provide additional preference information regarding various objectives (Gen and Cheng 2000). Multi-objective optimization results can be presented in two general ways: generating approaches and preference-based approaches. In generating approaches an entire set of non-dominated solutions would be

identified and would not consider any preferences among the objectives. Pareto approach is a generating approach. In preference-based approaches, a preferred solution based on the relative importance of objectives is identified. Typical preference approaches include: weighted sum, utility function, compromise, and lexicographic ordering (Gen and Cheng 2000). Preference-based approaches have the advantage of providing the decision maker with one solution based on a predefined importance structure of objectives. However, defining this importance structure (e.g. objective weights in weighted sum approach or utility function for utility function approach) is controversial for some optimization, since the resulting solutions are very sensitive to the values of the weights or the prescribed order of objectives (Gen and Cheng 2000). On the other hand, generating approaches would not require preference information to present results and provide the decision makers with a set of Pareto solutions to select from.

In this study, the multi-objective optimization results are presented in a generating format. A multi-objective GA using an elitist non-dominated sorting strategy (Deb et al. 2002) is implemented to perform the optimization. In order to preserve the diversity of the solutions in the Pareto front, a crowding distance methodology is used. Figure 16 is the graphical explanation of a non-dominated sorting genetic algorithm (NSGA-II) implemented for a problem with two optimization objectives f_1 and f_2. The closed markers in the Figure 16(b) represent the non-dominated solutions on the front. The first step in this optimization strategy is to randomly generate a population P_N and compute a fitness value for each parent individual in the population based on a non-dominated sorting. Fitness is assigned to individuals based on the number of solutions they dominate. An individual dominates another solution when it excels in both

objectives. A new child population Q_N is generated based on general GA methodology (roulette wheel selection, uniform crossover, and mutation). Next, a new population P_N^{New} is developed from the parent and child populations (size 2N) by grouping individuals into subsets of different fronts F_i based on the non-dominated sorting procedure. The next generation (size N) is populated with members for the first front F_1 (the most dominate front). If the new generation is not fully populated from the F_1 front pool, members are taken form the second front F_2, and so on, until the new generation P_N^{New} is fully populated. If there are fewer unfilled positions in the new generation than there are members in a front group, a crowding distance sorting strategy is applied where individuals with larger crowding distances (the distance between the individuals immediately before and after the individual j located on the Pareto front, as shown in Figure 16b) are chosen to fill out the parent population.

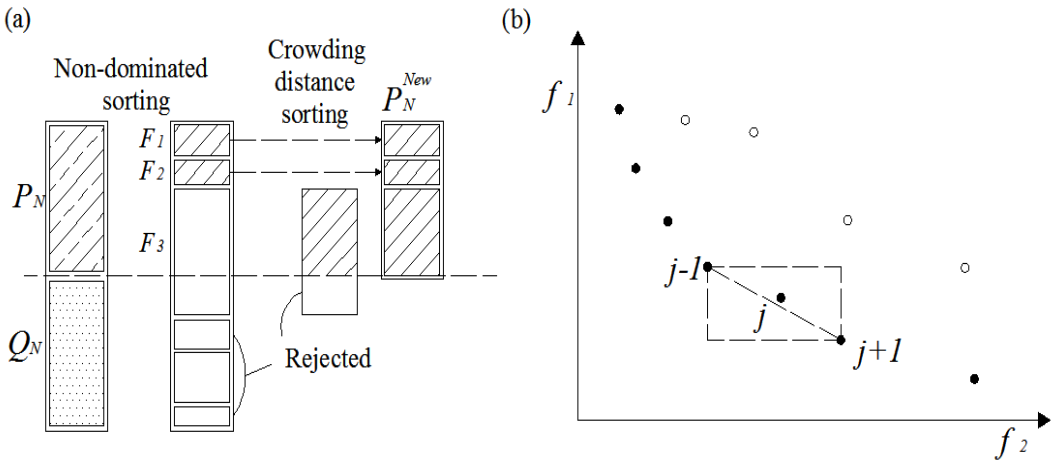

Figure 16. (a) NSGA-II procedure, (b) crowding distance calculation (Deb et al 2002)

3.3. Optimization Problems

Three different optimization problems are considered. The first two problems are optimized for two objectives. In the third optimization problem, three objectives are

considered. The first multi-objective optimization problem attempts to minimize the combination of the initial cost associated with the weight of the structural system *w* and EAL of a building while achieving the desired confidence levels for performance objectives and seismic design codes. The performance objectives are immediate occupancy performance level for the hazard level of 50% in 50 years and collapse prevention for the hazard level of 2% in 50 years, while satisfying design criteria for strong column-weak beam (AISC 2011).

In the second optimization problem, the objectives are defined as the lifetime cost of the structure or the present value of the total cost and direct social loss defined as the EASL.

The third optimization problem considers three optimization objectives defined as the initial cost of the structure, direct economic loss parameter *EAL*, and direct social loss parameter *EASL*. The formulation and the results of these optimization problems are discussed in more detail in Chapter 4.

3.4. Summary

In this chapter, a general introduction to optimization problems has been presented. Different optimization methods, including definite methods, based on direct search for exact mathematical solutions, and stochastic methods are introduced and the application of some of these optimization methods in engineering problems is briefly discussed. The basic formulation of a GA, an algorithm inspired by natural selection, is introduced in detail. Since the many practical engineering optimization problems involve multiple objectives, there has been much interest and research conducted in multi-objective optimization problems. There are several strategies proposed to address the

multi-objective optimization problems, including generating approaches and preference-based approaches. In this study a multi-objective elitist non-dominated sorting GA strategy is implemented for problems with various objectives.

CHAPTER 4

OPTIMIZATION DESIGN EXAMPLES

Multi-objective optimization has been implemented in the probabilistic performance-based design of various steel moment frame structures. The optimization objectives include combinations of initial cost, expected annual seismic economic loss, and expected annual seismic social loss. Three different optimization problems are considered. The first two problems are optimizing for two objectives. In third optimization problem, three objectives are considered. The following sections present each of the considered problems in details.

4.1 Optimization Problem I

This multi-objective optimization attempts to minimize the combination of the initial cost associated with the weight of the structural system *w* and EAL of a building, while achieving the desired confidence levels for performance objectives. An example 3-story steel moment frame is considered. The performance objectives are IO performance level for the hazard level of 50% in 50 years and CP for the hazard level of 2% in 50 years, while satisfying design criteria for strong column-weak beam (AISC 2011).

4.1.1 Problem Definition

The multi-objective optimization problem is formulated as two minimization problems for the considered objectives. The general form of the optimization statement is defined as

$$\begin{aligned} &Minimize\,(W, EL) \\ &Subjected\ \ to: c_i \quad (i = 1,3) \end{aligned} \tag{23}$$

where W and EL are the penalized values for the weight w and EAL of the structure, respectively; and c_i is the i^{th} constraint that is applied on the optimization problem. The penalized values W and L are calculated as

$$W = \varphi \times w \tag{24}$$

$$EL = \varphi \times EAL \tag{25}$$

where φ is the penalty function. The constraints for the confidence levels for collapse prevention CL_{CP} and immediate occupancy CL_{IO} are

$$c_1 : \frac{CL_{CP}}{CL_{CP,\min}} \geq 1.0 \tag{26}$$

$$c_2 : \frac{CL_{IO}}{CL_{IO,\min}} \geq 1.0 \tag{27}$$

where $CL_{CP,\min}$=90% and $CL_{IO,\min}$=50%, as recommended by FEMA 350 (FEMA 2000a). The constraint for ensuring the AISC strong column-weak beam criteria of for seismic design, calculated for each connection in the frame is

$$c_3 : \frac{\sum M^*_{pc}}{\sum M^*_{pb}} \geq 1.0 \tag{28}$$

where M^*_{pc} is the modified flexural strength of the column and M^*_{pb} is the modified flexural strength of beam sections (neglecting the additional moment due to shear amplification from the location of the plastic hinge to the column centerline). Equation (28) is calculated using the AISC (2011) specifications Section E3.

The penalty function φ is defined as

$$\varphi = \prod_{i=1}^{4} \varphi_i$$
$$where \begin{cases} \varphi_i = 2.0 - c_i & if \quad c_i < 1.0 \\ \varphi_i = 1.0 & if \quad c_i \geq 1.0 \end{cases} \tag{29}$$

Figures 17 and 18 show the example structure which is adopted from the SAC structure presented in FEMA (2000b). The structural steel is A992. The lumped masses are calculated based on the loading presented in FEMA (2000b) for this structure. Based on these loading definitions, the seismic mass for the structure is considered as 70.90 kips-sec^2/ft for the roof and 65.53 kips-sec^2/ft for the floors (the values are for the entire structure) (FEMA 2000b). Masses are lumped (LM_i) at the beam-to-column locations. Moment frame A-E/1 is considered for the design. Lean-on columns are used in the analysis to represents the gravity frame system that is tributary to the moment resisting frame. The gravity loads for lean-on columns are calculated as 100% of permanent dead load and 25% of transient live load. In this example, since there are two moment resisting frames in the considered direction, the tributary gravity load associated with one half of the structure is assigned to the moment frame A-E/1. Lean-on columns are pin-ended columns that are connected to the moment frame considered through rigid links, as shown in Figure 17.

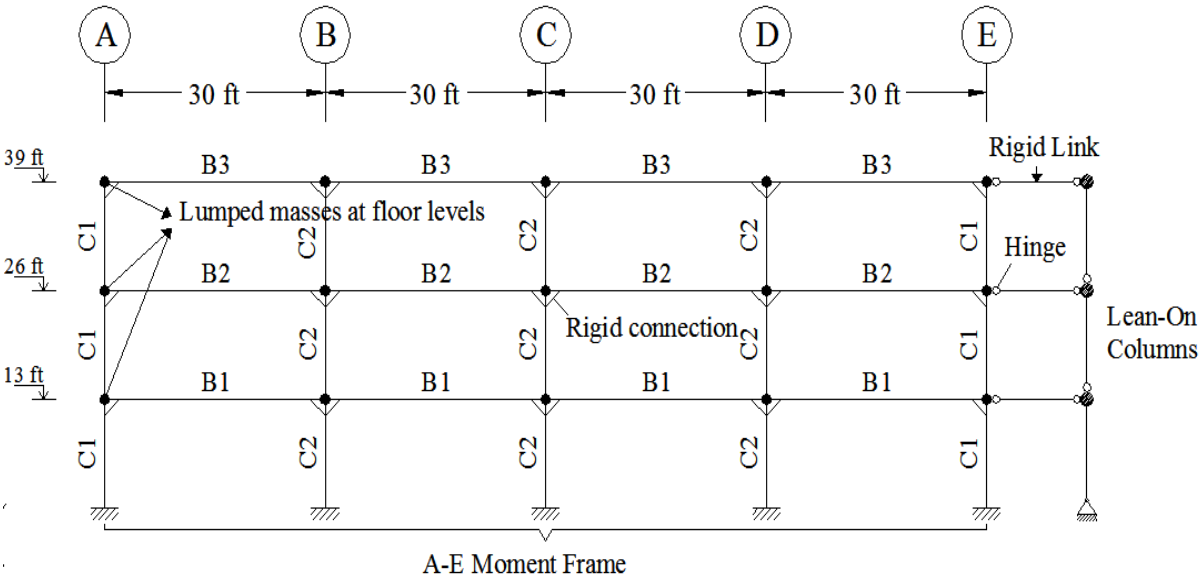

Figure 17. Elevation of the considered structure

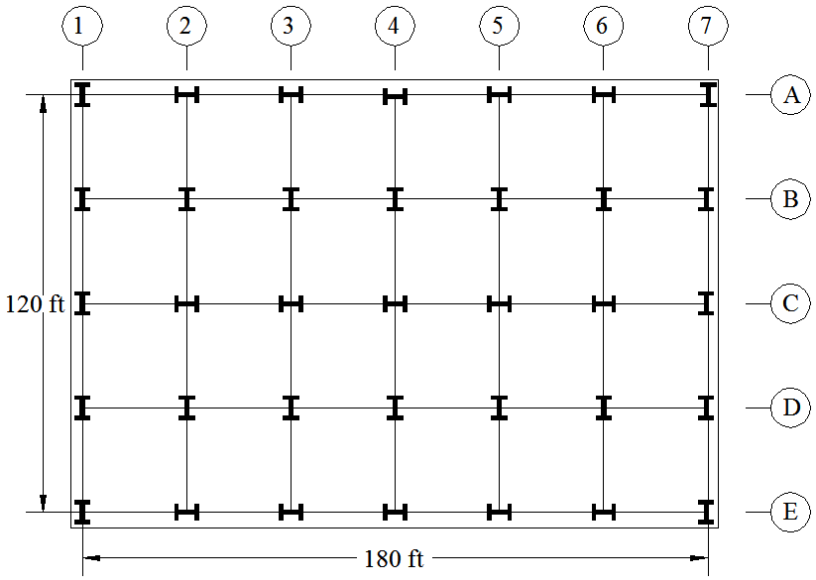

Figure 18. Plan view of the considered structure

Figure 17 shows the five design variables for the seismic PBD optimization (two column types C1 and C2 and three beam types B1, B2, and B3). The search space includes a list of 60 AISC W sections (W10, W12, and W14) for columns and another list

of 64 AISC W sections (W18, W21, W24, W27, W30, W33, W36, and W40) for beam elements. Therefore, the size of the search space for this problem would be approximately $9.44(10^8)$. The lists of the considered sections are presented in Appendix D. The genetic algorithm uses a population size of 100, maximum number of generations of 300, a roulette wheel selection method, a uniform crossover method with probability of 0.6, and a mutation probability of 0.03. Figure 19 shows the Pareto fronts obtained using the NSGA-II multi-objective optimization strategy (Deb et al. 2002) for the combination of structural weight and EAL. The Pareto fronts represent a range of feasible designs that are mathematically equivalent. Table 3 lists the design details for the example frame for three sample designs located on the Pareto front for both geographic locations: design associated with the minimum weight, design located on the middle of the front (which could be approximated as assigning similar importance or weight to the both optimization objectives), and design associated with the minimum EAL.

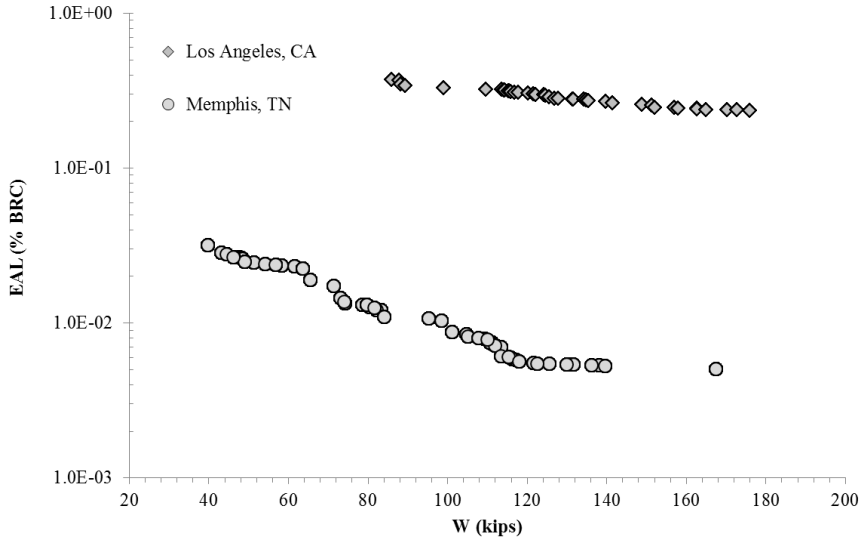

Figure 19. Pareto front for the example frame for sites located in Memphis, TN and Los Angeles, CA

Table 3. Comparison of the results for the example frame located in Memphis and Los Angeles

Memphis, TN							
Designs	C1	C2	B1	B2	B3	W (kips)	EAL(%BRC)
Min Weight	W12X152	W12X106	W21X44	W21X44	W18X40	39.78	0.03188
Midpoint front	W14X233	W14X233	W30X99	W30X99	W27X94	80.53	0.01268
Min EAL	W14X455	W14X550	W40X167	W40X199	W30X191	167.37	0.00508
Los Angeles, CA							
Designs	C1	C2	B1	B2	B3	W (kips)	EAL(%BRC)
Min Weight	W14X398	W14X233	W18X71	W27X114	W21X44	86.02	0.37296
Midpoint front	W14X370	W14X426	W30X124	W36X170	W27X94	125.48	0.28846
Min EAL	W14X605	W14X605	W33X130	W40X183	W40X167	175.91	0.23601

Figures 19 shows that values for EAL are significantly larger for a site located in Los Angeles, CA compared to the site located in Memphis, TN; the difference is associated with the seismicity characteristics of the two geographic locations characterized by the hazard curves and larger PGAs for the considered hazard levels in the Los Angeles site. Comparing Figures 12 and 13 shows that for frequent earthquakes, associated with larger values of λ, the PGA values are considerably larger on the Los Angeles hazard curve; the difference is less notable for rare events (smaller λ values). In addition, the slope of the hazard curve for Los Angeles, CA is greater than that for Memphis, TN and results in a considerable difference in the calculated EAL values for these two locations. The ratio of the change in EAL to the change in weight, computed from Figure 18, is several times greater in Los Angeles, CA than in Memphis, TN indicating an increase in weight would result in a significantly larger decrease in EAL.

Using the Pareto fronts, decision makers would have a wider range of EAL to choose from for a structure in Los Angeles, CA.

The present value of the total cost PC^T_t considering initial cost and seismic economic loss for a lifetime period of t years, is estimated as

$$PC^T_t = C^I + PL^S_t \tag{30}$$

.where C^I is the initial cost of the structure and PL^S_t is the present value of the seismic direct economic loss. The initial cost C^I is

$$C^I = \rho \times W \tag{31}$$

where W is the weight of the frame and ρ is the cost per unit weight of the frame. The present value of the seismic economic loss PL^S_t is calculated as

$$PL^S_t = EAL \times \frac{(1 - e^{-i_r t})}{i_r} \tag{32}$$

where i_r is the discount rate, assumed to be 2% (Porter et al. 2004), and t is considered as 50 years. The value of EAL in Equation (32) is calculated by considering the BRC to be equal to C^I.

Table 4 lists the calculated ratios C^I/PC^T_{50} and PL^S_{50}/PC^T_{50} for the structure designs. The ratio of seismic cost to the total cost of the structure is significantly higher in Los Angeles, CA than in Memphis, TN. Figures 20 and 21 show the distribution of losses for the designs. The following observation can be made from the obtained results:

- By moving from the lighter structures with larger EAL to heavier structures with smaller EAL, the contribution of structural and drift-sensitive non-structural components to the total loss value decreases and the contribution of acceleration sensitive non-structural components increases.
- Drift-sensitive non-structural components have the highest contribution to the calculated seismic loss for all hazard levels for the three selected designs in Memphis, TN and for the minimum weight and middle front designs in Los Angeles, CA. In general, NSD components have had a higher contribution in the calculated EAL.

Table 4. Costs for the example frame located in Memphis, TN and Los Angeles, CA

Memphis, TN						
Designs	W(kips)	EAL(%BRC)	CL_{CP}(%)	CL_{IO}(%)	C^{I}/PC^{T}_{50}	PL^{S}_{50}/PC^{T}_{50}
Min Weight	39.782	0.03188	98.7	100.00	0.990	0.0100
Midpoint front	80.529	0.01268	100.0	100.00	0.996	0.0040
Min EAL	167.37.060	0.00508	100.0	100.00	0.998	0.0016
Los Angeles, CA						
Designs	W(kips)	EAL(%BRC)	CL_{CP}(%)	CL_{IO}(%)	C^{I}/PC^{T}_{50}	PL^{S}_{50}/PC^{T}_{50}
Min Weight	86.020	0.37296	90.00	76.56	0.895	0.1054
Midpoint front	125.480	0.28846	99.50	99.98	0.916	0.0836
Min EAL	175.910	0.23601	100.00	100.00	0.931	0.0694

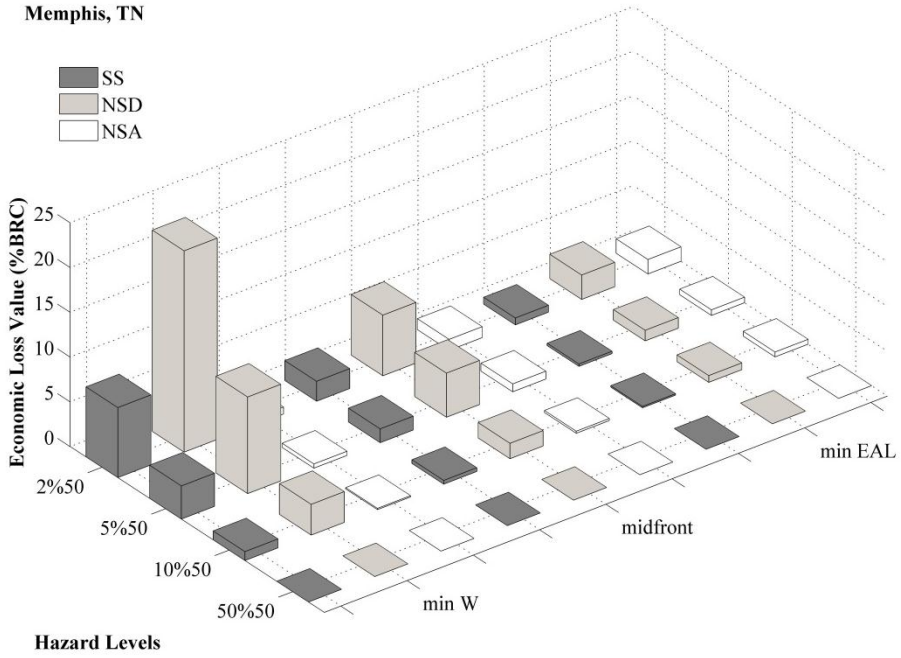

Figure 20. Distribution of losses for structures for Memphis, TN

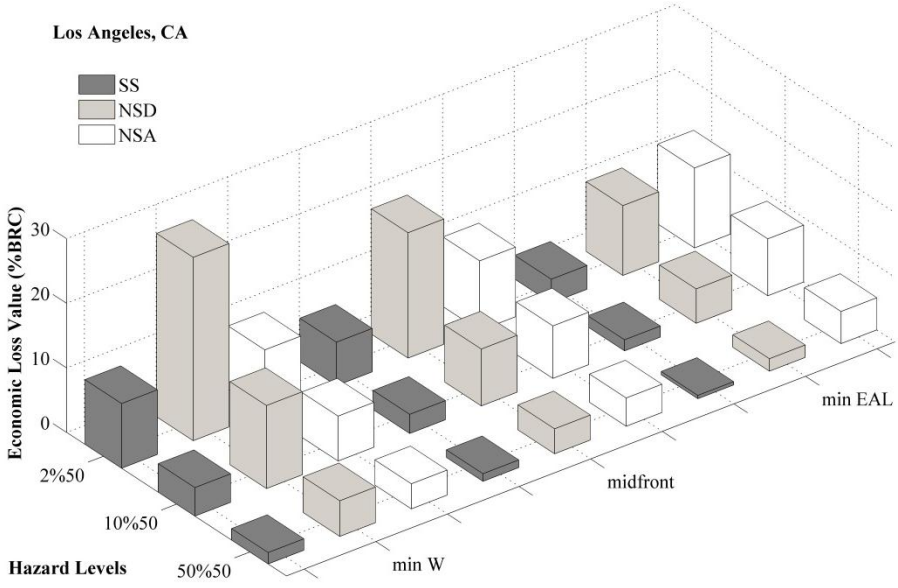

Figure 21. Distribution of losses for structures for Los Angeles, CA

4.1.2 Summary and Conclusions

In this problem, the EAL and the initial construction cost (the weight of the structure) are the optimization objectives for the PBD of structures. The obtained PBD Pareto fronts provide engineers with a decision making tool for designing structures considering both initial cost and EAL. Additionally, the effect of geographical location on the calculated loss values are evaluated by considering two different site locations: Memphis, TN (CUS) and Los Angeles, CA (WUS). Seismic PBD results show a significantly larger seismic loss for structures located in Los Angeles, CA than in Memphis, TN, which is attributed to the differences in the seismicity characteristics and the slopes of the hazard curves in these locations. Consequently, for structures in Los Angeles, CA, seismic loss should have a much greater role in real-state decision-making processes as compared to structures in Memphis, TN. Moreover, analyzing the distribution of losses indicates that, in general, NSD components have the highest contribution to the total seismic loss associated with direct economic losses for most designs in both geographic locations. Additionally, by moving along the Pareto front from lower weight designs to higher weight designs, the contribution of SS and NSD components to total loss decreases and the contribution of the NSA components increases.

4.2 Optimization Problem II

In the second optimization problem, two optimization objectives are defined as the lifetime cost of the structure (expressed as the present value of the total cost PC^T_t) and the expected annual social loss EASL.

The lifetime cost of the structure takes into account the initial cost and expected annual economic loss associated with earthquake events at the site of interest. The PBD of the example 3-story steel moment frame considered in Optimization Problem I is used. Moment frame A-E/1 is considered for the design.

The performance objectives are immediate occupancy performance level for the hazard level of 50% in 50 years and collapse prevention for the hazard level of 2% in 50 years, while satisfying design criteria for strong column-weak beam (AISC 2011). The search space includes a list of 60 AISC W sections (W10, W12, and W14) for columns and another list of 64 AISC W sections (W18, W21, W24, W27, W30, W33, W36, and W40) for beam elements. Therefore, the size of the search space for this problem would be approximately $9.44(10^8)$. The considered sections are listed in Appendix D.

4.2.1 Problem Definition

The Multi-objective optimization problem includes minimization of two specified objectives. The optimization problem would be expressed as

$$\begin{aligned} &Minimize\ (TC, SL) \\ &Subjected\ \ to: c_i \geq l_i\ \ (i = 1,3) \end{aligned} \tag{33}$$

where TC and SL are the penalized values of PC^T_t and $EASL$, respectively; and c_i is the i^{th} constraint that is applied on the optimization problem. The penalized values TC and SL are calculated as

$$TC = \varphi \times PC_t^T \tag{34}$$

$$SL = \varphi \times EASL \tag{35}$$

where φ is a penalty function. The constraints c_1, c_2, and c_3 and the penalty function implemented are the same as in Optimization Problem I.

Figure 22 shows the obtained Pareto fronts for the two sites for the specified optimization objectives.

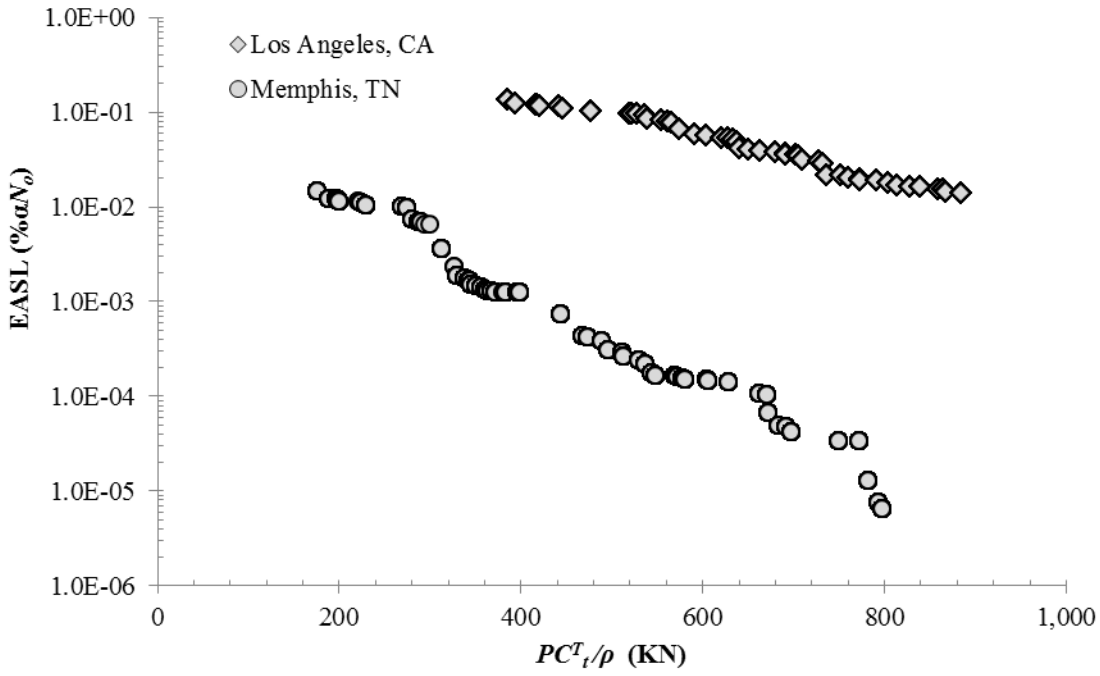

Figure 22. Pareto fronts for site locations in Memphis, TN and Los Angeles, CA

The results presented in Figure 22 show the significant difference between the calculated seismic loss values between the two considered sites. This variance can be explained by the difference in site seismicity characteristics and the less steep slope of the hazard curve for Memphis, TN as compared to Los Angeles, CA and indicates the significance of seismicity characteristics of the region in the evaluation of expected annual seismic loss parameters. Additionally, the ratio of change in PC^T_t to change in EASL between extreme designs along the Pareto front (i.e. min PC^T_t and min EASL designs) is several times larger for designs in Los Angeles as compared to Memphis. This higher ratio implies that for the structure located in Los Angeles, a specific increase in the value of PC^T_t would result in more reduction in the EASL value as compared to the structure located in Memphis.

In order to determine which constraint has the most effect on the optimization, the original constraints defined in Equations (26)-(28) are scaled as follows

$$C_i = \frac{c_i \times l_i - l_i}{1 - l_i} \quad (\textit{for } i = 1 \text{ and } 2) \tag{36}$$

$$C_3 = \frac{c_3 - l_3}{c_{3\max} - l_3} \tag{37}$$

Figures 23 to 28 show the scaled constraint values for the example steel structure located in Memphis and in Los Angeles; respectively. In all figures, darker colored circles specify smaller values for the C_i's for designs, which is an indicator of associated constraints being closer to the defined limit states. As expected, when designs move along the Pareto front towards higher cost, the values of C_1 and C_2, defined by confidence

levels for CP and IO performance objectives, increase. However, no specific pattern is observable for C_3 (SCWB criterion). Comparing the C_i values in Figures 23 to 28 shows that C_3 is often controlling for both sites, which implies that the strong column weak beam (SCWB) requirement is typically the controlling constraint in the optimization problem.

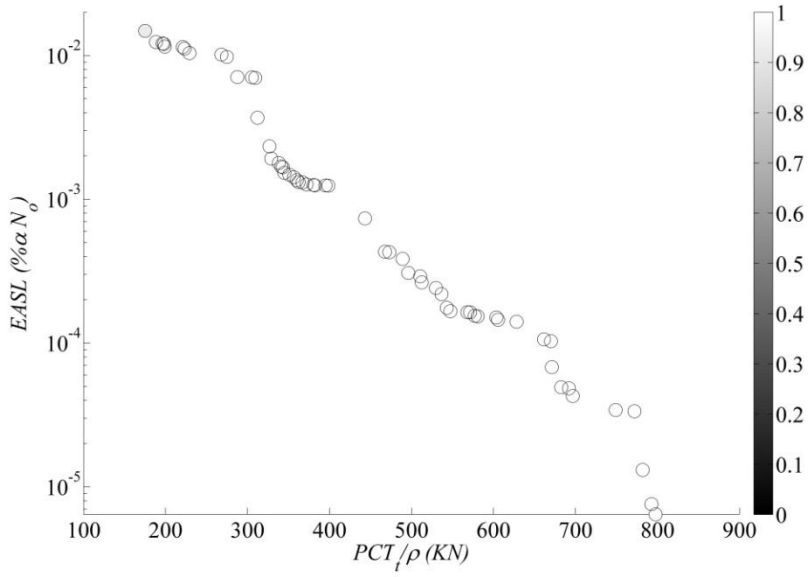

Figure 23. Variation in criteria C_1 along the Pareto front for structures located in Memphis, TN

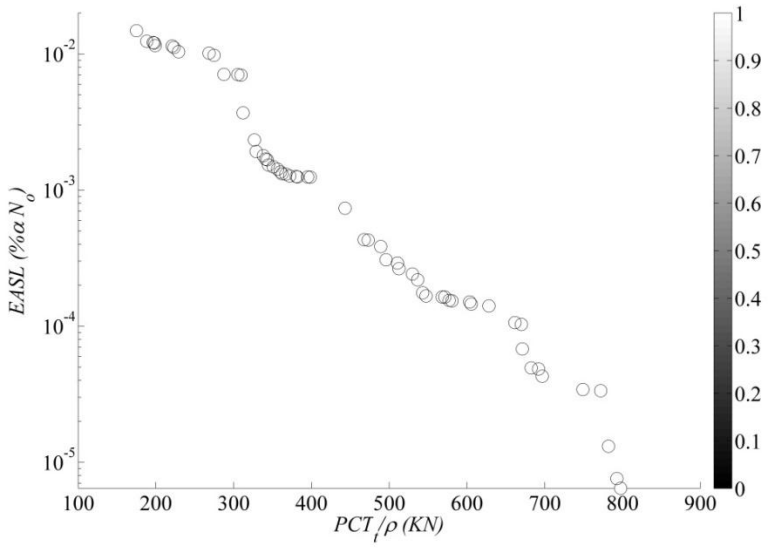

Figure 24. Variation in criteria C_2 along the Pareto front for structures located in Memphis, TN

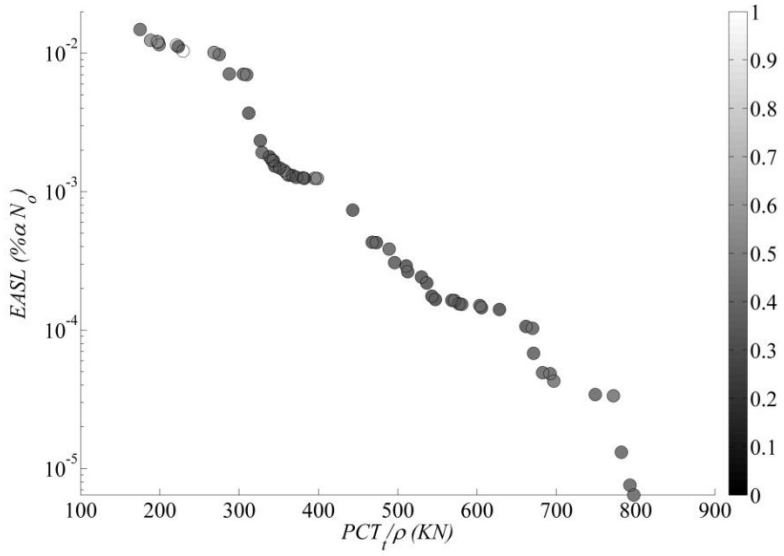

Figure 25. Variation in criteria C_3 along the Pareto front for structures located in Memphis, TN

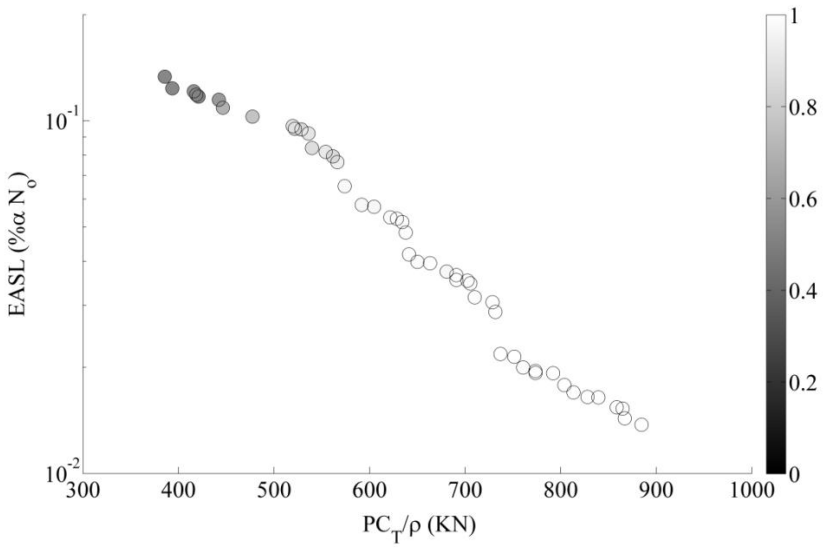

Figure 26. Variation in criteria C_1 along the Pareto front for structures located in Los Angeles, CA

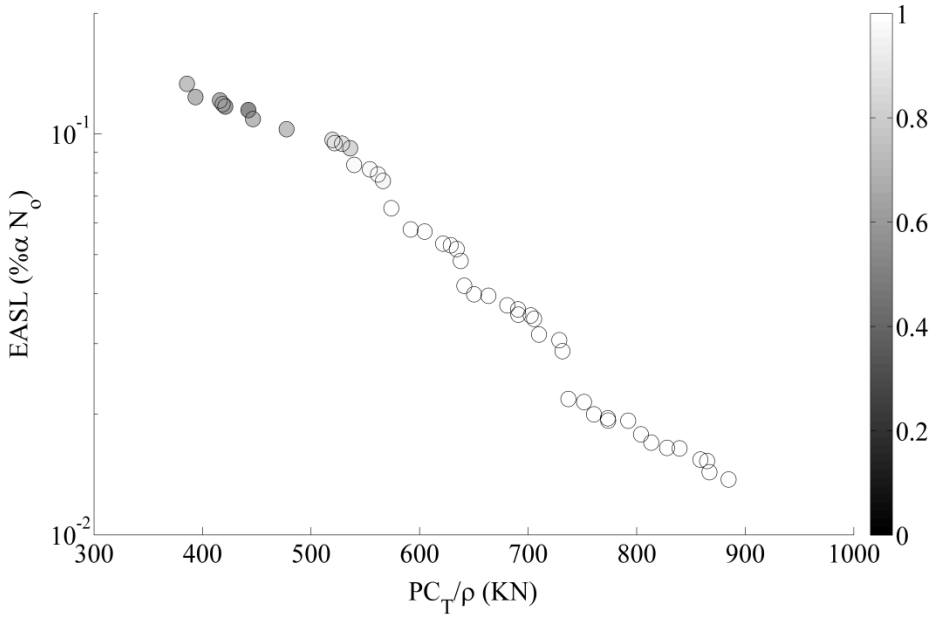

Figure 27. Variation in criteria C_2 along the Pareto front for structures located in Los Angeles, CA

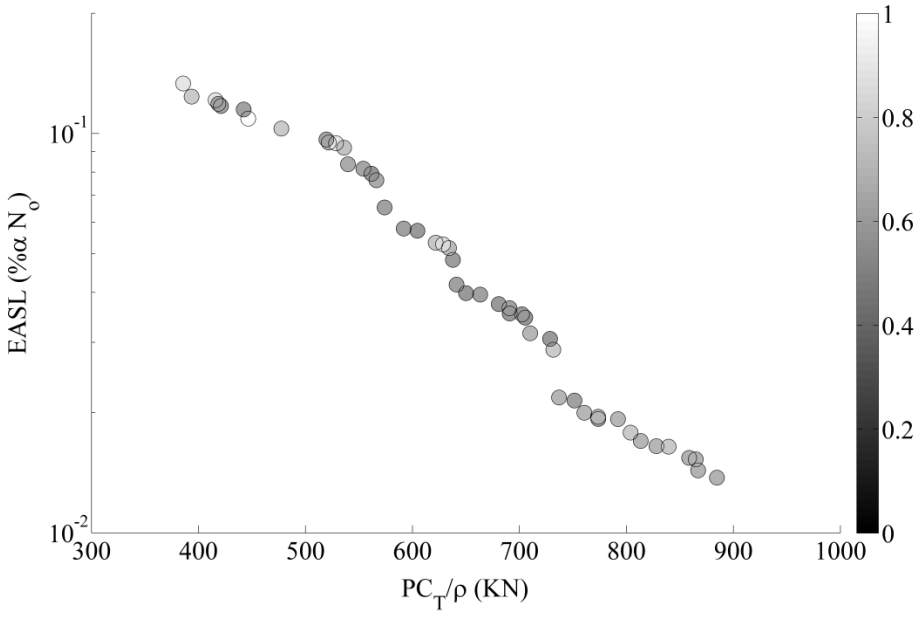

Figure 28. Variation in criteria C_3 along the Pareto front for structures located in Los Angeles, CA

In order to better compare the losses at the two sites, three designs are selected along the Pareto fronts for each site. These designs are associated with the solutions with minimum values for the PC^T_t and EASL objectives and one design with calculated objectives close to the mean value of the extreme points. Figure 29 shows the distribution of losses between different components for both site locations. Table 5 lists the selected designs and their corresponding values of optimization objectives. Table 6 lists the calculated loss values for these designs for both sites.

Table 5. Three designs selected from the obtained Pareto fronts for site locations in Memphis, TN and Los Angeles, CA.

Memphis, TN							
Designs	**C1**	**C2**	**B1**	**B2**	**B3**	PC^T_t/ρ **(KN)**	***EASL*** $(\%\alpha N_o)$
Min PC^T_t	W14X109	W14X109	W21X50	W21X44	W18X46	175.01	0.01485
Midpoint front	W14X176	W14X233	W27X94	W30X99	W18X46	312.01	0.00369
Min *EASL*	W14X550	W14X605	W40X183	W40X199	W36X160	797.61	0.00001
Los Angeles, CA							
Designs	**C1**	**C2**	**B1**	**B2**	**B3**	PC^T_t/ρ **(KN)**	***EASL*** $(\%\alpha N_o)$
Min PC^T_t	W14X257	W14X257	W27X84	W24X76	W24X68	385.69	0.13349
Midpoint front	W12X336	W14X398	W36X150	W30X116	W24X104	573.95	0.06531
Min *EASL*	W14X550	W14X605	W40X199	W40X199	W40X183	884.62	0.01375

Table 6. Calculated loss values for the designs located on Pareto front for site locations in Memphis, TN and Los Angeles, CA.

Memphis, TN						
Designs	**W(KN)**	**EAL(%BRC)**	PC^T_t/ρ **(KN)**	***EASL*** $(\%\alpha N_o)$	CL_{CP}**(%)**	CL_{IO}**(%)**
Min PC^T_t	173.33	0.0307	175.01	0.0149	98.50	100.00
Midpoint front	310.27	0.0177	312.01	0.0037	100.00	100.00
Min *EASL*	796.69	0.0036	797.61	0.0000	100.00	100.00
Los Angeles, CA						
Designs	**W(KN)**	**EAL(%BRC)**	PC^T_t/ρ **(KN)**	***EASL*** $(\%\alpha N_o)$	CL_{CP}**(%)**	CL_{IO}**(%)**
Min PC^T_t	345.73	0.3657	385.69	0.1335	90.95	76.02
Midpoint front	523.12	0.3076	573.95	0.0653	99.55	99.62
Min *EASL*	818.16	0.2571	884.62	0.0138	98.50	100.00

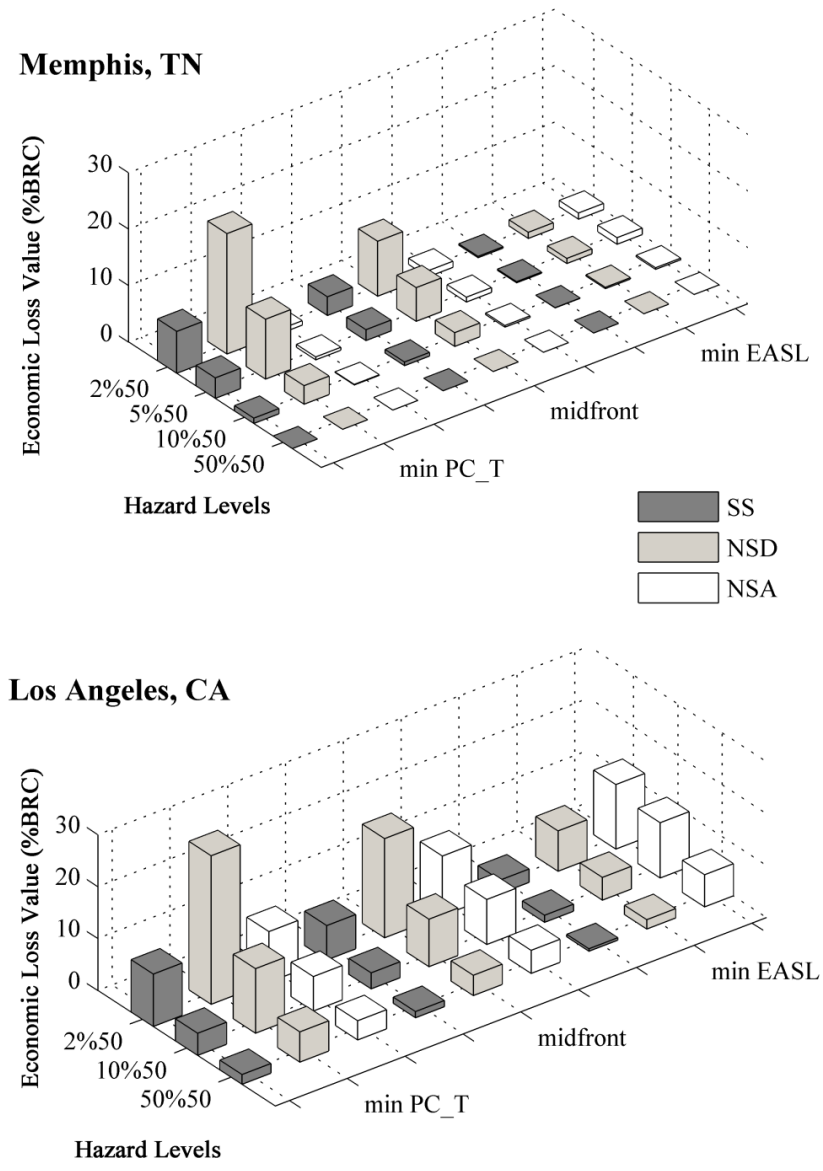

Figure 29. Distribution of economic losses for different components of the building for structures located in Memphis, TN and Los Angeles, CA

Figures 30 and 31 present a comparison between the distributions of economic and social losses for the structures at both sites. Both loss parameters have a descending trend from the designs that minimized for PC_t^T to the designs minimized for *EASL*.

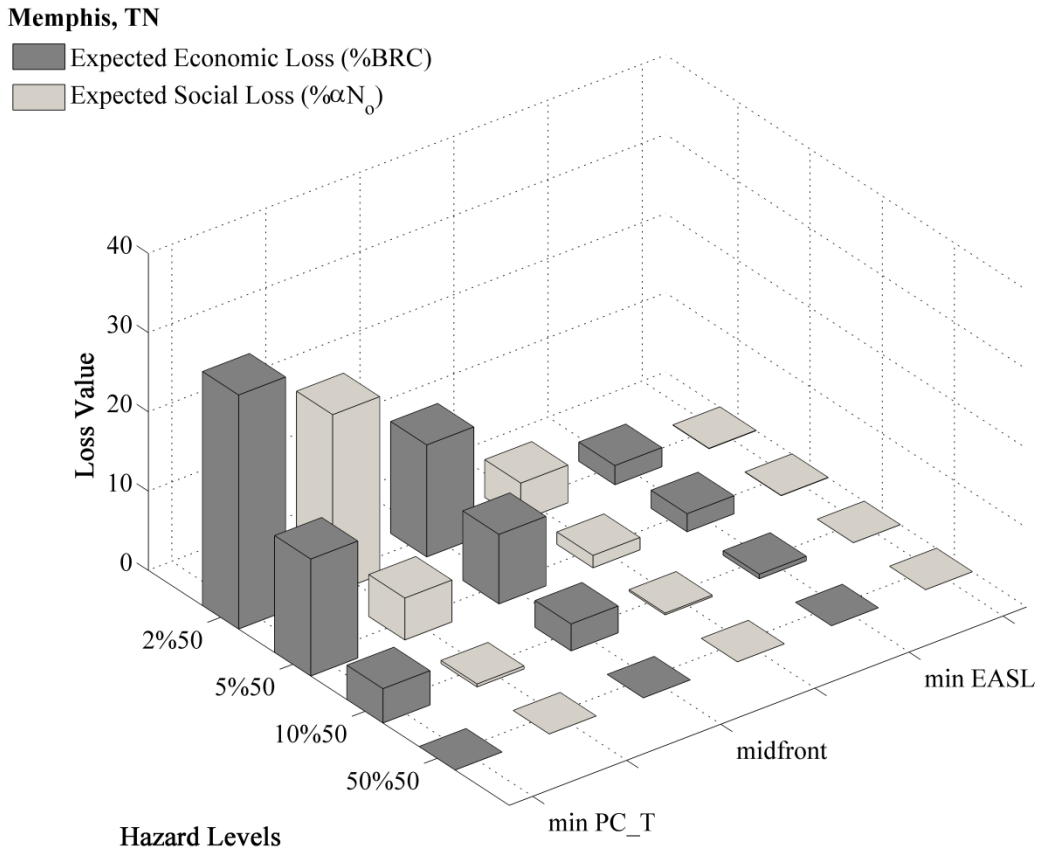

Figure 30. Comparison between distribution of direct economic losses and direct social losses for structures in Memphis, TN

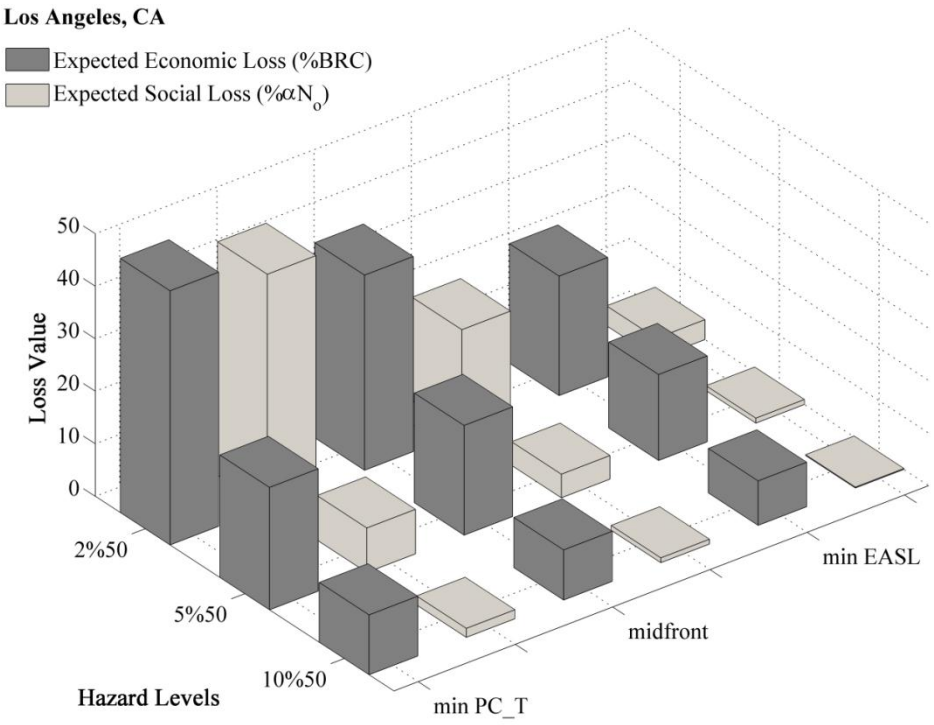

Figure 31. Comparison between distribution of direct economic losses and direct social losses for structures in Los Angeles, CA

Figures 31 to 33 show the comparison of the calculated loss values for an example design with frame sections of W12x336 and W14x398 for C1 and C2 and W36x150, W30x116, and W24x104 for B1, B2, and B3 for the two considered site locations.

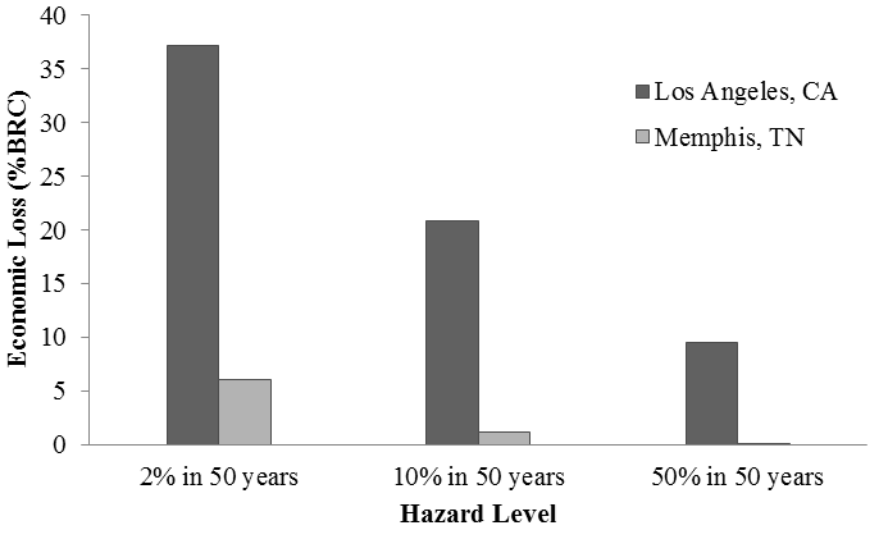

Figure 32. Economic losses for an example structure located in Los Angeles, CA and Memphis, TN

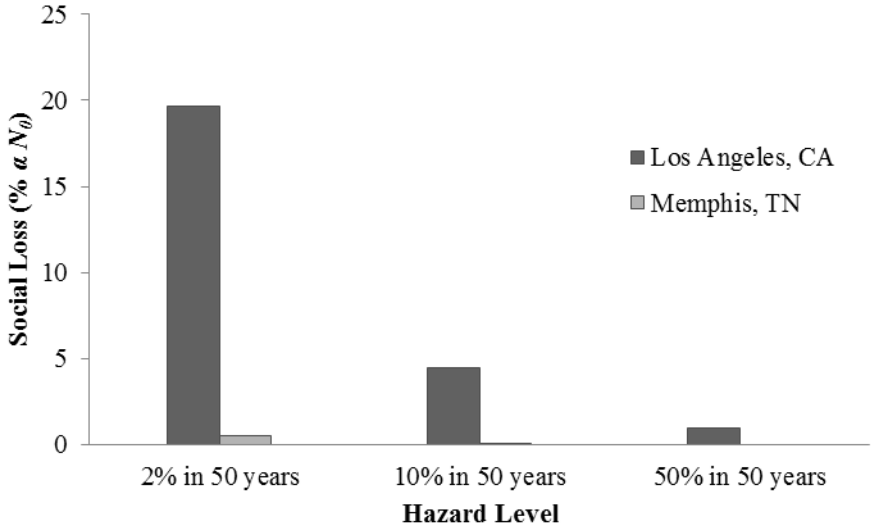

Figure 33. Social losses for an example structure located in Los Angeles, CA and Memphis, TN

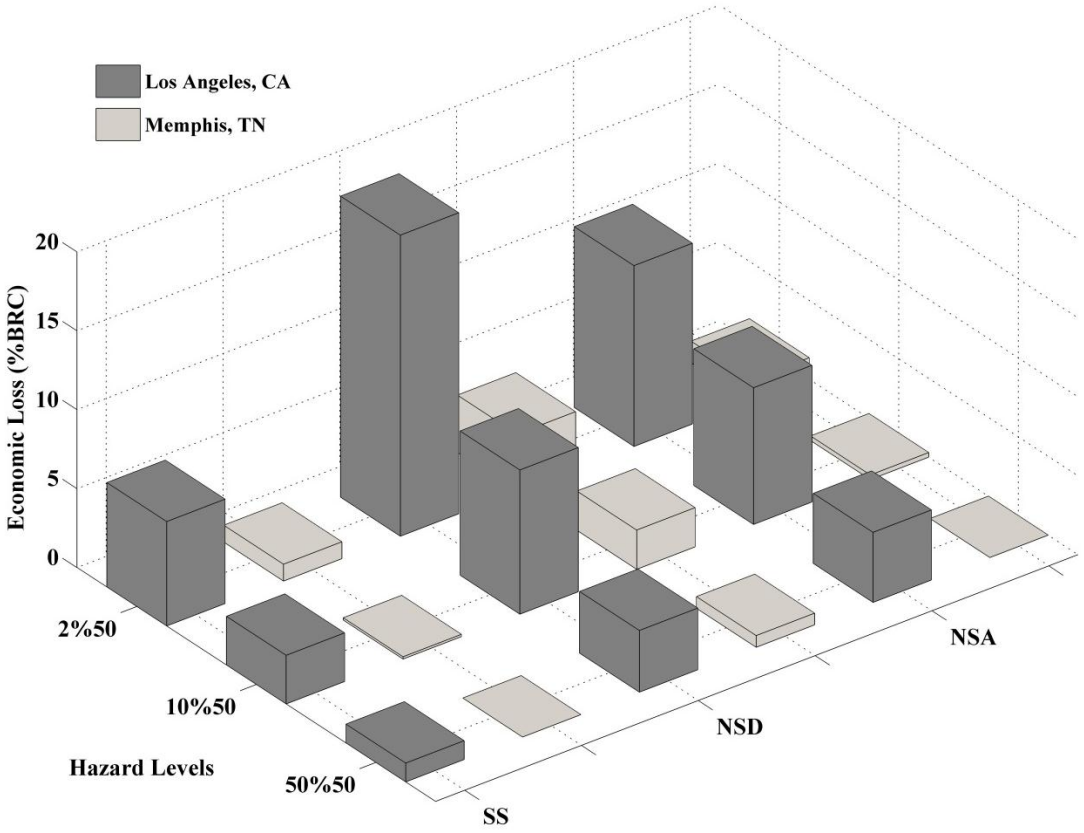

Figure 34. Distribution of economic losses for different components for an example structure located in Los Angeles, CA and Memphis, TN

4.2.2 Summary and Conclusions

The objective of this study is to develop an optimal PBD procedure that considers the economic and social losses associated with probable future earthquakes. Designs for a steel moment frame structure are developed using the proposed PBD procedure. The PBD of a structure is accomplished using a multi-objective optimization considering two objectives. Seismic losses are used to evaluate optimization objectives, which are calculated through the integration of four steps of probabilistic seismic hazard analysis, probabilistic demand analysis, probabilistic damage analysis, and probabilistic loss analysis, by implementing total probability theorem. The first optimization objective is the present value of the total cost, calculated based on the initial construction cost and

EAL associated with seismic direct economic losses. The second optimization objective is the direct social loss modeled as EASL, which is a parameter developed in this study to facilitate the interpretation of social loss in calculations and to provide a comparison tool between economic and social loss parameter values. The multi-objective optimization results are presented in the form of Pareto fronts which could be used to visualize the trade-offs between the various objectives.

An evaluation of the critical optimization criteria for designs along the Pareto fronts indicates that the strong-column weak-beam constraint often controls the feasibility of designs generated by the optimization.

A comparison of the economic and social expected annual losses shows that these loss values are considerably lower for a site located in Memphis, TN than a site located in Los Angeles, CA, as observed in the previous problem. This variance can be explained by the difference in site seismicity characteristics and the hazard curves for Memphis, TN as compared to Los Angeles, CA and indicates the significance of seismicity characteristics of the region in the evaluation of expected annual seismic loss parameters. Additionally, the ratio of change in PC^T_t to change in EASL between extreme designs along the Pareto front (i.e. min PC^T_t and min *EASL* designs) is several times larger for designs in Los Angeles as compared to Memphis. This higher ratio implies that for the structure located in Los Angeles site, a specific increase in the value of PC^T_t would result in more reduction in the *EASL* value as compared to the structure located in Memphis site.

4.3. Optimization Problem III

In this multi-objective optimization problem, in order to better compare the relationship between the initial cost and two loss parameters, three optimization objectives are defined as the initial cost of the structure, *EAL*, and *EASL*. The performance objectives are immediate occupancy performance level for the hazard level of 50% in 50 years and collapse prevention for the hazard level of 2% in 50 years, while satisfying design criteria for strong column-weak beam (AISC 2011).

4.3.1 Problem Definition

The multi-objective optimization problem includes minimization of the three specified objectives. The optimization problem would be expressed as

$$\begin{aligned} &Minimize\ (W, EAL_P, EASL_P) \\ &Subjected\ \ to: c_i \geq l_i\ \ (i = 1,3) \end{aligned} \tag{39}$$

where W, EAL_P, and $EASL_P$ are the penalized values of w, EAL, and $EASL$, respectively; and c_i is the i^{th} constraint that is applied on the optimization problem. The penalized values EAL_P and $EASL_P$ are calculated as

$$EAL_P = \varphi \times EAL \tag{39}$$

$$EASL_P = \varphi \times EASL \tag{40}$$

where φ is a penalty function. c_1, c_2, and c_3 and the penalty function implemented are given in Equations (26) to (29).

4.3.2 Example Structures

The multi-objective SPBD optimization problem is applied to 3-story and 7-story steel structures shown in Figures 34 to 36. The search space includes a list of 60 AISC W sections (W10, W12, and W14) for columns and another list of 64 AISC W sections (W18, W21, W24, W27, W30, W33, W36, and W40) for beam elements. Therefore, the size of the search space for this problem would be approximately $3.40(10^{12})$ for the 3-story structure and $4.40(10^{19})$ for the 7-story structure. The lists of the considered sections are presented in Appendix D. For the 3-story frame, four groups are considered for columns: ground floor exterior and interior columns and 2nd and 3rd floor exterior and interior columns. One group is considered for beams at each floor level. For the 7-story frame, eight groups are considered for columns: exterior and interior ground floor, 2nd & 3rd floor, 4th & 5th floor, and 6th & 7th floor. Three groups are considered for beams. The structural steel is A992. The seismic masses for the 3-story structure are 73.10 kips-sec^2/ft for the roof, 67.86 kips-sec^2/ft for the 2nd floor and 69.86 kips-sec^2/ft for the 1st floor. The seismic masses for the 7-story structure are 73.10 kips-sec^2/ft for the roof, 67.86 kips-sec^2/ft for the 2nd to 6th floors and 69.86 kips-sec^2/ft for the 1st floor (the values are for the entire structure). Masses are lumped (LM_i) at the beam-to-column locations. Moment frame A-E/1 is considered for the design.

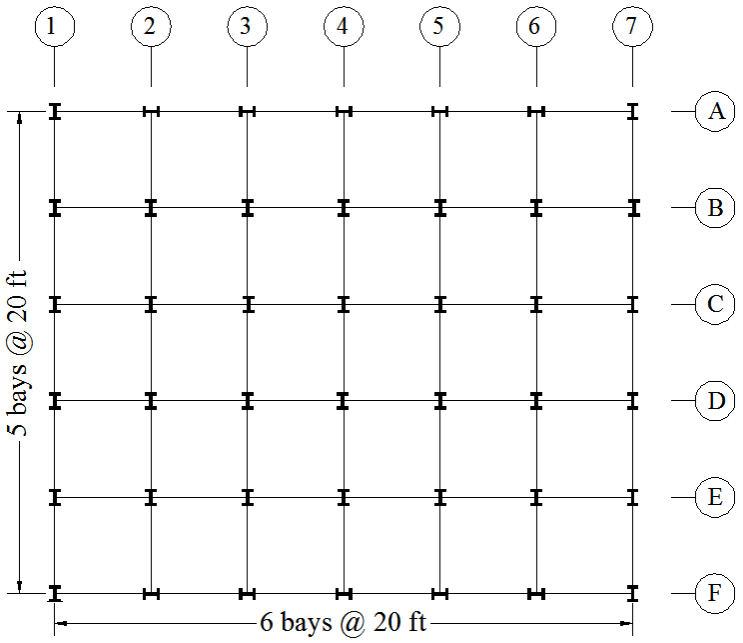

Figure 35. Plan view of the example structures

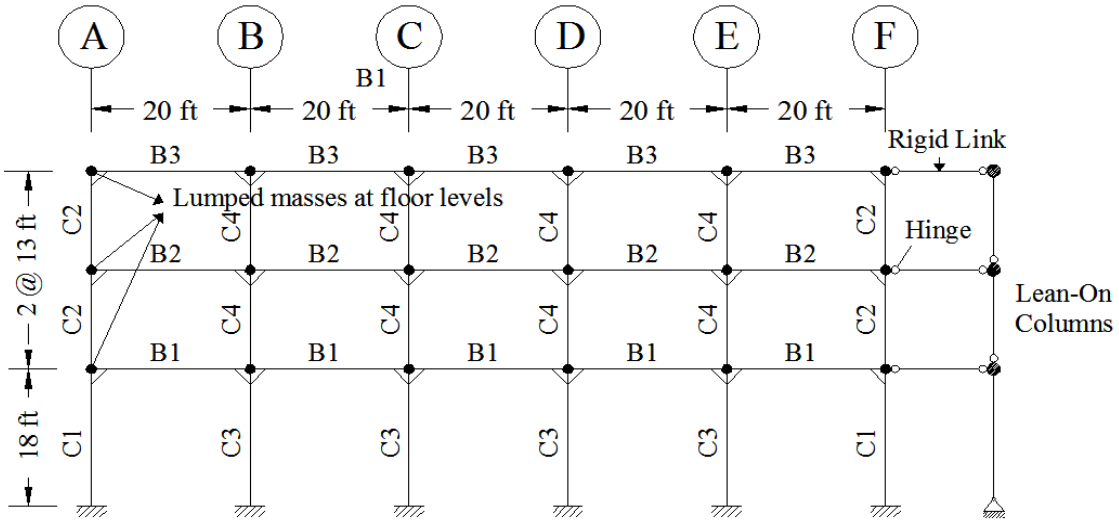

Figure 36. Elevation for the example 3-story structure

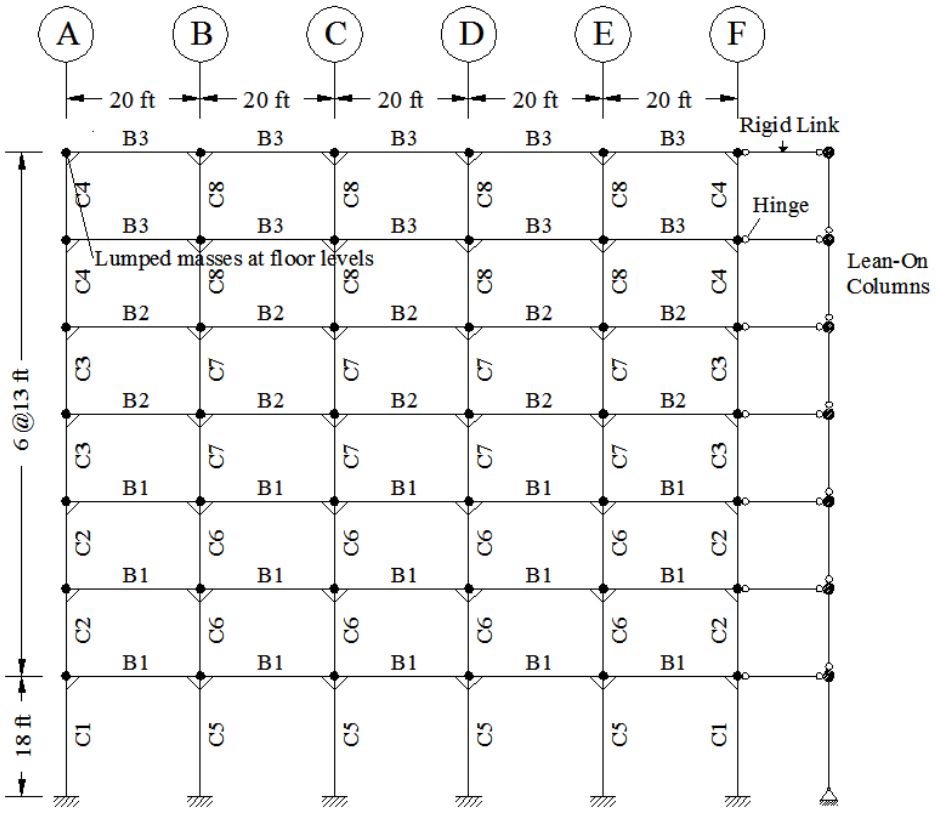

Figure 37. Elevation for the example 7-story structure

Figures 37-40 relate the optimization objective values for the solutions on the Pareto front for the 3-story and 7-story structure examples, respectively for the two considered sites of Memphis, TN and Los Angeles, CA. For each site, approximately similar patterns of relationships between pairs of objectives, i.e. W and EAL, W and EASL, and EAL and EASL, is observed. An increase in initial construction cost (associated with W) would result in a decrease in both EAL and EASL values. EAL and EASL have a direct relationship and an increase in one, as expected, would be associated with an increase in the other. Figures 41 and 42 combine the results from Figures 35-38 to facilitate comparison between the 3-story and 7-story solutions for both sites. In these figures it should be taken into account that BRC and N_o would be considerably different

for 3-story and 7-story buildings. The percentile values can be compared in this figure but not the net loss values.

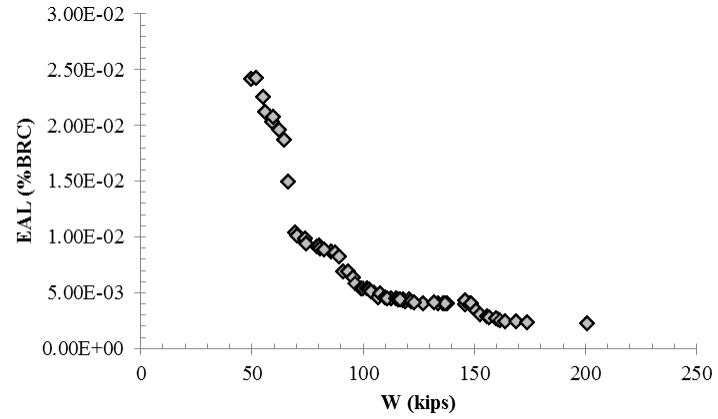

(a)

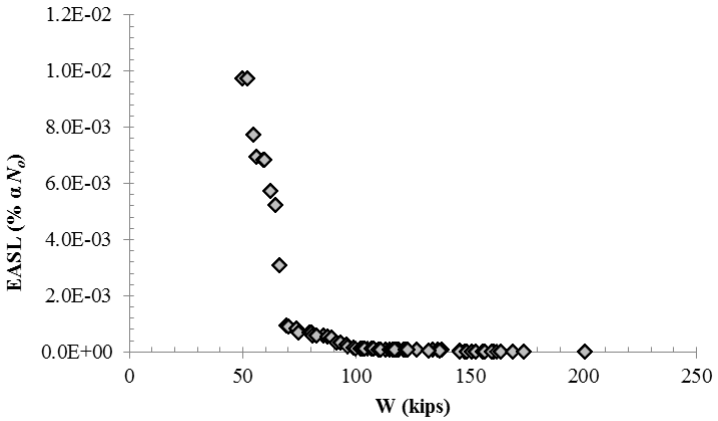

(b)

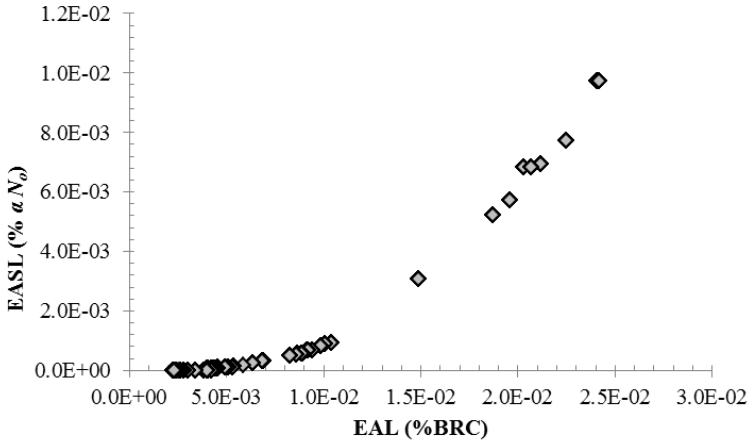

(c)

Figure 38. Comparison of the optimization objective values for the solutions on the Pareto front for the 3-story example structure located in Memphis, TN: (a) W (kips) versus EAL (%BRC), (b) W (kips) versus EASL (%α N_o), (c) EAL (%BRC) versus EASL (%α N_o)

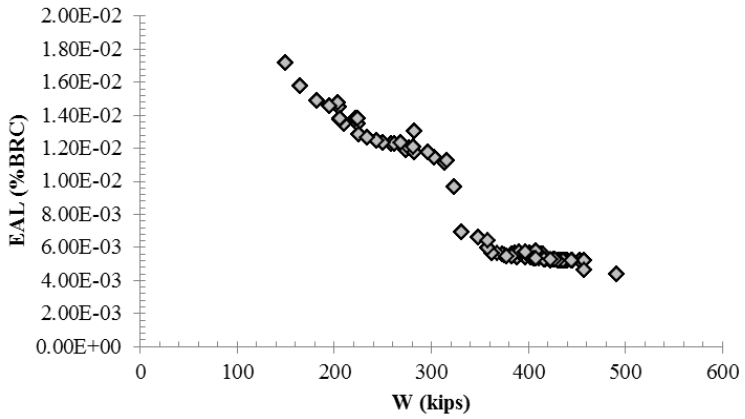

(a)

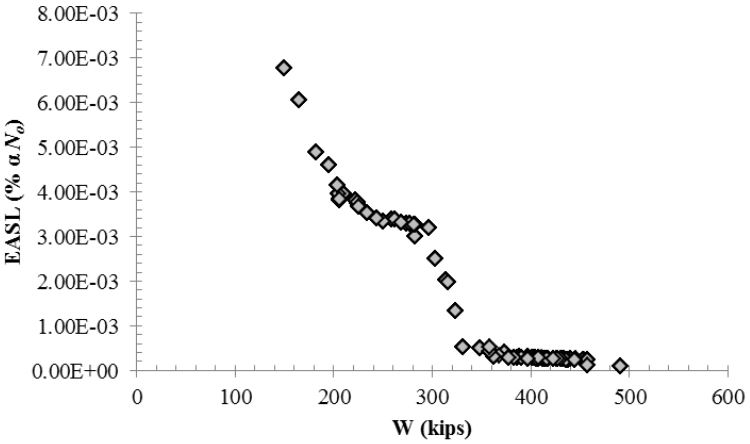

(b)

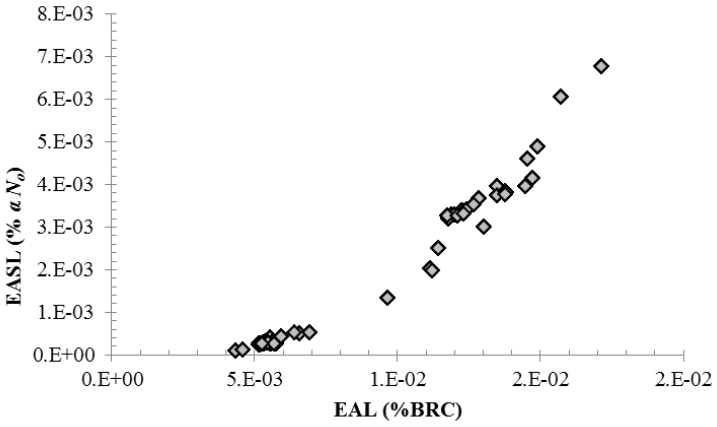

(c)

Figure 39. Comparison of the optimization objective values for the solutions on the Pareto front for the 7-story example structure located in Memphis, TN: (a) W (kips) versus EAL (%BRC), (b) W (kips) versus EASL (%α N_o), (c) EAL (%BRC) versus EASL (%α N_o)

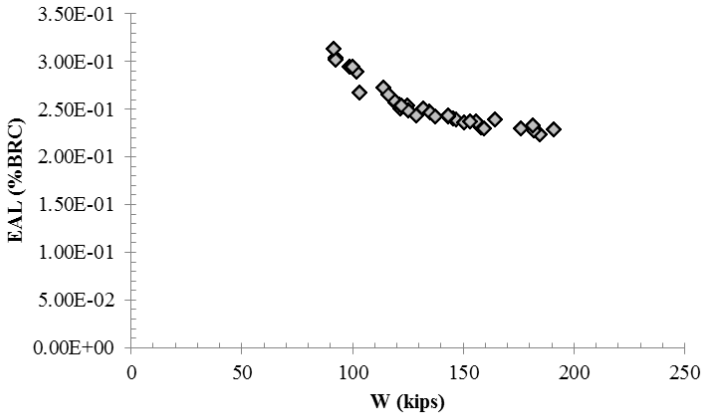

(a)

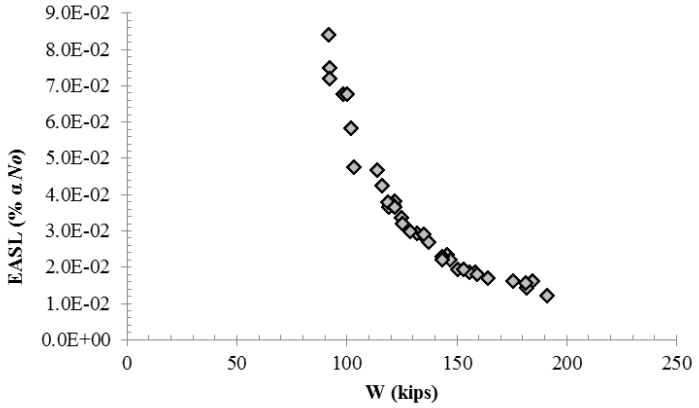

(b)

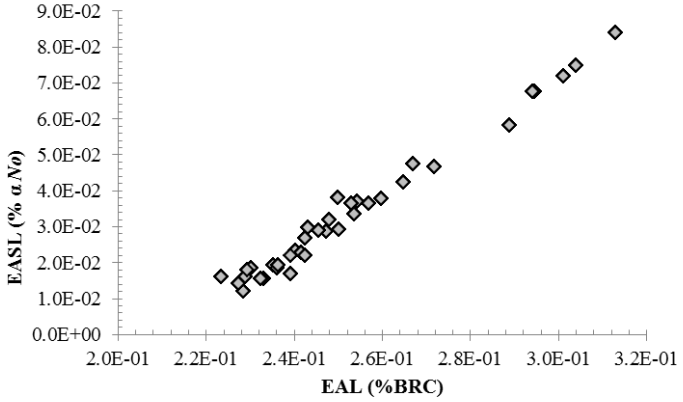

(c)

Figure 40. Comparison of the optimization objective values for the solutions on the Pareto front for the 3-story example structure located in Los Angeles, CA: (a) W (kips) versus EAL (%BRC), (b) W (kips) versus EASL (%α N_o), (c) EAL (%BRC) versus EASL (%α N_o)

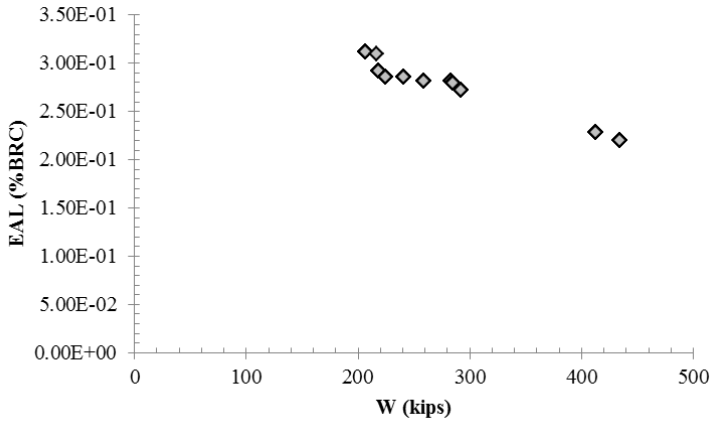

(a)

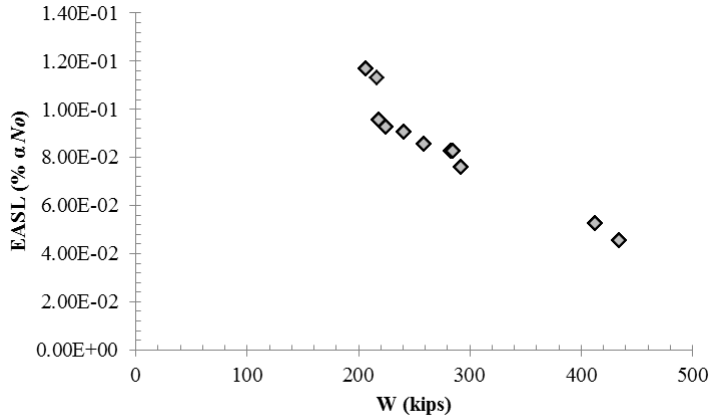

(b)

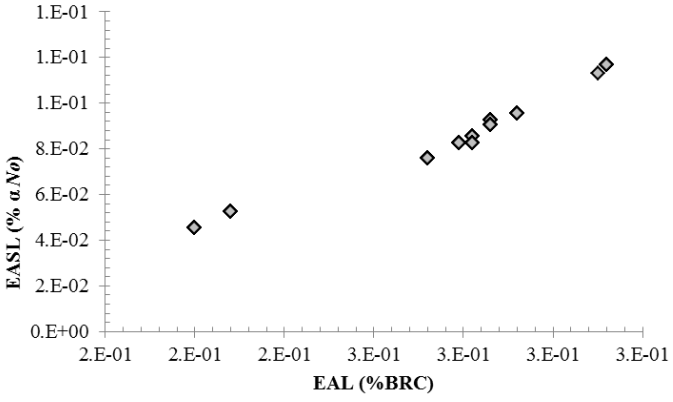

(c)

Figure 40. Comparison of the optimization objective values for the solutions on the Pareto front for the 7-story structure example located in Los Angeles, CA: (a) W (kips) versus EAL (%BRC), (b) W (kips) versus EASL (%α N_o), (c) EAL (%BRC) versus EASL (%α N_o)

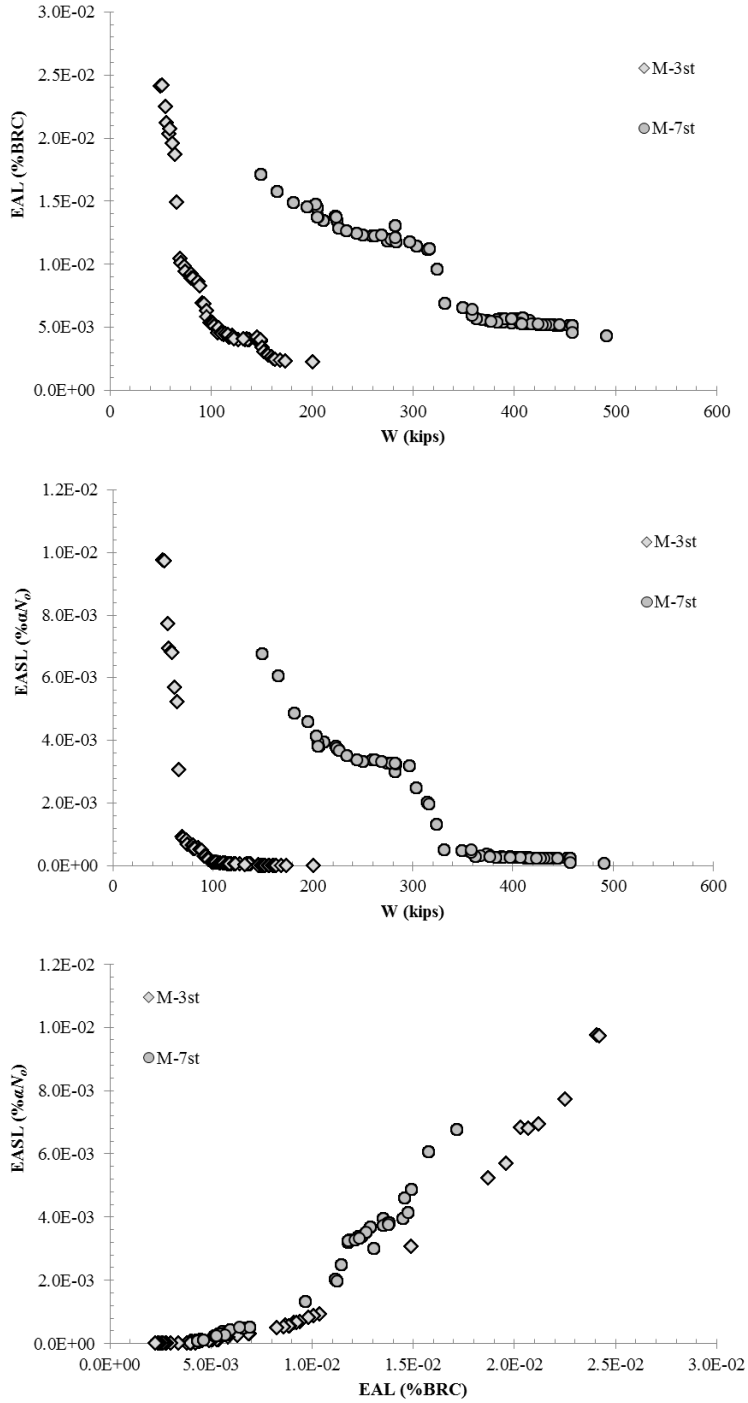

Figure 41. Comparison of the optimization objective values for the solutions on the Pareto front for the 3-story and 7-story structures, located in Memphis, TN.

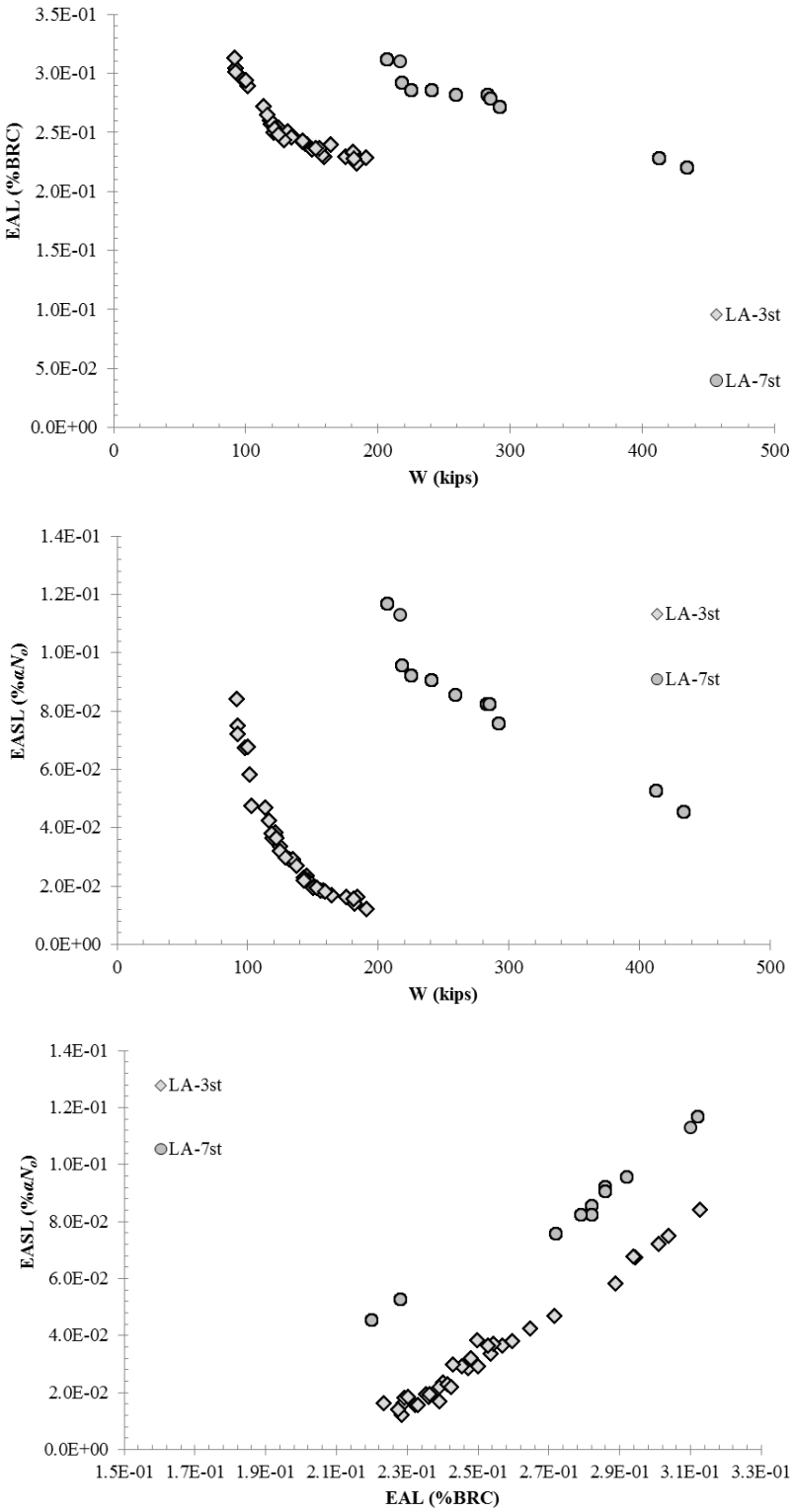

Figure 42. Comparison of the optimization objective values for the solutions on the Pareto front for the 3-story and 7-story structures, located in Los Angeles, CA.

Figures 43 and 44 show a comparison of the Pareto fronts for the 3-story and 7-story structures for both sites in the 3D space, with each axis presenting one of the three objectives. In these figures the EAL is presented as a percentage of the replacement cost for one story of the building ($\%BRC_{1st}$), assuming that %BRC would be approximately equivalent to 3 times $\%BRC_{1st}$ for the 3-story building and 7 times $\%BRC_{1st}$ for the 7-story building. Similarly, EASL is presented as $\%\alpha\ N_{o1st}$, where N_{o1st} is the number of occupants in one story of the building which implies that N_o for the three and seven story buildings would be equivalent to $3N_{o1st}$ and $7N_{o1st}$, respectively. The reason for presenting the losses this way is to be able to better compare the net loss values for structures with different numbers of floors, since the BRC and N_o values would depend on the number of floors.

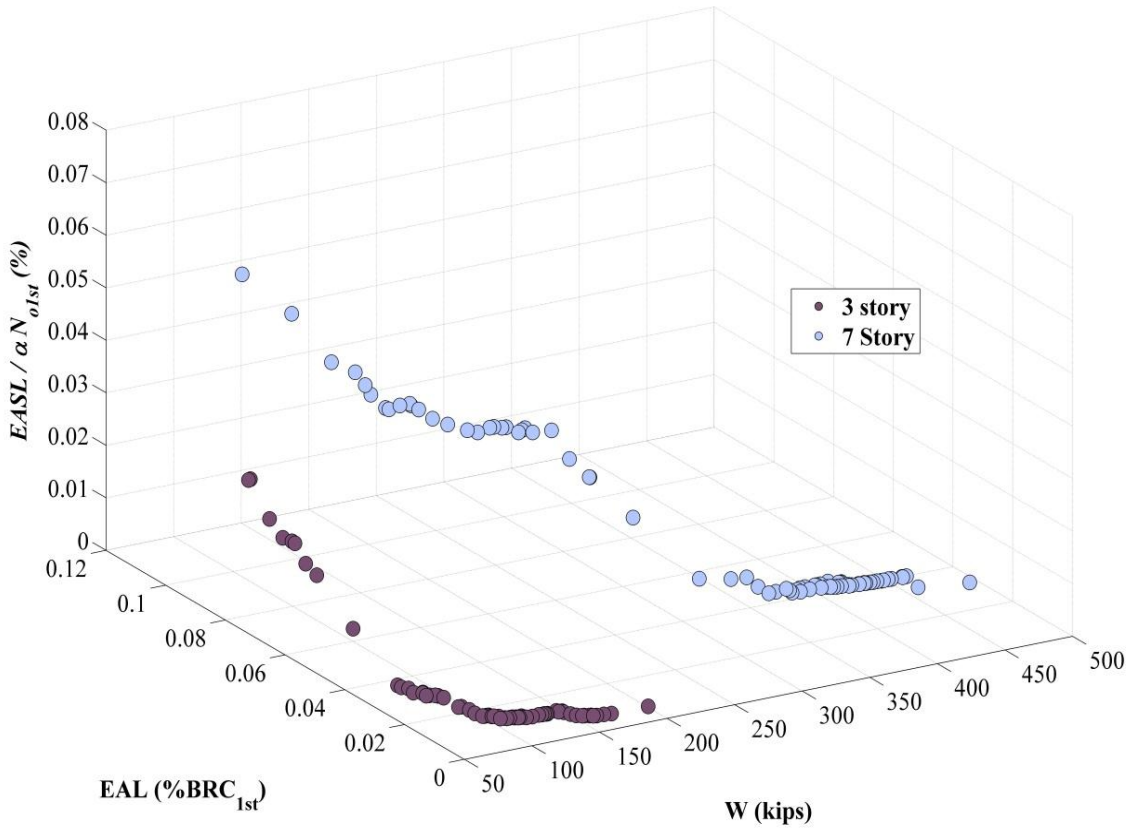

Figure 41. Comparison of the Pareto fronts for the 3-story and 7-story structures located in Memphis, TN.

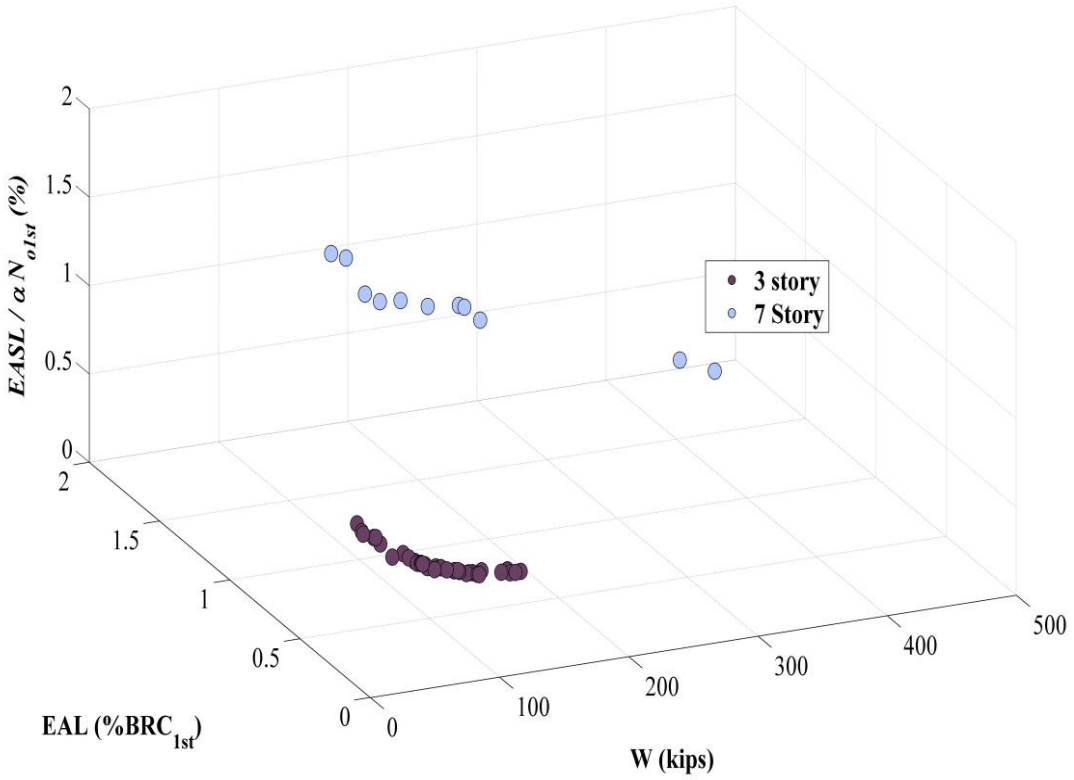

Figure 42. Comparison of the Pareto fronts for the 3-story and 7-story structures located in Los Angeles, CA.

Tables 7 and 8 list the calculated loss and confidence level parameters for designs associated with minimum weight, minimum EAL and minimum EASL for the 3-story and 7-story structures located in Memphis, TN and Los Angeles, CA, respectively. For some cases, similar designs are obtained for the minimum EAL and minimum EASL objectives.

Table 7. Calculated loss and confidence level parameters for designs associated with minimum weight, minimum EAL and minimum EASL, for 3-story and 7-story structures located in Memphis, TN.

7-Story Structure					
Designs	**W(kips)**	**EAL(%BRC)**	**EASL ($\%\alpha N_o$)**	**CL_{CP}(%)**	**CL_{IO}(%)**
Min *W*	149.57	0.017149	0.006779	99.41	100.00
Min EAL	491.08	0.004345	0.000096	100.00	100.00
Min *EASL*	491.08	0.004345	0.000096	100.00	100.00
3-Story Structure					
Designs	**W(kips)**	**EAL(%BRC)**	***EASL* ($\%\alpha N_o$)**	**CL_{CP}(%)**	**CL_{IO}(%)**
Min *W*	50.00	0.024100	0.009740	99.88	100.00
Min EAL	201.00	0.002260	2.20E-11	100.00	100.00
Min *EASL*	174.00	0.002280	2.75E-12	100.00	100.00

Table 8. Calculated loss and confidence level parameters for designs associated with minimum weight, minimum EAL and minimum EASL, for 3-story and 7-story structures located in Los Angeles, CA.

7-Story Structure					
Designs	**W(kips)**	**EAL(%BRC)**	**EASL ($\%\alpha N_o$)**	**CL_{CP}(%)**	**CL_{IO}(%)**
Min *W*	207.00	0.31	0.12	90.96	99.81
Min EAL	434.00	0.22	0.05	99.27	100.00
Min *EASL*	434.00	0.22	0.05	99.27	100.00
3-Story Structure					
Designs	**W(kips)**	**EAL(%BRC)**	***EASL* ($\%\alpha N_o$)**	**CL_{CP}(%)**	**CL_{IO}(%)**
Min *W*	91.72	0.31	0.08	98.69	97.29
Min EAL	184.57	0.22	0.02	99.98	100.00
Min *EASL*	191.20	0.23	0.01	99.99	100.00

Tables 9 to 13 show the design parameters for the 3-story and 7-story structures for Memphis and Los Angeles sites. The design parameters can be compared for the three selected designs on the Pareto front, which are the designs with the minimum values for each of the three considered objectives.

Table 9. Design parameters for the 3-story structure located in Memphis, TN.

3-Story Structure			
Design Parameter	Min *W*	Min EAL	Min *EASL*
C1	W14X193	W14X605	W14X605
C2	W14X193	W14X605	W14X605
C3	W14X132	W14X605	W14X455
C4	W14X109	W14X605	W14X455
B1	W18X40	W36X182	W36X182
B2	W18X40	W27X161	W33X130
B3	W18X40	W24X68	W27X94

Table 10. Design parameters for the 7-story structure located in Memphis, TN.

7-Story Structure			
Design Parameter	Min *W*	Min EAL	Min *EASL*
C1	W14X370	W14X605	W14X605
C2	W14X311	W14X605	W14X605
C3	W14X257	W14X605	W14X605
C4	W14X257	W12X136	W12X136
C5	W14X257	W14X605	W14X605
C6	W12X120	W14X605	W14X605
C7	W12X106	W14X605	W14X605
C8	W12X106	W14X605	W14X605
B1	W18X40	W40X199	W40X199
B2	W18X40	W36X150	W36X150
B3	W18X40	W27X102	W27X102

Table 11. Design parameters for the 3-story structure located in Los Angeles, CA.

3-Story Structure			
Design Parameter	Min *W*	Min EAL	Min *EASL*
C1	W14X342	W14X605	W14X550
C2	W14X342	W14X605	W14X550
C3	W14X233	W14X605	W14X605
C4	W14X233	W14X550	W14X605
B1	W27X102	W27X114	W30X132
B2	W21X57	W27X102	W30X132
B3	W21X44	W27X84	W27X94

Table 12. Design parameters for the 7-story structure located in Los Angeles, CA.

7-Story Structure			
Design Parameter	Min *W*	Min EAL	Min *EASL*
C1	W14X605	W14X605	W14X605
C2	W14X550	W14X605	W14X605
C3	W14X342	W14X370	W14X370
C4	W14X257	W12X252	W12X252
C5	W14X211	W14X605	W14X605
C6	W14X211	W14X455	W14X455
C7	W14X159	W14X455	W14X455
C8	W14X159	W14X455	W14X455
B1	W21X57	W18X175	W18X175
B2	W21X57	W30X173	W30X173
B3	W18X40	W27X102	W27X102

Comparisons of the distribution of losses for the 3-story and 7-story structures located in Memphis, TN and Los Angeles, CA are presented in Appendix E. Comparisons are presented in percentages of BRC and αN_o and it is important to take into account their difference for 3-story and 7-story structures when comparing the losses.

4.3.3 Summary and Conclusions

The objective of this optimization problem has been to compare the relationship between the initial cost and two loss parameters, EAL and EASL, for structures with different heights. Two steel structures, one 3-story and another 7-story, are considered

and the multi-objective optimization method is implemented to optimize the probabilistic performance-based design of the structures. The results are compared for two different sites with different seismicity characteristics: Memphis, TN and Los Angeles, CA. The three optimization objectives considered are initial construction cost (modeled as the weight of the structure), EAL associated with expected annual economic loss, and EASL associated with expected annual social loss. The optimization results are presented in the form of three-dimensional Pareto fronts. In most cases, the Pareto fronts are presented in , 3D space, with each axis presenting one of the three objectives. For all cases, an increase in the initial cost would be associated with a decrease in both loss parameters. For some cases, the design associated with minimum EAL and minimum EASL are similar. As in previous problems, considerable difference exists between the calculated loss values for the two sites for all structures which can be explained by the differences in the seismicity characteristics of the regions.

CHAPTER 5

CONCLUSION AND DISCUSSION

The objective of this study has been to consider seismic loss values, which are of interest in the recent frameworks for performance-based design of structures, in the optimized probabilistic PBD. A multi-objective optimization method has been implemented for several example problems with different sets of optimization objectives. The optimization objectives include combinations of initial cost, expected annual seismic economic loss parameter, EAL, and expected annual seismic social loss parameter, EASL. Three different optimization problems are considered. The first problem considers two optimization objectives of initial cost, modeled as the weight of the structure and EAL. The results are presented for an example three-story steel moment frame structure for two different site locations of Memphis, TN and Los Angeles, CA. In the second problem, initial cost and EAL are combined as one objective, defined as the present value of the total cost, and the second objective is the social loss parameter, EASL. The results of this optimization problem are presented for a three-story structure located at the same two sites considered in the first problem. In the third optimization problem, three objectives are considered as weight, EAL, and EASL. The obtained designs for example 3-story and 7-story structures located in Memphis, TN and Los Angele, CA are presented and compared.

The multi-objective optimization results are presented in the form of Pareto fronts. For the first two problems with two optimization objectives the fronts are two dimensional. For these problems, three designs, two located on the extremes and one located on the mid-front are selected to demonstrate and compare calculated loss values

for the two sites. For the third problem, with three optimization objectives, the Pareto fronts are three dimensional. The obtained Pareto fronts provide engineers with a decision-making tool for designing structures considering different objectives.

Seismic PBD results show a significantly larger seismic loss for structures located in Los Angeles, CA than in Memphis, TN, which is attributed to the differences in the seismicity characteristics and the slopes of the hazard curves in these locations. Consequently, for structures in Los Angeles, CA, seismic loss should have a greater role in real-estate decision-making processes. Moreover, analyzing the distribution of losses indicates that, in general, NSD components have the highest contribution to the total seismic loss associated with direct economic losses for most designs in both geographic locations. In addition, an evaluation of the critical optimization criteria for designs along the Pareto fronts indicates that the strong-column weak-beam constraint often controls the feasibility of designs generated by the optimization. Additionally, by moving along the Pareto front from lower weight designs to higher weight designs, the contribution of structural (SS) and drift-sensitive non-structural (NSD) components to total loss decreases and contribution of acceleration-sensitive non-structural (NSA) components increases.

FUTURE WORKS

The implemented methodology for the seismic loss evaluation could be applied to a wider range of geographic locations to obtain a better understanding of the effect of the seismicity characteristics in the calculation of seismic loss parameters. In addition, other types of hazard could be considered in the calculation of the expected annual losses.

REFERENCES

Allahabadi, R (1987) DRAIN-2DX – Seismic Response and Damage Assessment for 2D Structures, Ph.D. dissertation, University of California, Berkeley

Allahabadi, R., Powell, G. H. (1988) DRAIN-2DX – User Guide, report No. UCB/EERC-88/06

Alimoradi, A. (2004) Probabilistic Performance-Based Seismic Design of Nonlinear Steel Structures Using Genetic Algorithm, Ph.D. Dissertation, The University of Memphis.

Alimoradi, A., Pezeshk, S., Foley, C. M. (2007) Probabilistic Performance-Based Optimal Design of Steel Moment-Resisting Frames. II: Applications, ASCE Journal of Structural Engineering / 767.

American Concrete Institute (2011) Building code requirements for structural concrete and commentary. ACI 318-11

American Institute of Steel Construction (AISC) (2011) Seismic Design Manual, Second Edition

American Society of Civil Engineers (ASCE) (1997) Guide to Structural Optimization, ASCE Manuals and Reports on Engineering Practice No. 90

American Society of Civil Engineers (2010) Minimum design loads for buildings and other structures. ASCE/SEI 7-10

American Association of State Highway and Transportation Officials (AASHTO) (2009) AASHTO Guide Specifications for LRFD Seismic Bridge Design

American Institute of Steel Construction (AISC) (2011) Seismic Design Manual, Second Edition

American Society for Testing and Material (ASTM) (2007) E 2026-07, Standard Guide for Seismic Risk Assessment of Buildings

Applied Technology Council (ATC) (2007) Guidelines for Seismic Performance Assessment of Buildings, Applied Technology Council. ATC-58 35% Draft

Augusti, G., Ciampoli, M. (2008) Performance-Based Design in risk assessment and reduction, Probabilistic Engineering Mechanics 23 496–508.

Bazzurro, P., Cornell, C. A. (1999) Disaggregation of Seismic Hazard, Bulletin of the Seismological Society of America, 89(2): 501-520

Bachman, R. E. (2004) The Atc-58 Project Plan For Nonstructural Components, Bled, Slovenia, PEER 2004/05, 125-136.

Baker, Jack W. (2008) An Introduction to Probabilistic Seismic Hazard Analysis (PSHA), 72.

Bazeos, N. (2009) Comparison of three seismic design methods for plane steel frames, Soil Dynamics and Earthquake Engineering 29: 553– 562.

Beck, J. L., Irfanoglu, A., Papadimitriou, C., and Au, S. K. (2000) A Performance-Based Optimal Design Methodology Incorporating Multiple Criteria, 12th World Conference on Earthquake Engineering, Auckland, New Zealand, 314

Blickle, T,. Thiele L. (1995) A Comparison of Selection Schemes used in Genetic Algorithms, Computer Engineering and Communication Networks Lab (TIK)-Reprt Nr. 11, December 1995, Version 2

Boore, D. M. (2000) SMSIM—Fortran Programs for Simulating Ground Motions from Earthquakes: Version 2.0—a Revision of OFR 96–80–A, <http://geopubs.wr.usgs.gov/open-file/of00-509/>

Caldas, L. G., Norford, L. K. (2003) Genetic Algorithms for Optimization of Building Envelopes and the Design and Control of HVAC Systems" J. Sol. Energy Eng. 125(3): 343-351

Camp C., Pezeshk S., Cao G. (1998) Optimized design of Two-Dimensional Structures Using a Genetic Algorithms, Journal of Structural Engineering, 124(5): 551-559

Castro, L. N. (2006) Fundamentals of Natural Computing: Basic Concepts, Algorithms, and Applications, Chapman & Hall/CRC, Taylor & Francis Group

Coley, D. A. (1999) An Introduction to Genetic Algorithms for Scientists and Engineers, World Scientific Publishing Co. Pte. Ltd.

Cornell, C. A. (1968) Engineering Seismic Risk Analysis, Bulletin of the Seismological Society of America. Vol. 58, No. 5, pp. 1583-1606. October, 1968

Deb, K., Pratap, A., Agarwal, S., Meyarivan, T. (2002) A Fast and Elitist Multiobjective Genetic Algorithm: NSGA-II, IEEE Transactions on Evolutionary Computation, 6(2).

Electric Power Research Institute (EPRI) (1993) Guidelines for Determining Design Basis Ground Motions, Volume 2: Appendices for Ground Motion Estimation, TR-102293 Project 3302 Final Report.

"EZ-FRISK" -Software for site-specific earthquake hazard analysis, Risk Engineering Inc. (2013) <http://www.riskeng.com/software/ez-frisk/>

Federal Emergency Management Agency (FEMA) (1997a) NEHRP Guidelines for the Seismic Rehabilitation of Buildings, FEMA 273

Federal Emergency Management Agency (FEMA) (1997b) NEHRP Recommended Provisions for Seismic Regulations for New Buildings and Other Structures-Part 1: Provisions (FEMA 302), prepared by the Building Seismic Safety Council (BSSC) for the FEMA

Federal Emergency Management Agency (FEMA) (2000a) Recommended Seismic Design Criteria for New Steel Moment-Frame Buildings, FEMA 350

Federal Emergency Management Agency (FEMA) (2000b) State of the Art Report on Systems Performance of Steel Moment Frames Subject to Earthquake Ground Shaking, FEMA 355C

Federal Emergency Management Agency (FEMA) (2006) Next-Generation Performance-Based Seismic Design Guidelines-Program Plan for New and Existing Buildings, FEMA 445

Federal Emergency Management Agency (FEMA) (2008) HAZUS MH Estimated Annualized Earthquake Losses for the United States, FEMA 366

Federal Emergency Management Agency (FEMA) (2012) Seismic Performance Assessment of Buildings Volume 1 - Methodology, FEMA P-58

Foley, C., Pezeshk, S., Alimoradi, A. (2007) Probabilistic Performance-Based Optimal Design of Steel Moment-Resisting Frames. I: Formulation. J. Struct. Eng., 133(6), 757–766.

Fragiadakis, M., Lagaros, N. D., Papadrakakis, M. (2006) Performance-based multiobjective optimum design of steel structures considering life-cycle cost, Struct Multidisc Optim 32: 1–11

Ganzerli, S., Pantelides, C. P., and Reaveley, L. D. (2000) Performance-Based Design Using Structural Optimization, Earthquake Engineering and Structural Dynamics, 29: 1677-1690

Gen, M. and Cheng, R. (2000) Genetic Algorithms and Engineering Optimization, A Wiley-Interscience Publication.

Gencturk, B., Elnashai, A. S. (2011) Multi-Objective Optimal Seismic Design Of Buildings Using Advanced Engineering Materials, Mid-America Earthquake (MAE) Center Report No. 11-01

Goldberg, D. E. (1989) Genetic Algorithms in Search, Optimization and Machine Learning, Addison-Wesley Publishing Company, Inc.

Hamburger, R., Rojahn, C., Moehle, J., Bachman, R., Comartin, C., Whittaker, A. (2004) The Atc-58 Project: Development of Next-Generation Performance-Based Earthquake Engineering Design Criteria for Buildings, 13th World Conference on Earthquake Engineering, Vancouver, BC, Canada, Paper No. 1819

Hazus-MH (2003a) Hazus-MH MR1 Technical and User's Manual- Multi-hazard Loss Estimation Methodology, FEMA.

Hazus-MH (2003b) Hazus-MH MR4 Technical Manual- Multi-hazard Loss Estimation Methodology, FEMA.

Holland, J. H. (1975) Adaptation in Natural and Artificial Systems. Ann arbor: The University of Michigan Press.

Idriss, I. M., Sun, J.I. (1992) User's Manual for SHAKE91, Center for Geotechnical Modeling, University of California Davis

Jenkins, W. M. (1997) On the application of natural algorithms to structural design optimization, Journal of Engineering Structures, 19(4): 302-308

Kappos, A., Lekidis, V., Panagopoulos, G., Sous, I., Thedulidis, N., Karakostas, Ch., Anastasiadis, T., Margaris, B., (2007), Analytical Estimation of Economic Loss for Buildings in the Area Struck by the 1999 Athens Earthquake and Comparison with Statistical Repair Costs, Earthquake Spectra, 23(2): 333–355

Krawinkler, H. (2005) Van Nuys Hotel Building Testbed Report: Exercising Seismic Performance Assessment, PEER Report 2005/11

Kramer, L. K. (1996) Geotechnical Earthquake Engineering, Pearson Education, Inc.

Li, Q. S., Liu, D.K., Fang, J.Q., and Tam, C.M. (2000) "Multi-level optimal design of buildings with active control under winds using genetic algorithms" Journal of Wind Engineering and Industrial Aerodynamics 86: 65-86

Liu, M., Burns, S. A, Wen, Y. K. (2005) Multiobjective optimization for performance-based seismic design of steel moment frame structures, Earthquake Engineering & Structural Dynamics, 34(3): 289–306

Mastuzaki, K., Irohara, T., Yoshimoto, K. (1999) Heuristic algorithm to solve the multi-floor layout problem with the consideration of elevator utilization Journal of Computers & Industrial Engineering 36: 487-502

McCormac, J. (1992) Structural Steel design ASD Method (4th edition), Harpers Collins Publishers, Inc.

Mitchell, M. (1999) An Introduction to Genetic Algorithms, A Bradford Book, The MIT Press, Fifth printing,

Moehle, J., Deierlein, G. (2004) A Framework Methodology for Performance-Based Earthquake Engineering. 13th World Conference on Earthquake Engineering, Vancouver, BC, Canada.

National Safety Council (NSC) (2013) Injury Facts, 2013 Edition. NSC Press Product No. 02320-0000

Pareto, V., (1906) Manuale di Econòmica Plìttica, Società Editrice Libràia, Milan, Italy; translated into English by A. S. Schwier, as Manual of Political Economy, Macmillan, New York, 1971

Park, M., Ha, S., Lee, H. S., Choi, Y.K., Kim, H., Han, S. (2013) Lifting Demand-Based Zoning for Minimizing Worker Vertical Transportation Time in High-Rise Building Construction, Journal of Automation in Construction 32: 88-95

Powel, G. H. (1973) DRAIN-2D user guide, Report No. UCB/EERC 73-22, Earthquake Engineering Research Center, University of California, Berkeley, CA

Powel, G. H. (1993) DRAIN-2DX, Element Description and user guide for element Type01, Type02, Type04, Type06, Type09, And Type15, version 1.10, Report No. UCB/SEMM-93/18

Porter, K. A., Beck, J. L., and Shaikhutdinov, R. (2004) Simplified Estimation of Economic Seismic Risk for Buildings, Earthquake Spectra, 20(4): 1239–1263, Earthquake Engineering Research Institute

Prakash, V., Powel, G. H. and Campbell, S. (1993) DRAIN-2DX Base Program Description and User Guide, Report No. UCB/SEMM-93/17

Ramirez, C. M., Liel, A. B., Mitrani-Reiser, J., Haselton, C.B., Spear, A.D., Steiner, J., Deierlein, G.G., Miranda, E., 2012. Expected Earthquake Damage and Repair Costs in Reinforced Concrete Frame Buildings, Earthquake Engineering & Structural Dynamics, 41(11): 1455-1475

Rojas, H. A. (2008) Automating the Design of Steel Moment-Frames Using a Probabilistic Performance-Based Approach and Evolutionary Computation, Ph.D. Dissertation, The University of Memphis

Rojas, H. A., Foley, C., and Pezeshk, S. (2011) Risk-Based Seismic Design for Optimal Structural and Nonstructural System Performance. Earthquake Spectra, 27(3), 857–880.

Romero, S. and Rix, G.J. (2001) Regional Variations in Near Surface Shear Wave Velocity in Greater Memphis Area, Engineering Geology 62: 137-158.

Shahbazian, A. and S. Pezeshk. (2010) Improved Velocity and Displacement Time Histories in Frequency-Domain Spectral-Matching Procedures, Bulletin of the Seismological Society of America, 100(6): 3213–3223

Schnabel, P. B., Lysmer, J., and Seed, H. B. (1972) SHAKE, a computer program for earthquake response analysis of horizontal layered sites, Report No. EERC72-12, December.

Soliman, S.A, Mantawy A.H. (2012) Modern Optimization Techniques with Applications in Electric Power Systems, Energy Systems, DOI 10.1007/978-1-4614-1752-1_2, # Springer Science+Business Media, LLC 2012

Somerville, P. G., Smith, N. F., Graves, R. W., Abrahamson, N. A. (1997) Modification of Empirical Strong Ground Motion Attenuation Relations to Include the Amplitude and Duration Effects of Rupture Directivity, Seismological Research Letters, 68:.199-222.

Spears, W. M., De Jong K. A. (1991) On the Virtues of Uniform Crossover, the 4th International Conference on Genetic Algorithms, La Jolla, California.

Spall, J. C. (2004) Stochastic Optimization-Handbook of Computational Statistics (Gentle J., Härdle W., and Mori Y. ,eds) Copyright Springer Heidelberg

U.S. Geological Survey (USGS) (2008) Documentation for the 2008 Update of the United States National Seismic Hazard Maps, Open-File Report 2008–1128.

U.S. Geological Survey (USGS) (2013) <http://www.usgs.gov/>

Vasiliev, V.V., Gurdal, Z. (1999) Optimal Design-Theory and Applications to Materials and Structures

Xu, L., Yanglin, G., Grierson, D. E. (2006) Seismic Design Optimization of Steel Building Frameworks, Journal of Structural Engineering,132 : 277-286

NOTATIONS

Notation	Definition	Notation	Definition
EAL	Expected Annual Loss	SL_{indoor}	Social Loss associated with indoor injuries
EASL	Expected Annual Social Loss	CSL_j	Casualty Severity Level j
TC	Penalized value of the PC^T_t	α	Comprehensive cost for CSL_1*($/person)*
PC^T_t	Present value of the total economic cost	N_o	Number of occupants in building
SL	Penalized value of the EASL	t	Lifetime period
φ	Penalty Function	C^I	Initial Cost
CL_{CP}	Confidence Levels for Collapse Prevention	PL^S_t	Present value of the seismic direct economic loss
CL_{IO}	Confidence Levels for Immediate Occupancy	$EN_{OI,IM}$	Expected number of occupants injured or killed in an event with intensity measure *IM*
c_i	i^{th} constraint	W	Weight of the frame
C_i	Scaled i^{th} constraint	ρ	Cost per unit weight of the frame
DV	Decision Variable	i_r	Discount rate
DM	Damage Measure	BRC	Building Replacement Cost
EDP	Engineering Demand Parameter	λ_{CL}	Confidence parameter
IM	Intensity Measure	γ	Demand variability factor
L_c	Direct economic loss for each component	γ_a	Analysis uncertainty factor
L	Direct economic loss	D	Calculated demand on a structure
$RC_{DMi,c}$	Repair Cost for each component c	C	Median estimate of the capacity of the structure

Notation	Definition	Notation	Definition
λ	Annual rate of exceedance for each intensity measure	ϕ	Uncertainty in the prediction of structural capacity
$\Delta\lambda_i$	change in annual rate of exceedance associated with dividing the hazard curve into m different segments	K_x	Standard Gaussian variant
$SL_{outdoor}$	Social loss associated with outdoor injuries	β_{UT}	Uncertainty measure
m	Number of hazard levels considered	CL	Confidence Level

APPENDIX A

CL Parameters and Injury Classifications

Table A-1. Interstory Drift Angle Analysis Uncertainty Factors γ_a (FEMA 2000a)

Analysis Procedure	**LSP**		**LDP**		**NSP**		**NDP**	
System Characteristic	I.O.	C.P.	I.O.	C.P.	I.O.	C.P.	I.O.	C.P.
Special Moment Frames (SMF)								
Low Rise (3 stories or less)	0.94	0.7	1.03	0.83	1.13	0.89	1.02	1.03
Mid Rise (4 – 12 stories)	1.15	0.97	1.14	1.25	1.45	0.99	1.02	1.06
High Rise (> 12 stories)	1.12	1.21	1.21	1.14	1.36	0.95	1.04	1.1
Ordinary Moment Frames (OMF)								
Low Rise (3 stories or less)	0.79	0.98	1.04	1.31	0.95	1.31	1.02	1.03
Mid Rise (4 – 12 stories)	0.85	1.14	1.1	1.53	1.11	1.42	1.02	1.06
High Rise (> 12 stories)	0.8	0.85	1.39	1.38	1.36	1.53	1.04	1.1

Table A-2. Interstory Drift Angle Demand Variability Factors γ (FEMA 2000a)

Building Height	**γ**	
	Immediate Occupancy (I.O.)	Collapse Prevention (C.P.)
Special Moment Frames (SMF)		
Low Rise (3 stories or less)	1.5	1.3
Mid Rise (4 – 12 stories)	1.4	1.2
High Rise (> 12 stories)	1.4	1.5
Ordinary Moment Frames (OMF)		
Low Rise (3 stories or less)	1.4	1.4
Mid Rise (4 – 12 stories)	1.3	1.5
High Rise (> 12 stories)	1.6	1.8

Table A-3. Global Interstory Drift Angle Capacity C and Resistance Factors φ for Regular SMF and OMF Buildings (FEMA 2000a)

Building Height	Performance Level			
	Immediate Occupancy		Collapse Prevention	
	Interstory Drift Angle Capacity *C*	Resistance Factor *φ*	Interstory Drift Angle Capacity *C*	Resistance Factor *φ*
Special Moment Frames (SMF)				
Low Rise (3 stories or less)	0.02	1	0.1	0.9
Mid Rise (4 – 12 stories)	0.02	1	0.1	0.85
High Rise (> 12 stories)	0.02	1	0.085	0.75
Ordinary Moment Frames (OMF)				
Low Rise (3 stories or less)	0.01	1	0.1	0.85
Mid Rise (4 – 12 stories)	0.01	0.9	0.08	0.7
High Rise (> 12 stories)	0.01	0.85	0.06	0.6

Table A-4. Injury Classification Scale (Hazus-MH, 2003b)

Injury Severity Level	Injury Description
Severity1	Injuries requiring basic medical aid that could be administered by paraprofessionals. These types of injuries would require bandages or observation. Some examples are: a sprain, a severe cut requiring stitches, a minor burn (first degree or second degree on a small part of the body), or a bump on the head without loss of consciousness. Injuries of lesser severity that could be self-treated are not estimated by HAZUS.
Severity 2	Injuries requiring a greater degree of medical care and use of medical technology such as x-rays or surgery, but not expected to progress to a life threatening status. Some examples are third degree burns or second degree burns over large parts of the body, a bump on the head that causes loss of consciousness, fractured bone, dehydration or exposure.
Severity3	Injuries that pose an immediate life threatening condition if not treated adequately and expeditiously. Some examples are: uncontrolled bleeding, punctured organ, other internal injuries, spinal column injuries, or crush syndrome.
Severity 4	Instantaneously killed or mortally injured

APPENDIX B

PSHA Using EZ-FRISK

EZ-FRISK is a software package to perform site-specific earthquake hazard analysis. It has database of earthquake faults characteristics and ground motion attenuation equations that could be implemented to perform probabilistic seismic hazard analysis (PSHA) for the site of interest. The advantage of this software is that database for an extensive collection of attenuation equations and seismic sources for different regions are included. EZ-FRISK has been used to perform PSHA for Memphis site, considering the attenuation relationships recommended by USGS (2008). The considered attenuation relationships are listed in Table B-1.

The New Madrid seismic zone (NMSZ) and CEUS gridded data are considered as the seismic sources. EZ-FRISK generates the uniform hazard response spectra (UHRS) for different hazard levels. The obtained UHRS for the Memphis site are presented in Figure 7.

Table B-1. Attenuation relationships used for the Memphis, TN site

Number	Attenuation Relationship
1	Atkinson-Boore (2006) -140 Bar Mw and 200 Bar Mw
2	Cambpell (2003)
3	Frankel (1996)
4	Silva et al (2002)
5	Tavakoli-Pezeshk (2005)
6	Toro (1999)
7	Somerville (2001)

APPENDIX C

DRAIN-2DX

The computer program DRAIN-2D (Dynamic Response Analysis of Inelastic 2-Dimensional Structures) was first released in 1973 (Powell 1973). DRAIN-2DX (Allahabadi 1987 and Allahabadi and Powell 1988, Prakash et al. 1993) is a modification to the program DRAIN-2D. The program is written in FORTRAN-77 and performs nonlinear static and dynamic analyses. For dynamic analysis considers ground accelerations, ground displacements, imposed dynamic loads (e.g., wind), and specified initial velocities (e.g., impulse loading).

Considered yielding surfaces for the nonlinear response-history analysis for beam and beam-column members in DRAIN-2DX are shown in Figure D-1 (Rojas et al. 2011). In this figure, P_{yt} is the axial tensile yield capacity of a beam-column in the absence of bending moment. P_n is the axial compression capacity of the beam column in the absence of bending moment. M_p^+ and M_p^- are the positive and negative plastic moment capacities of the cross-section in the absence of axial loading (Rojas et al. 2011, AISC 2011).

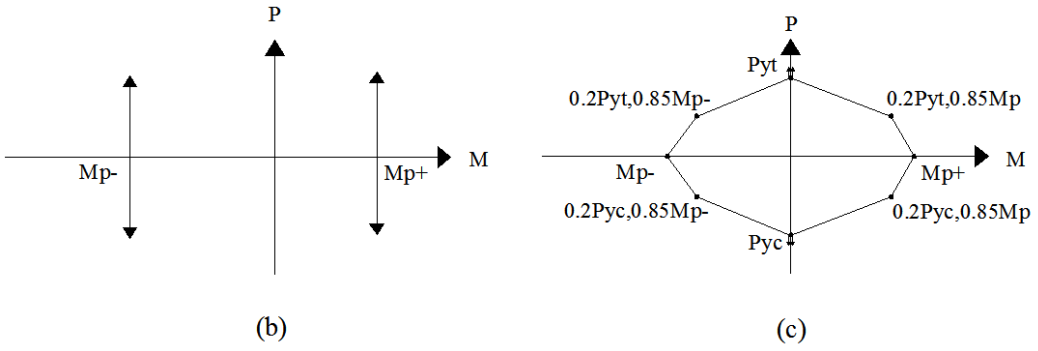

Figure C-1 Yield surfaces in the nonlinear response history analysis for: (a) beam members, (b) beam-column members

The nonlinear analysis for the frame shown in Figure C-2 is performed using two different programs: DRAIN-2DX and Zeus-NL, to compare the results. The frame sections are W14x455 for C1 and C2 and W30x108, W36x170, and W30x99 for B1, B2, and B3, respectively. The considered ground motion is shown in Figure C-3.

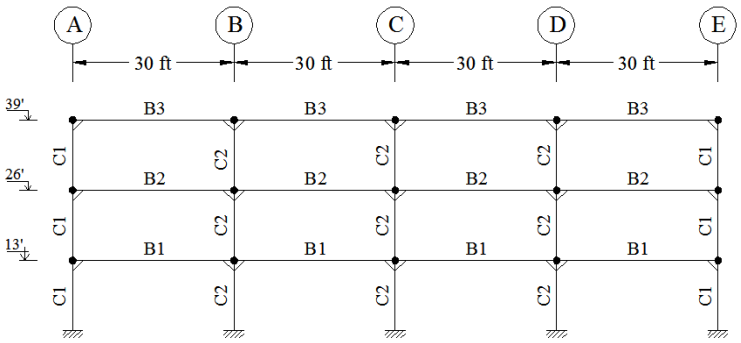

Figure C-2 Example frame

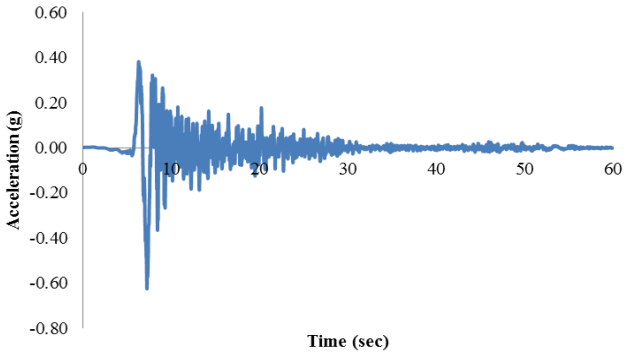

Figure C-3 Considered ground motion

The compatibility of the obtained maximum top-story displacements for the specified example using the two analysis approaches (using DRAIN-2DX and Zeus-NL) could be observed from the results presented in Table C-2.

Table C-1 Comparison of the results

Max Displacement	DRAIN-2DX	Zeus-NL
Top-Story Disp. (in)	3.84	4.07

APPENDIX D

List of Considered W-Sections

Table D-1. List of the considered AISC W-sections for the beams search space

	Section Name	Area (in^2)	$I_x(in^4)$	$I_y(in^4)$	M_y(kips.in)	M_p(kips.in)
1	W18X40	11.8	612	19.1	3420	3920
2	W21X44	13	843	20.7	4080	4770
3	W18X46	13.5	712	22.5	3940	4535
4	W21X50	14.7	984	24.9	4725	5500
5	W21X55	16.2	1140	48.4	5500	6300
6	W21X57	16.7	1170	30.6	5550	6450
7	W18X60	17.6	984	50.1	5400	6150
8	W24X62	18.2	1550	34.5	6550	7650
9	W18X65	19.1	1070	54.8	5850	6650
10	W24X68	20.1	1830	70.4	7700	8850
11	W18X71	20.9	1170	60.3	6350	7300
12	W21X73	21.5	1600	70.6	7550	8600
13	W24X76	22.4	2100	82.5	8800	10000
14	W21X83	24.4	1830	81.4	8550	9800
15	W27X84	24.7	2850	106	10650	12200
16	W18X86	25.3	1530	175	8300	9300
17	W21X93	27.3	2070	92.9	9600	11050
18	W27X94	27.6	3270	124	12150	13900
19	W18X97	28.5	1750	201	9400	10550
20	W30X99	29	3990	128	13450	15600
21	W21X101	29.8	2420	248	11350	12650
22	W27X102	30	3620	139	13350	15250
23	W24X103	30.3	3000	119	12250	14000
24	W24X104	30.7	3100	259	12900	14450
25	W18X106	31.1	1910	220	10200	11500
26	W30X108	31.7	4470	146	14950	17300
27	W21X111	32.6	2670	274	12450	13950
28	W27X114	33.6	4080	159	14950	17150
29	W30X116	34.2	4930	164	16450	18900
30	W24X117	34.4	3540	297	14550	16350
31	W18X119	35.1	2190	253	11550	13100
32	W21X122	35.9	2960	305	13650	15350
33	W30X124	36.5	5360	181	17750	20400
34	W27X129	37.8	4760	184	17250	19750
35	W33X130	38.3	6710	218	20300	23350
36	W24X131	38.6	4020	340	16450	18500

Table D-1 (continued). List of the considered AISC W-sections for the beams search space

	Section Name	Area (in^2)	$I_x(in^4)$	$I_y(in^4)$	M_y(kips.in)	M_p(kips.in)
37	W30X132	38.8	5770	196	19000	21850
38	W33X141	41.5	7450	246	22400	25700
39	W18X143	42	2750	311	14100	16100
40	W27X146	43.2	5660	443	20700	23200
41	W21X147	43.2	3630	376	16450	18650
42	W30X148	43.6	6680	227	21800	25000
43	W36X150	44.3	9040	270	25200	29050
44	W33X152	44.9	8160	273	24350	27950
45	W18X158	46.3	3060	347	15500	17800
46	W36X160	47	9760	295	27100	31200
47	W27X161	47.6	6310	497	22900	25750
48	W24X162	47.8	5170	443	20700	23400
49	W21X166	48.8	4280	435	19000	21600
50	W40X167	49.3	11600	283	30000	34650
51	W33X169	49.5	9290	310	27450	31450
52	W36X170	50	10500	320	29050	33400
53	W30X173	50.9	8230	598	27050	30350
54	W18X175	51.4	3450	391	17200	19900
55	W24X176	51.7	5680	479	22500	25550
56	W27X178	52.5	7020	555	25250	28500
57	W40X183	53.3	13200	331	33750	38700
58	W36X182	53.6	11300	347	31150	35900
59	W30X191	56.1	9200	673	30000	33750
60	W24X192	56.5	6260	530	24550	27950
61	W36X194	57	12100	375	33200	38350
62	W27X194	57.1	7860	619	27950	31550
63	W40X199	58.8	14900	695	38500	43450
64	W33X201	59.1	11600	749	34300	38650

Table D-2. List of the considered AISC W-sections for the columns search space

	Section Name	Area (in^2)	$I_x(in^4)$	$I_y(in^4)$	M_y(kips.in)	M_p(kips.in)
1	W10X19	5.62	96.3	4.29	940	1080
2	W10X26	7.61	144	14.1	1395	1565
3	W10X30	8.84	170	16.7	1620	1830
4	W10X33	9.71	171	36.6	1750	1940
5	W10X39	11.5	209	45	2105	2340
6	W12X40	11.7	307	44.1	2575	2850
7	W12X45	13.1	348	50	2885	3210
8	W10X45	13.3	248	53.4	2455	2745
9	W14X48	14.1	484	51.4	3510	3920
10	W10X49	14.4	272	93.4	2730	3020
11	W12X50	14.6	391	56.3	3210	3595
12	W12X53	15.6	425	95.8	3530	3895
13	W14X53	15.6	541	57.7	3890	4355
14	W10X54	15.8	303	103	3000	3330
15	W12X58	17	475	107	3900	4320
16	W10X60	17.7	341	116	3335	3730
17	W14X61	17.9	640	107	4605	5100
18	W10X68	19.9	394	134	3785	4265
19	W14X68	20	722	121	5150	5750
20	W12X72	21.1	597	195	4870	5400
21	W14X74	21.8	795	134	5600	6300
22	W10X77	22.7	455	154	4295	4880
23	W12X79	23.2	662	216	5350	5950
24	W14X82	24	881	148	6150	6950
25	W12X87	25.6	740	241	5900	6600
26	W10X88	26	534	179	4925	5650
27	W12X96	28.2	833	270	6550	7350
28	W10X100	29.3	623	207	5600	6500
29	W12X106	31.2	933	301	7250	8200
30	W14X109	32	1240	447	8650	9600
31	W10X112	32.9	716	236	6300	7350
32	W12X120	35.2	1070	345	8150	9300
33	W14X120	35.3	1380	495	9500	10600
34	W14X132	38.8	1530	548	10450	11700
35	W12X136	39.9	1240	398	9300	10700
36	W14X145	42.7	1710	677	11600	13000
37	W12X152	44.7	1430	454	10450	12150

Table D-2 (continued). List of the considered AISC W-sections for the columns search space

	Section Name	Area (in^2)	$I_x(in^4)$	$I_y(in^4)$	M_y(kips.in)	M_p(kips.in)
38	W14X159	46.7	1900	748	12700	14350
39	W12X170	50	1650	517	11750	13750
40	W14X176	51.8	2140	838	14050	16000
41	W12X190	56	1890	589	13150	15550
42	W14X193	56.8	2400	931	15500	17750
43	W12X210	61.8	2140	664	14600	17400
44	W14X211	62	2660	1030	16900	19500
45	W12X230	67.7	2420	742	16050	19300
46	W14X233	68.5	3010	1150	18750	21800
47	W12X252	74.1	2720	828	17650	21400
48	W14X257	75.6	3400	1290	20750	24350
49	W12X279	81.9	3110	937	19650	24050
50	W14X283	83.3	3840	1440	22950	27100
51	W12X305	89.5	3550	1050	21750	26850
52	W14X311	91.4	4330	1610	25300	30150
53	W12X336	98.9	4060	1190	24150	30150
54	W14X342	101	4900	1810	27900	33600
55	W14X370	109	5440	1990	30350	36800
56	W14X398	117	6000	2170	32800	40050
57	W14X426	125	6600	2360	35300	43450
58	W14X455	134	7190	2560	37800	46800
59	W14X550	162	9430	3250	46550	59000
60	W14X605	178	10800	3680	52000	66000

APPENDIX E

Distribution of Losses for Optimization Problem III

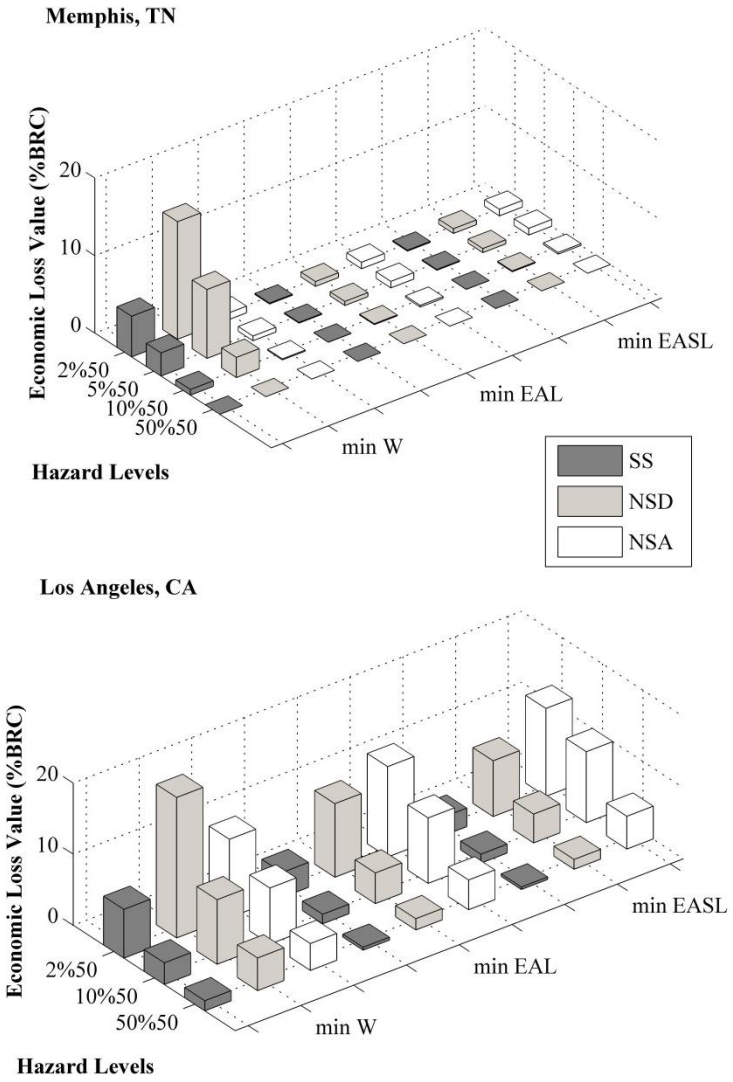

Figure E-1. Comparison of the distribution of losses between different components for the 3-story structures located in Memphis, TN and Los Angeles, CA

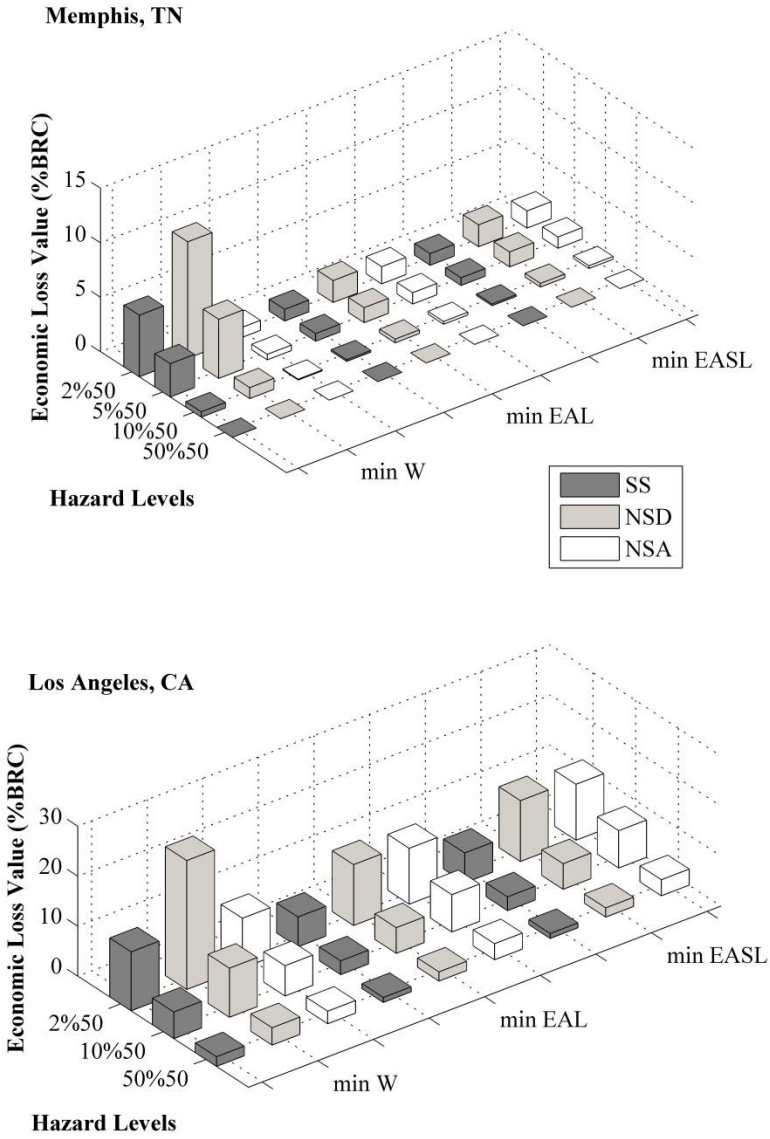

Figure E-2. Comparison of the distribution of losses between different components for the 7-story structures located in Memphis, TN and Los Angeles, CA

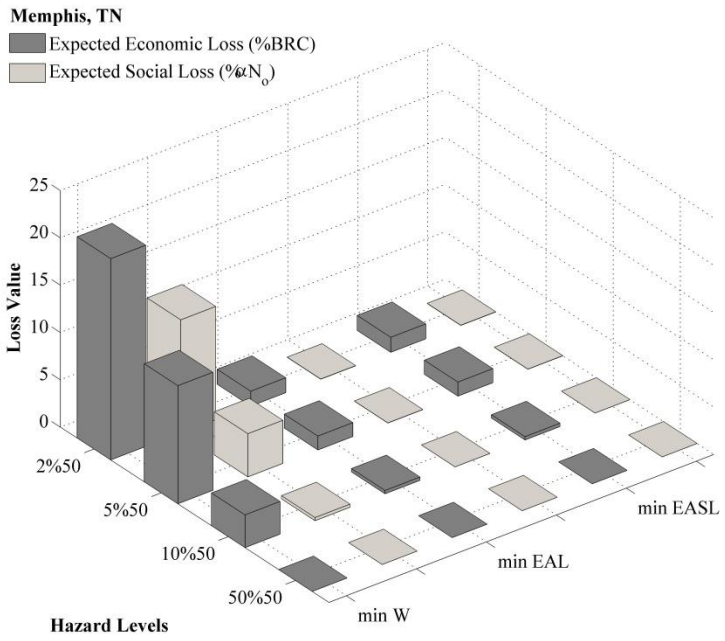

Figure E-3. Comparison of the economic and social losses between for the 3-story structures located in Memphis, TN

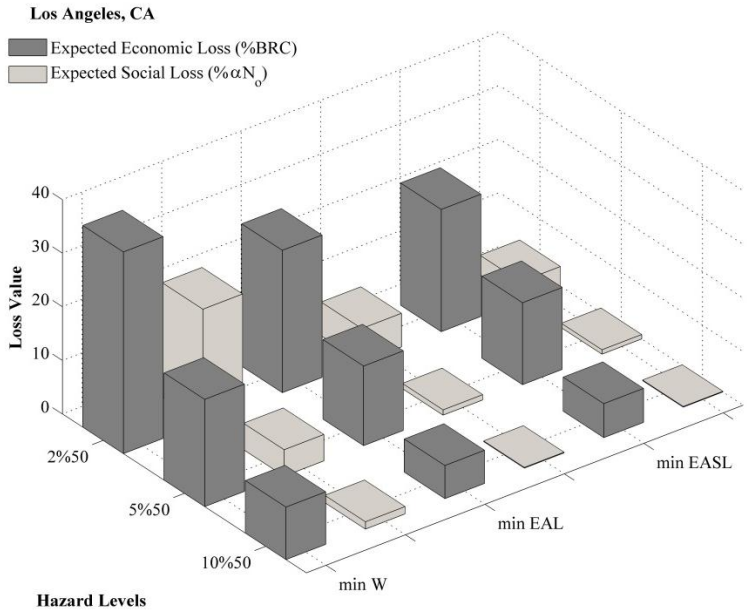

Figure E-4. Comparison of the economic and social losses between for the 3-story structures located in Los Angeles, CA

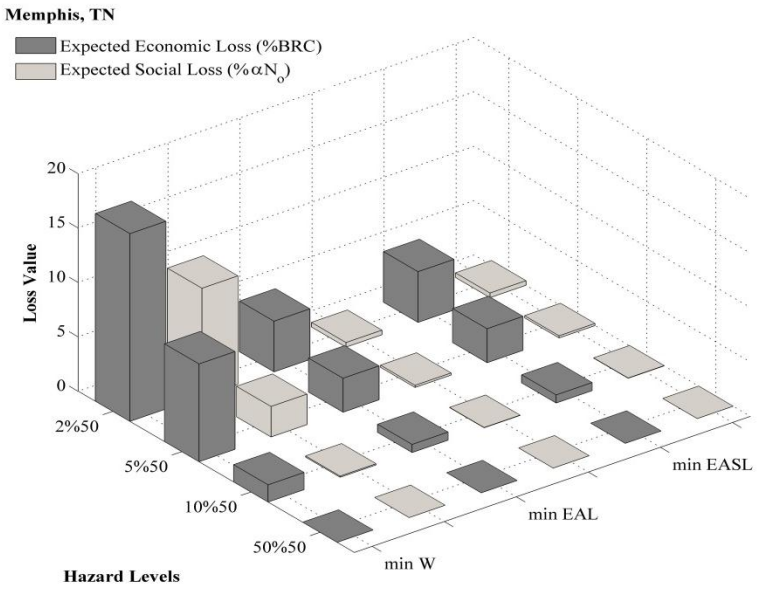

Figure E-5. Comparison of the economic and social losses between for the 7-story structures located in Memphis, TN

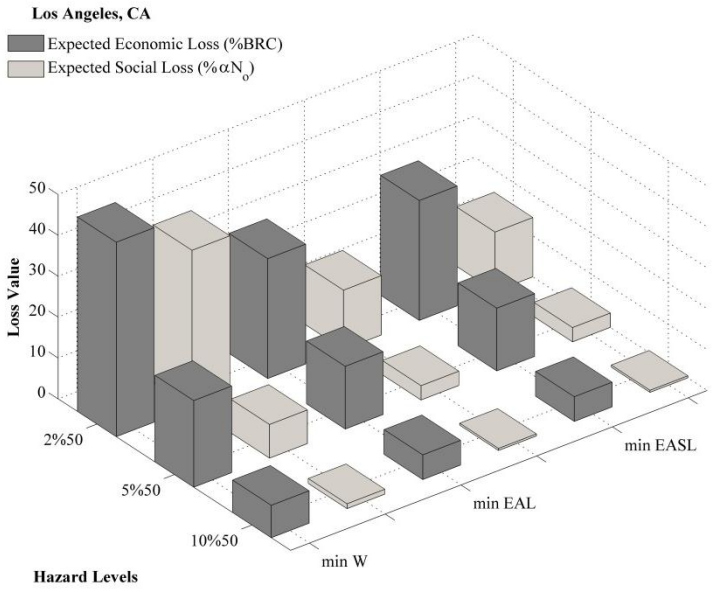

Figure E-6. Comparison of the economic and social losses between for the 7-story structures located in Los Angeles, CA